UNIVERSITÀ
DI PARMA

UNIVERSITA' DEGLI STUDI DI PARMA

Dottorato di ricerca in Scienze Chimiche

Ciclo XXX (2014-2017)

Synthesis of novel hybrid nanosystems composed by *core-shell* SiC/SiO_x nanowires conjugated with porphyrins for X-ray-excited PDT

Coordinatori: Chiar.mo Prof. Roberto Corradini

Tutor: Chiar.ma Prof. Franca Bigi

Dottoranda: Cecilia Loffi

Anni 2014/2017

Introduction

Synthesis of novel hybrid nanosystems composed by core-shell SiC/SiOx nanowires conjugated with porphyrins for X-ray-excited PDT

Abstract

My PhD thesis dealt with the preparation and characterization of hybrid nanosystems for possible application in nanomedicine, in particular for the treatment of deep solid tumours by X-Ray activated PhotoDynamic Therapy, according to the "*self lighting photodynamic therapy*" recently proposed in the literature. The activity has been performed in the framework of the BioNiMED Project funded by the CARIPARMA foundation and coordinated by IMEM-CNR (Parma). The project aims to develop a nanosystem capable of causing oxidative stress through the production of singlet oxygen, a cytotoxic species, when exposed to a source of X-Ray.

During my PhD work, I functionalized cubic SiC/SiO_x nanowires, grown at IMEM (CNR), and prepared nanosystems consisting of "*core shell*" cubic $SiC@SiO_x$ nanowires conjugated with porphyrins. $SiC@SiO_x$ nanowires work as scintillators: indeed, when they are irradiated with X-Ray, they emit light in the wavelength range corresponding to the porphyrin absorption. This energy transfer excites the porphyrin, which in turns produces singlet oxygen. Indeed, porphyrins are a wide class of photosensitizers, largely used in conventional PDT. Cubic SiC is known to be a biocompatible material, employed in biomedical field, and the biocompatibility of the SiC/SiO_x nanowires was also assessed and previously published.

In a previous PhD work developed in our laboratory the *tetra*-(4-carboxyphenyl)porphyrin (H_2TCPP) was covalently linked to the SiC/SiO_x NWs by a 'click' reaction, giving a novel nanosystem able to promote X-ray-excited PDT, as evidenced by *in vitro* studies.

During my thesis work, I conjugated the selected porphyrin to the nanowires by the formation of the covalent amide bond and introduced different ending chains in the porphyrin moiety in order to increase the dispersion of the nanosystem in aqueous medium.

The formation of the amide bonds required the previously functionalization of the nanowire surface with amino groups reacting the silica hydroxyl groups with APTES (aminopropyltriethoxysilane). To bind the porphyrin to the nanowire surface, the carboxylic groups of H_2TCPP porphyrin were previously activated with typical condensation agents (EDC, HOBt, and DMAP) and then reacted with the amino groups to give the amide bond formation.

This conjugation approach resulted to give a higher degree of porphyrin loading, as evidenced by fluorescence spectra, and occurred under very mild conditions (r.t. *vs*. high temperature used in the thermal click reaction). In addition, it was possible to bind polar chains to the conjugated porphyrin.

It was planned to introduce short PEG chains to modulate the polarity of the nanosystem. In particular, two different ending NH_2-PEG chains were introduced, PEG_6-CH_2COOH and –PEG_8-OH.

In the first case, I prepared $NH_2CH_2CH_2(OCH_2CH_2)_5OCH_2CO_2H$ by a multistep synthesis starting from hexaethylene glycol.

Then this chain was bound to the residual activated carboxylic groups of the porphyrin conjugated to the nanowires. Finally, deprotection with trifluoroacetic acid gave free acid carboxylic functions at the end of the PEG-chains. The nanosystem was characterized by fluorescence spectroscopy that confirmed that functionalization occurred successfully.

Last, the nanowires were detached from the support using an ultrasound microtip. *In vitro* experiments (clonogenic tests) performed on the adenocarcinoma human alveolar basal epithelial (A549) cell line evidenced the ability to significantly reduce the survival fraction with respect to simple radiotherapy.

To prepare the second chain, NH_2-PEG_8-OH, without the ionizable acid group, I started from tetraethylene glycol by a multistep synthesis. The residual activated carboxylic groups of the H_2TCPP porphyrin conjugated to the nanowires were reacted with this chain giving a less polar nanosystem. The activity of the nanowires, after detachment from the support, was tested by *in vitro* experiment on A549 tumoural cell line. The lower activity observed could be attributed to lower internalization due to the formation of boundles in the biological medium.

To increase the cytotoxic activity, a further aim was to obtain a thicker porphyrin coating. Thus, it was planned to link a second different porphyrin on the conjugated H_2TCPP porphyrin. In particular, tetra(4-aminophenyl)porphyrin could be successfully reacted and in vitro experiments are in progress.

To face the open problem of the number of porphyrin arms involved in the conjugation, we planned to apply XPS spectroscopy to study the nanosystem conveniently modified by the presence of bromine atom.

To check the possibility of evaluating the C=O/Br ratio in XPS spectra, I synthesized the bromophenyl tetra-derivative of H_2TCPP porphyrin as

reference compound. Then H_2TCPP and the bromine derivative porphyrins were deposited on Pt-metalized wafer by drop casting. XPS spectra will give us information on the utility of this approach.

Last, to evaluate the porphyrin loading, I synthesized the Cu-TCPP porphyrin, a metal derivative stable enough to be conjugated to the nanowires. Indeed, the complete removal of copper from the porphyrin requires the treatment with conc. sulfuric acid. The determination of Cu amount by atomic absorption was performed.

To explore a different type of linker to anchor a porphyrin to a solid support, I successfully synthesized a metal tetra-phosphonated porphyrin. In particular, starting from the tetra(4-hydroxyphenyl)porphyrin (H_2THPP) it was possible to obtain the Zn-THPP functionalized with four phosphonic acid chain ($–CH_2)_6PO_3H$), compound that is not reported in the literature. This type of porphyrins is of great interest for both energy transfer process and electron transfer process.

The anchorage of this porphyrin on a flat silicon support will be useful to study the porphyrin position on the surface, parallel or not, by X-ray-excited optical luminescence (XEOL).

Nanomedicine and nanomaterials

1.1 Nanomedicine

Nanomedicine is the medical application of nanotechnology. It is a new branch of medicine, which relies on the potentiality and specific properties of nanomaterials. Nanomedicine ranges from the medical applications of nanomaterials and biological devices, to nanoelectronic biosensors, and even possible future applications of molecular nanotechnology such as biological machines[1]. Nanomaterials can be suitable for different applications in this field. Current problems for nanomedicine involve understanding the issues related to toxicity and environmental impact of nanoscale materials (materials whose structure is on the scale of nanometers, i.e. billionths of a meter, or with nano and under micron size). Functionalities can be added to nanomaterials by interfacing them with biological molecules or structures. The size of nanomaterials is similar to that of most biological molecules and structures; therefore, nanomaterials can be useful for both in vivo and in vitro biomedical research and applications.

Thus far, the integration of nanomaterials with biology has led to the development of diagnostic devices, contrast agents, analytical tools, physical therapy applications, and drug delivery vehicles.

Nanomedicine was defined (by the European Science Foundation, ESF) as "the science and technology of diagnostic treating and preventing disease and traumatic injury, of relieving pain, and of preserving and improving human health, using molecular tools and molecular knowledge of the human body". Nanomedicine is defined as the application of nanometer technologies in medical areas (from biomedical imaging to drug delivery and therapeutics).

Others, instead, prefer to focus on the original word meaning "nanomedicine" as one technique that makes use of physical effects occurring only in nanoscale objects and that exist at the interface between the molecular and macroscopic world, in which quantum mechanics still reigns[2].

This is a new and fast expanding medical field. The overall goal of nanomedicine is the same as it is for traditional medicine: early and accurate diagnosis, effective treatments that are free of side effects, and *non*-invasive evaluation of the efficacy of the treatment[3]. Nanotechnology is a very broad interdisciplinary research field that involves various areas of science and chemistry. Physics and engineering properties of nanomaterial can change

completely if you compare the nanosystem with bulk materials. Some of these nanosystems are already appearing in the market place or in clinical trials.
In the world and also in Italy, the interest in nanodevices and nanosystems for biomedical applications is growing rapidly.

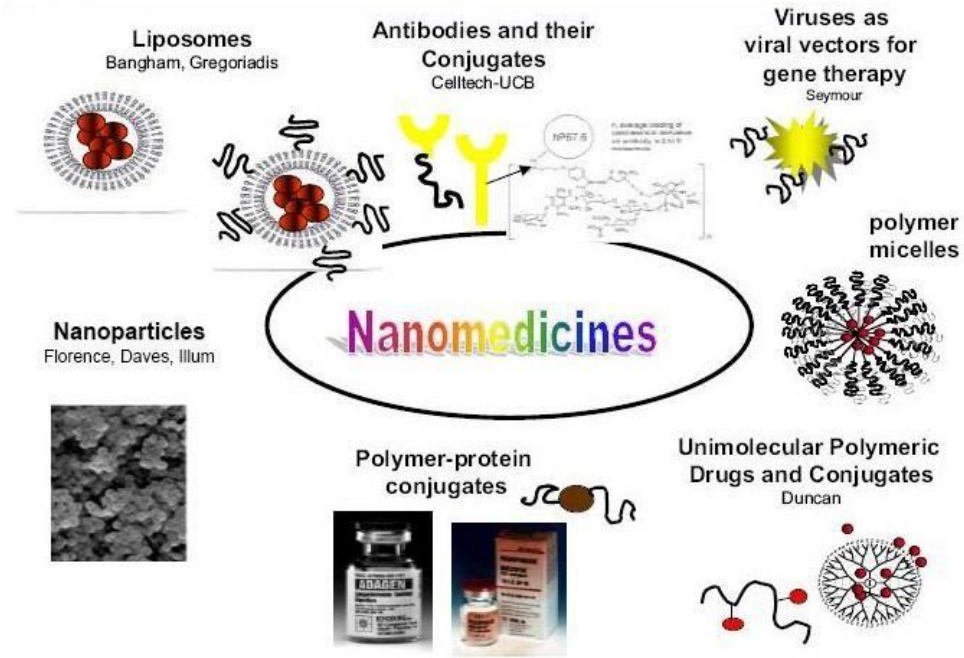

Figure 1*: Some examples of nanomedicines*

Applications of nanomedicine

Recently nanomedicine has focused on a wide range of applications and, going hand in hand with new technologies and new nanomaterials, found new fields of employment.
In this paragraph the main application fields of nanomedicine are summarized.

Drug delivery: Drug delivery refers to approaches, formulations, technologies, and systems for transporting a pharmaceutical compound in the body as needed to safely exert its desired therapeutic effect. The drug delivery technique is based on nanoscale particles/molecules that have been developed to target specific sites in the body, to improve the bioavailability and pharmacokinetics of therapeutics. Multifunctional targeted devices are capable of bypassing biological barriers to deliver multiple therapeutic agents directly to the cells and also to tissues in the microenvironment.[4]

Therapy techniques: Several nanostructure have unique medical properties themselves, showing therapeutic effects in biological systems.[5]
These properties can be exploited in therapeutic treatments. Indeed, several nanostructures have intrinsic properties or can be enriched with bioactive agents and can be useful to treat specific systems.
Magnetic hyperthermia or photodynamic therapy, for example, can be used for cancer treatment[6].

Imaging: Nanoparticles can be used to mark biological structure and they are used particularly for MRI and ultrasound scans, providing an improved contrast and favorable biodistribution. For example, superparamagnetic iron oxide nanoparticles have been used as MRI contrast agents.[7]

Cell and Tissue Repair and replacement: damaged tissues and organs often need to be replaced by artificial substitutes. Nanotechnology offers a range of new biocompatible coatings for the implants that improves their adhesion, durability and lifespan or as a scaffold. New types of nanomaterials are being evaluated to improve interface properties for tissue replacement and regeneration. For example, nanopolymers can be used to coat devices in contact with blood (e.g. artificial hearts, catheters), to disperse clots or prevent their formation.[8]

Implantable devices: Nanomaterials have the capability to improve device properties or can be used to develop a new generation of electrical bio-devices, smaller and more efficient.[9]

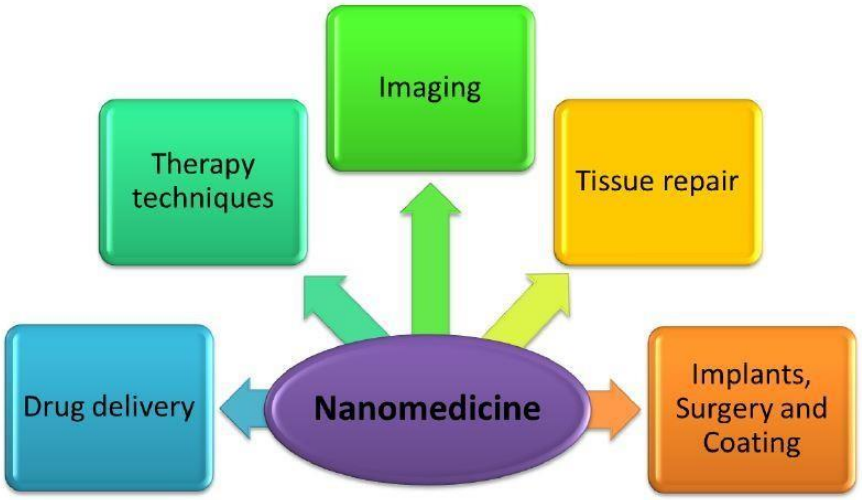

***Figure 2**: Scheme of the different nanostructural applications in nanomedicine.*

1.2 Nanomaterials and Nanowires

Nanomaterials describe, in principle, materials of which a single unit is sized between 1 and 1000 nanometers (10^{-9} meter) but is usually 1—100 nm (the usual definition of nanoscale[10]).
Nanomaterial research is nowadays widespread, due to the fact that these materials, with structure at the nanoscale, often have unique optical, electronic, or mechanical properties.[11]
Furthermore, nanomaterials are highly versatile, due to their easy functionalization: they have a high surface area, so that they can be decorated with a wide variety of molecules with different features. Their small size makes them suitable for many purposes, ranging from electronics, to catalysis, to biological and medical field: nanomaterials, in fact, are small enough to penetrate biological tissues, thus being internalized by cells.
Several nanostructures and materials with different shape and dimensionality (0D: nanoparticles, 1D: nanotubes and nanowires, 2D: nanosheets) are

employed in nanotechnology. These characteristics play an important role on the cell fate. The size and shape is the key of the interaction between nanostructure and the biological system and one dimension nanostructures find a large purpose in this field.

1D nanostructure are interesting because mime the biological systems. Among the plethora of nanomaterials we know, nanowires are nowadays growing a special importance in this field.

A nanowire is a nanostructure, with the diameter in the order of a nanometer. It can also be defined as the ratio of the length to width being greater than 1000. Alternatively, nanowires can be defined as structures that have a thickness or diameter constrained to tens of nanometers or less and an unconstrained length.

In the last decade nanowires became very important in different fields, such as mechanics, electronics and in nanomedicine. Many different types of nanosystems exist and nowadays are being studied, such as carbon nanotubes (single-walled and multi-walled), metallic nanowires (e.g. based on gold, iron and silver), semiconducting nanowires (e.g. silicon, GaN, InP and other III-V elements), superconducting nanowires (e.g. YBCO) and oxide nanowires (e.g. ZnO, SiO_x, and TiO_2).

These differ considerably one from each other for both composition and the structure, and, therefore the effect induced on cell behavior must be carefully studied for each kind of nanowire.

It was demonstrated that TiO_2-based nanofilaments had a strong dose-dependent effect on cell proliferation and cell death[14] and TiO_2 nanowires induced persistent pathologic alterations in the lung tissue in mice[13]. ZnO nanowires resulted in vitro cytotoxic for human monocyte macrophages[12], and the cell viability resulted decreased on ZnO nanorods for NIH_3T_3 fibroblasts, human umbilical vein endothelial cells[15] and mouse macrophages[12]

Metal nanowires (e.g. silver, iron, iron oxide nanowires) and Si based nanowires, on the contrary, turned out to be essentially cytocompatible. The best results on NWs biocompatibility were obtained from Si-based nanosystems, which recently showed a stability of about two weeks in biological environments.

2. *Nanowires*

In the last decade, materials science focused its attention on new nanotechnologies, novel materials and innovative growth methods.
The growing interest in nanomaterials is due to the fact that they have superior properties, if compared to the respective bulks. These properties allow the realization of new nano devices with outstanding performances in many application fields. Research on nanomaterials crosses different areas, from nanoelectronic devices (e.g. nano field-effect transistors) to nanophotonics and to nanomedicine, as stated in the previous chapter.
Among the world of nanomaterials, nanowires (NWs) open promising near-future perspectives for the design and fabrication of nano-scale devices. The main application fields are nanoelectronic devices (e.g. nano field effect transistors), nano-electromechanical systems able to operate even in harsh environments, nano-sensors, nanomedicine and nano-probes for biological systems.
A nanowire refers to a 1D structure with two dimensions in the nanometer range and the third (length) in the micron one. A nanowire can have characteristics completely different from its massive counterpart, due to the very high surface/volume ratio and, below certain critical dimensions, due to quantum confinement effect.
In this chapter the properties and the applications of silicon-based nanowires will be discussed: in particular, I'll shine light on *core-shell* SiC/SiOx nanowires, for their special features and their potential role in the biomedical field.

2.1 Silicon Carbide

Silicon Carbide (SiC) is known to be a robust, hard material and a high-temperature semiconductor for advanced applications.
Single-crystal silicon carbide presents a high Young modulus (370 GPa), excellent hardness (9 on the Mohs scale), low friction coefficient (0.17), and

high resistance to wear and corrosion: for these reasons SiC works well also in harsh environments, such as body fluids [16,17].
For instance, SiC does not react with any known material at room temperature, the only efficient etchant being molten potassium hydroxide (KOH) at temperatures above 400ºC [18]. Moreover, single-crystal SiC is a wide energy band-gap semiconductor with gaps varying from 2.4 to 3.2 eV depending on the polytype. Hence, crystalline SiC shows excellent tribological properties to a vast sensing potentiality.
These features, together with low thermal expansion coefficient, low weight, and transparency to visible light, elevate SiC as a candidate biomaterial that could be used in a wide variety of cutting-edge applications varying from smart medical implants to environmental and space exploration biosensors. However, in many of these bioapplications, the degree of success of a material depends on its biocompatibility and on its capability of directly interfacing cells. The capability of SiC of integrating with living tissue and safely contacting blood has been largely reported by the biomedical research community.

Silicon carbide is a refractory material consisting of covalently bound Si and C atoms, typically in biatomic layers. These form tetrahedrally oriented molecules of Si–C, with a very short bond length and, hence, a very high bond strength. This is the origin of the extremely high chemical and mechanical stability of SiC [20].

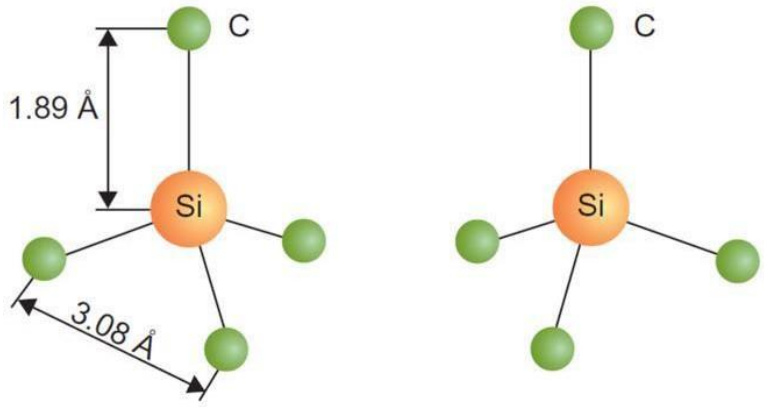

***Figure 3**: All SiC crystals are made up of bilayers of C and Si, covalently bound to form a tetrahedron. Four carbon atoms are covalently bonded with a silicon atom in the center (conversely four Si atoms are covalently bonded with a C atom as this arrangement is crystallographically identical and represents the next atomic layer in the crystal). Two types exist—one is rotated 180° around the c-axis with respect to the other, as shown. This tetrahedrally bonded molecule then forms the basic building block of all SiC materials [19]*

SiC can exist in amorphous, polycrystalline, and monocrystalline solid forms. The bilayers of Si and C (Figure 3) can be stacked one upon the other in different crystal systems: cubic, hexagonal, and rhombohedral. Among more than 200 known polytypes reported in the literature, the three technologically relevant forms are one purely cubic form (β-SiC) and two hexagonal forms that actually have some cubic symmetry (α-SiC). These three polytypes are shown in Figure 4.

The cubic form is named as 3C-SiC, where the "3" indicates that 3 bilayers of Si–C are needed to form the basic structure and the "C" indicates that the crystal form is cubic. The hexagonal forms are 4H-SiC and 6H-SiC, where the "4" and "6" delineate that 4 and 6 bilayers are needed, while the "H" indicates that the crystal form is hexagonal. These forms of SiC all have different properties, which allow applications in various fields: 3C-SiC has the highest electron mobility and saturation velocity because of
reduced phonon scattering resulting from the higher symmetry. The band gaps differ widely among the polytypes ranging from 2.3 eV for 3C-SiC to 3 eV in 6H SiC to 3.3 eV for 2H-SiC. Among the SiC polytypes, 6H is most

easily prepared and best studied, while the 3C and 4H polytypes are attracting more attention for their superior electronic properties.
In this work, when SiC is cited, it means that only 3C-SiC is used even if not specified. Indeed, this is the most interesting crystal phase in this context for two main reasons: it can be grown over silicon substrates and it is the best polytype for possible biomedical applications.

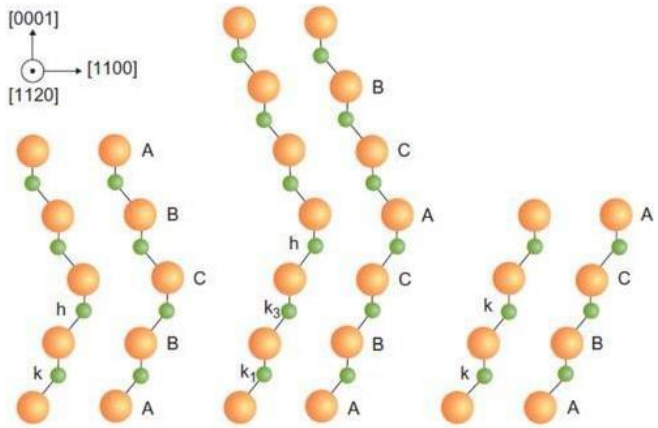

***Figure 4**: Atomic stacking sequence of the three technologically relevant SiC polytypes. From left to right, 4H-SiC (ABCB), 6H-SiC (ABCACB), and 3C-SiC (ABC). The letters "k" and "h" denote crystal symmetry points that are cubic and hexagonal, respectively. [19]*

Moreover, SiC can be easily covered with silicon oxide (SiO_x).
SiO_x shows relevant physical and chemical properties like elastic modulus, bending strength and hardness, chemical durability [21][22][23]. Then, it can be easily functionalized and decorated with a wide variety of macro-molecules and nanoparticles [24][25][26].
NWs based on cubic silicon carbide (3C-SiC), either bare (3C-SiC NWs) or surrounded by an amorphous shell (3C-SiC/SiO_x core/shell NWs), and silicon oxycarbide nanowires (SiOxCy NWs) can meet the chemical, mechanical and electrical requirements for tissue engineering and have a strong potential to

pave the way for the development of a novel generation of implantable nano-devices.
Among different types of nanowires, SiC nanowires gained a special interest in the biomedical field for their cytocompatibility and their better features with respect to other materials.
In particular, core-shell SiC/SiO_x nanowires have unique properties, due to their special structure, consisting of a SiC core and a silica shell: the latter, in fact, can be easily functionalized with a wide variety of organic molecules, tuning the properties of the material according to a specific purpose.
Furthermore, the presence of silica shell determines SiC emission as a scintillator. When SiC is irradiated with a X-ray radiation, it absorbs this, thus emitting and transferring the excitation to an organic molecule (e.g. porphyrins or phtalocyanines), for instance. Silica shell is responsible for this phenomenon, which is at the basis of X-Ray-excited PDT: SiC alone does not have such properties.

2.2 Core-shell SiC/SiOx nanowires

During my PhD work, I managed to functionalize *core-shell* SiC/SiO_x nanowires ($1.8<x<2$) with different porphyrins, to develop nanosystems useful in the field of photodynamic therapy.
Core-shell SiC/SiO_x nanowires are supplied by the IMEM-CNR Institute of Parma, where they are grown and characterized. The technique employed for the preparation of the nanowires is called chemical vapor deposition (CVD) and consists of growing nanowires on a silicon substrate <100>, without removing the native oxide, in the presence of metal catalysts.
In this technique, the substrate is pretreated with an iron salt, then exposed to a stream of CO mixed with N_2 and Ar as carrier gas. The growth of the nanowires is catalyzed by an iron salt and occurs at temperatures between 1050-1100 °C. During this time, the carbon monoxide diffuses across silica and at the interface between SiO_x and Si.
The following carbothermic reaction between CO and Si occurs (Figure 5):

$$4\ CO\ (g) + 6\ Si\ (s) = 4\ SiC(s) + 2\ SiO_2$$

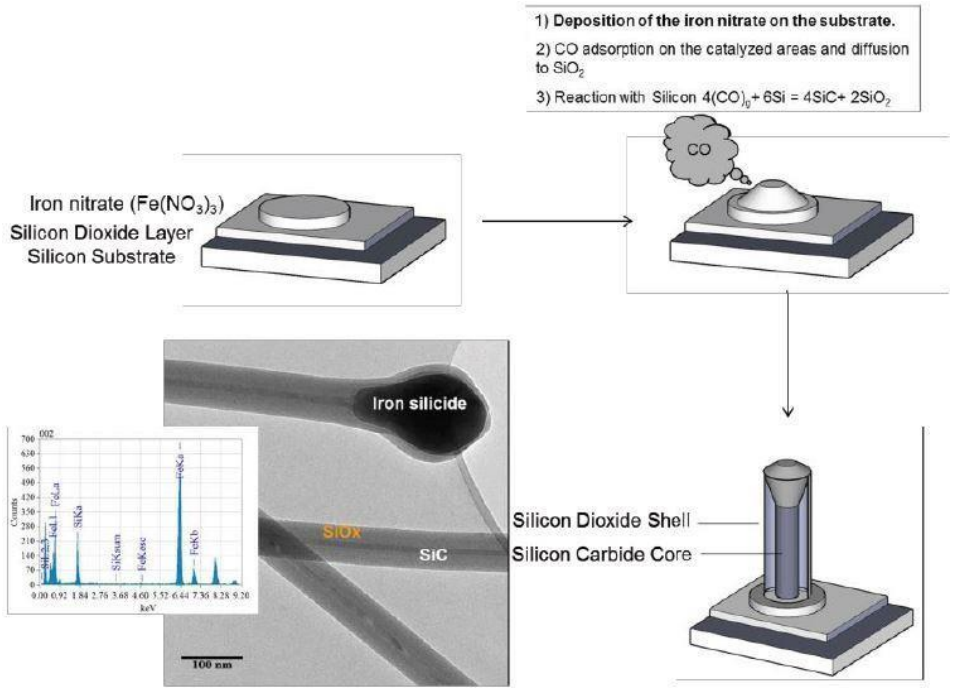

Figure 5*: Scheme showing the process to grow nanowires*

The process is metal assisted. Nickel based compounds (e.g. nickel nitrate ($Ni(NO_3)_2$)) perform as the most effective catalyst, but safety standards for applications in biological environment require
to minimize the employment of nickel, which could stimulate neoplastic transformations.
Therefore, the growth was performed using iron catalysts (e.g. ferric nitrate ($Fe(NO_3)_3$), more suitable for biomedical applications.

In agreement with the preferential mechanism of nucleation at the interface vapor-liquid (VLS), the formation of a dense forest of nanowires SiC/SiO_x can be observed (Figure 6).

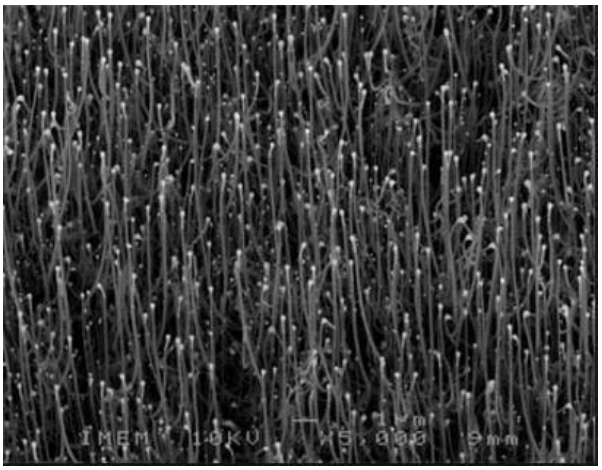

Figure 6: *TEM image representing a "forest" of nanowires grown on a silicon support*

The nanowires obtained were characterized with different analytical techniques, including transmission electron microscope (TEM), cathodoluminescence (CL), X-Ray and Raman spectroscopy. The results confirm that the nanowires actually have a "core-shell" structure, with a core of about 15-20 nm and a coating of approximately equal thickness, for total diameter of about 60 nm (Figure 7).

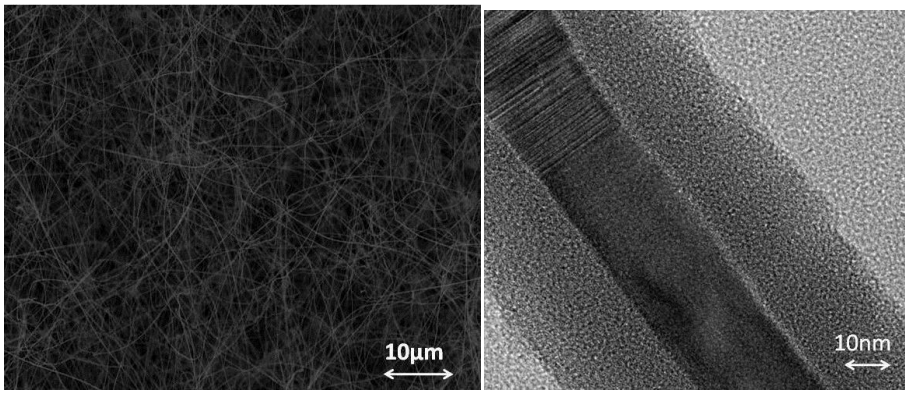

Figure 7*: Left: Typical SEM-image of SiC/SiOx core-shell NWs bundle. Right: Typical TEM image of a single SiC/SiOx NW, showing the planar defects of the SiC crystalline core.*

Furthermore, Fabbri et al. observed that the silica shell improves the emission of the SiC core[28], [29]: in core-shell SiC/SiOx NWs the silica shell is functional to enhance the luminescence intensity of the crystalline SiC core.
The core-to-shell ratio influences the luminescence of the nanosystem as proved, for instance, by cathodoluminescence (CL) spectroscopy. The standard luminescence of the core–shell NWs is a broad visible emission (Figure 8).

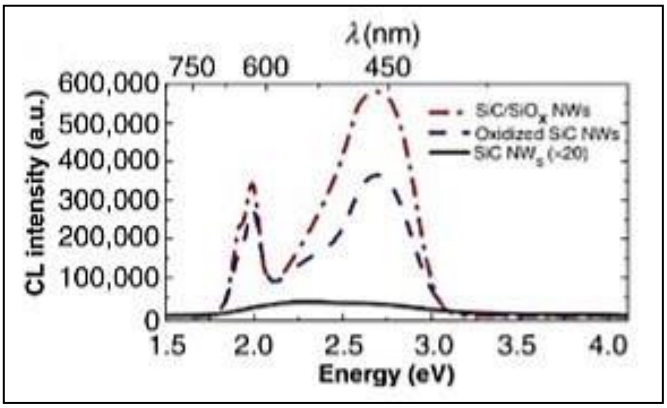

***Figure 8**: Room temperature CL spectra of bare SiC NWs (solid line) and core–shell SiC–SiOx NWs (dash-dotted line: as-grown, shell thickness 20 nm; dashed line: etched and reoxidized, shell thickness 5 nm).*

Gaussian deconvolution reveals that the broad emission is composed of three main features: the most intense at 2.69 eV, a shoulder at 2.38 eV, and a narrow emission at 2.00 eV. Two of these emissions are related to radiative centers of silicon oxide.
At a core-to-shell ratio of 1:1, the silicon oxide shell is beneficial to enhance the light emission yield of the 3C–SiC core [27], [28].
It has to be noted that the enhancement takes place mainly when the shell thickness is comparable to the core diameter. As the shell thickness increases, this beneficial effect is no longer observed and, instead, the shell becomes

detrimental. At a shell thickness of about five times that of the core diameter (core-to-shell ratio 1:5), the SiOx-related emissions play a dominant role [29]. As stated above, SiC is biocompatible and can be of great interest for biomedical applications, in particular if functionalized with specific organic molecules and photosensitizers, like porphyrins, for example (described later) Such a hybrid inorganic-organic nanosystem can create an active antitumoural device if excited by energetic X-Ray radiation: this deep and penetrating radiation, in fact, is able to activate the green emission of SiC in its cubic phase, which in turn excites phorphyrin (Figure 9).

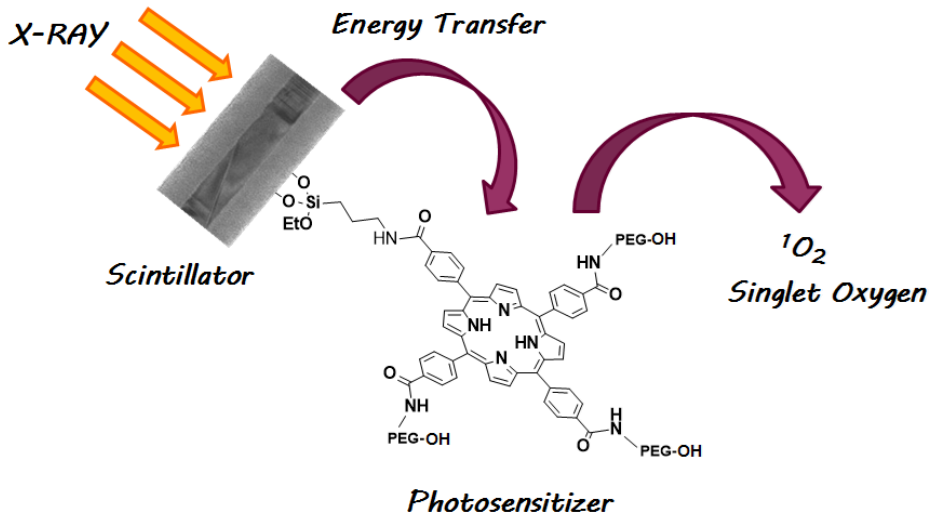

***Figure 9**: Scheme describing the energy transfer process between inorganic donor and organic acceptor: SiC core in nanowires, when exposed to a source of X-ray, is excited, then transfers its excitation to the porphyrin, which, in turns, produces singlet oxygen, a cytotoxic agent.*

In this frame, SiC enhanced fluorescence becomes crucial, since it is responsible for an efficient energy transfer from the inorganic part to the organic molecule. As a result of this process, singlet oxygen is produced: this reactive species is known to be cytotoxic and able to destroy cancerous cells.

3. Porphyrins

Porphyrins are an important class of organic compounds with a characteristic purple colour and a wide variety of application fields: pharmacology, material sciences, biology, catalysis and nanotechnologies are only some of their possible areas of applications.

Porphyrins are macrocyclics formed by four pyrroles linked one to each other with four methine bridges: the overall structure consists of 16 atom rings containing four nitrogen atoms.

These macrocycles contain only sp^2 hybridized bridging meso carbon atoms in their framework and the resulting structure is completely aromatic, with 18 π-electrons and a total number of 22 electrons.

IUPAC nomenclature numbers all carbon atoms in the ring, then all nitrogen atoms, so that the two saturated nitrogens are number 21 and 23. Positions 1,4,6,9,11,14,16 and 19 are named α-pyrrolic, whereas positions 2,3,7,8,12,13,17 and 18 are called β-pyrrolic; positions 5,10,15,20 are named meso (Figure 10).

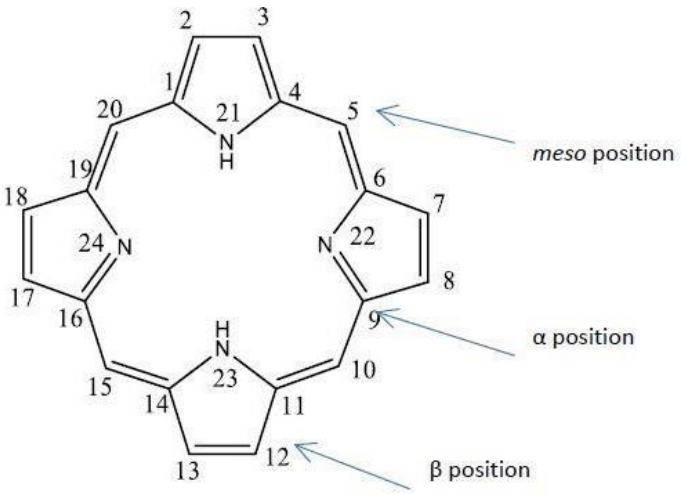

***Figure 10**: Basic structure of porphyrins and nomenclature*

The atoms of alkyl chain substituents are indicated with the number of carbon porphyrin which are linked to, with an apex that represents the number of links away.
NMR analysis, crystallographic and theoretical studies have shown that the forms thermodynamically more favored for symmetrically substituted porphyrins are the two degenerate tautomers *trans* NH. The migration of protons between the two seems to proceed
through a mechanism in stages, though the less favored *cis* tautomer.

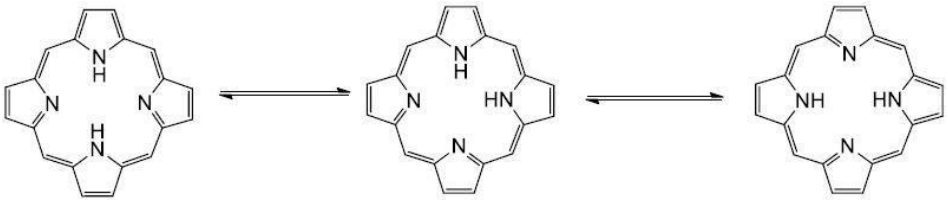

***Figure 11**: Tautomers in porphyrins*

Porphyrins are both naturally occurring (e.g. protoporphyrin IX in heme group) and synthetic compounds: their versatility relies on their intrinsic structure, which can be tailored according to the desired field of application. Naturally occurring porphyrins are synthetized by living systems. Among the best known natural porphyrin-based molecules, there are vitamin B_{12}, chlorophyll and Heme. Heme, the most important porphyrin for human life, is an iron-protoporphyrin complex functionalized in β position, as depicted in *Figure 12*. Protoporphyrin IX, with highly reactive vinyl groups, is the fundamental skeleton of Heme B, and it is present in living systems, since hemoglobin and myoglobin are examples of oxygen transport proteins containing Heme B.

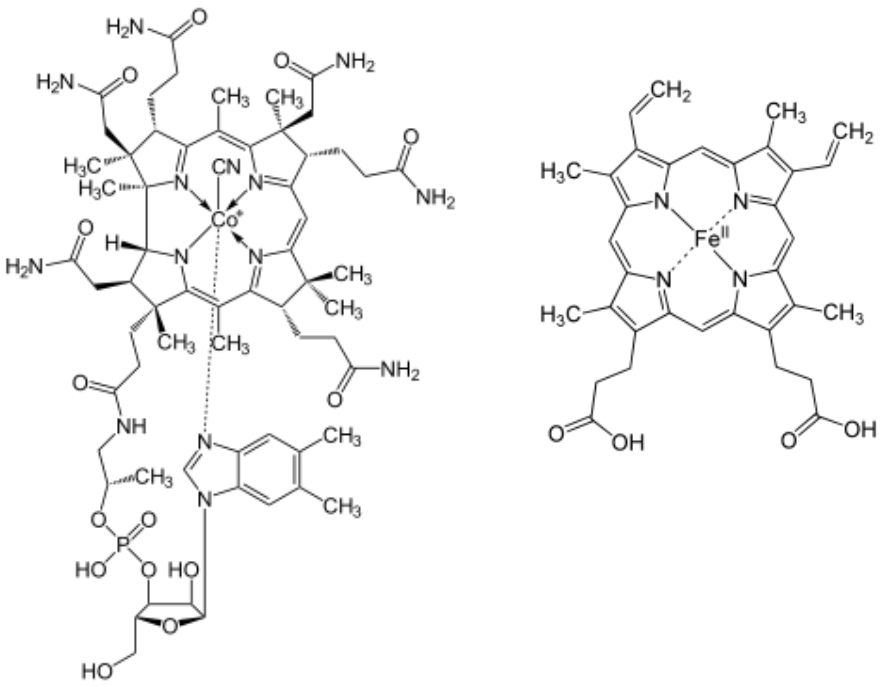

***Figure 12**: Left: Vitamin B12 (Cyanocobalamine); Right: Heme group*

Porphyrins are interesting for many applications: for example, as catalysts in oxidation reactions[30], or in electron transport chains or as a photosensitizer for photodynamic therapy in cancer treatment.[31]
Carboxy-substituted porphyrins are attractive synthetic targets since they are present in many different natural compounds. Moreover, the presence of carboxy groups allows the further functionalization of porphyrins and allows to anchor them on different inorganic surfaces: by so doing, it is possible to obtain hybrid-nanosystems.

By substituting hydrogens in meso positions with other functional groups, more complex porphyrins can be obtained. Depending on the synthesis, the new substituents in meso positions can either be the same or different.

Symmetric porphyrins are more easily synthetized than asymmetrical ones. Their synthesis is based on the condensation of pyrrole and an aldehyde with different reaction conditions (like *Adler-Longo conditions*).
On the other hand, asymmetrical porphyrins are much less synthetically accessible. Their preparation is based on various stepwise approaches (like *Adler-Longo* conditions or 2+2 approach, 3+1 approach and so on).
In all the cases the final addition of an oxidant to obtain the aromatic porphyrin ring is mandatory.
The Linsdey method, which involves pyrrole and aldehydes, is employed for the synthesis of porphyrins with four identical groups in the *meso* positions , and it can be also used for porphyrins having different substituents.
This method consists of mixing an aldehyde and pyrrole in a specific ratio, at room temperature in presence of BF_3*OEt_2, followed by the addition of an oxidizing reagent. If different aldehydes are present, a mixture of various isomeric products is obtained, thus a burdensome chromatography work is required for separation.
A simpler synthesis involves dipyrromethanes units formed by two pyrrole rings linked through a methine bridge. In this case, the synthesis of the macrocycle occurs via [2 + 2] condensation in the same conditions as the Lindsey's method. By employing dipyrromethanes, other intermediates are generated, participating in the condensation [3 + 1] with a fourth unit or other tetrapyrrolic intermediates: these are also useful in the synthesis of asymmetric porphyrins through intramolecular cyclization.

Among the various properties of porphyrins, optical, photochemical (e.g. photosensitizers in photodynamic therapy, catalysts in organic photosynthesis) and supramolecular (e.g. self-assembled systems in nanotechnologies) are noteworthy.
Optical properties of porphyrins are well characterized with absorption and fluorescence spectroscopy in the UV-VIS range. These macrocycles show intense absorption band in the visible region, at 400-500 nm, with a variability that depends on the substituents in meso positions. These intense bands are called B bands or Soret bands: they are due to a S0→S2 transition, from the ground state to the second electronic excited state. At higher wavelengths, between 480 and 650 nm, the so called Q bands can be

observed: these are less intense than the previous one, because they are due to a forbidden transition (according to UV-VIS spectroscopy selection rules). Number and relative intensity of Q-bands are diagnostic to know the symmetry of a porphyrin and the presence of a metal in the porphyrin core.

3.1 Porphyrins and photodynamic therapy

3.1.1 Photodynamic therapy

Photodynamic Therapy (PDT) is a brand-new therapeutic approach in the treatment of different kind of pathologies: cardiovascular, dermatological, ophthalmic. The most important application of PDT, however, is in the oncological field, to treat various kind of both superficial and deep solid tumours, with a curative or palliative approach, depending on the disease stage [32] [33]

Even if the clinical potential of this therapy has been well known for many years, only recently FDA approved the use of PDT for the treatment of oncological diseases[34].

Since then, PDT was employed to treat some kind of tumours, like head and neck, brain, lung, pancreas, intraperitoneal cavity, breast, prostatic and skin cancer[35].

PDT shows a huge number of advantages, if compared to traditional approaches for cancer treatment, like chemotherapy, radiotherapy and surgery[36]: these are a solution, but are massive and highly invasive, thus often damaging involved and nearby organs.

On the other hand, photodynamic therapy is an anticancer treatment with more controllable and finite side effects: it is less invasive and selectively destroys neoplastic tissues, leaving undamaged healthy ones[37]. Then, it can be applied in specific cases, when it is not possible to use surgery or any conventional anticancer treatment

The most important feature of PDT, however, is the photosensitizing agent: the latter, once introduced, selectively accumulates in neoplastic tissues, rather than in healthy ones, for EPR effect (Enhanced Permeation and Retention). This selective accumulation allows to repeat the treatment without remarkable side effects, thus achieving the reduction or complete

destruction of the tumour mass. Furthermore, PDT saves extracellular matrix, thus allowing an easy regeneration of healthy tissues after the treatment[38]: differently from chemotherapy and radiotherapy, which require several weeks or months of treatment, and from surgery, which leads the patient to a prolonged stay, PDT is often an outpatient therapy, and it can also lead to a long-termed control of tumours.

3.1.2 History of PDT

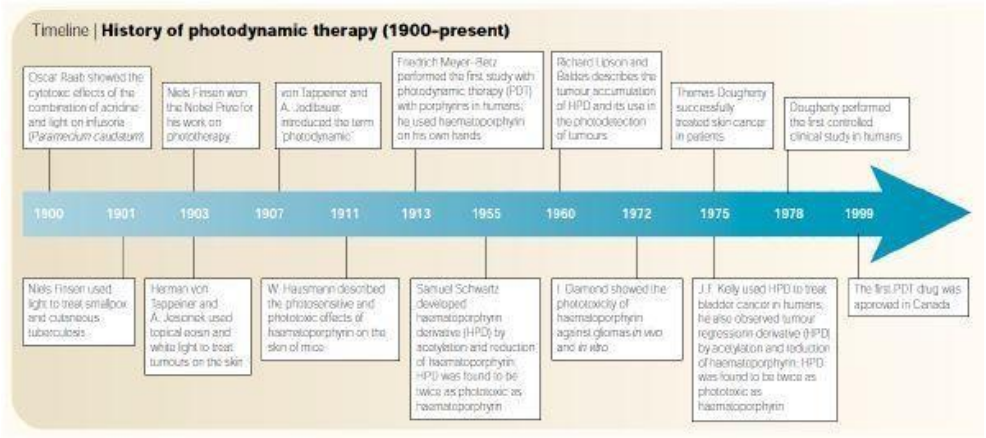

Figure 13: *History of PDT (Dolmans et al., 2003).*

Therapeutical properties of light are being well known for centuries. Ancient civilizations, like Egyptians, or Indian and Chinese, used to employ light for the treatment of a huge number of diseases, like psoriasis, vitiligo and skin tumours. At the end of XIX century, in Denmark, Niels Finsen studied in deep the properties of light and noticed that ultraviolet light was almost mandatory for cutaneous treatment of tubercolosis. For his relevant contribution in the rising field of phototherapy, he won a Nobel prize in 1903.

In the same period, in Germany, professor Von Tappeiner, which was the Director of Pharmacology Department at Monaco University, noticed that params cultures died when exposed to light.

In the following years he showed that cancerous lesions and cutaneous ulcers remarkably reduced, after being treated with acridine and eosin in combination with light of an appropriate wavelength.
Moreover, he showed the fundamental importance of oxygen to activate the mechanism of photodynamic therapy.
However, only in 1907 Von Tappeiner and A. Jobidauer introduced for the first time the term "photodynamic", thus sanctioning its employing in modern age.
The effects of PDT were widely studied in cells and animals and subsequently also in humans. A german physician, Meyer Betz, in 1923 injected himself with 200 mg of hematoporphyrin and registered no ill effects until he exposed himself to sunlight, whereupon for several months he suffered extreme swelling.
In the following years, however, the rising pharmaceutical industry lost interest in photodynamic therapy, for the sudden discovery of antibiotics. The interest in photodynamic therapy for antibacterial purpose grew again in the 50's, when Samuel Schwartz identified HPD (haematoporphyrin derivative), a complex mixture of porphyrin monomers, dimers and oligomers, linked one to each other by ester and ether bonds.
Five years later Richard Lipson and his colleague Baldes showed how HPD was able to be localized in the tumour mass and, above all, could emit fluorescence. The mechanism, however, was very complex and remained largely unknown.
In 1975 Thomas Dougherty and co-workers proved that HPD in combination with a red light was a good strategy to remove mammalian cancer in mice. Furthermore, J.F Kelly and co-workers showed that the same approach was effective also in treating bladder cancer.
For the continuous development of new photosensitizing agents, PDT is nowadays employed in the oncological field to treat lung, esophagus, gastrointestinal, bladder, prostatic, head, neck and skin tumours [39].

3.1.3 Mechanism of PDT action

A PDT-based clinical treatment can be schematically divided into four phases:

- photosensitizer injection
- accumulation in tumour
- activation of the photosensitizer by light and subsequent generation of cytotoxic species
- cellular death

Photodynamic therapy involves administration of a tumor-localizing photosensitizing agent (PS), like a porphyrin or a phtalocyanine, followed by activations of the agent by light of a specific wavelength. This results in a sequence of photochemical and photobiological processes that cause irreversible photodamage in tumor tissues. The overall goal of PDT is intracellular oxidative stress mediated by reactive oxygen species.
The mechanism of action of PDT can be divided into different phases: first of all, a photosensitizer is introduced in human body, intravenously or intraperitoneally, then it distributes into the tissues, thus reaching the ill ones. After that, the photosensitizer is excited with an appropriate radiation, causing chemical and biological damage of cancerous cells and tissue necrosis (Figure 14).

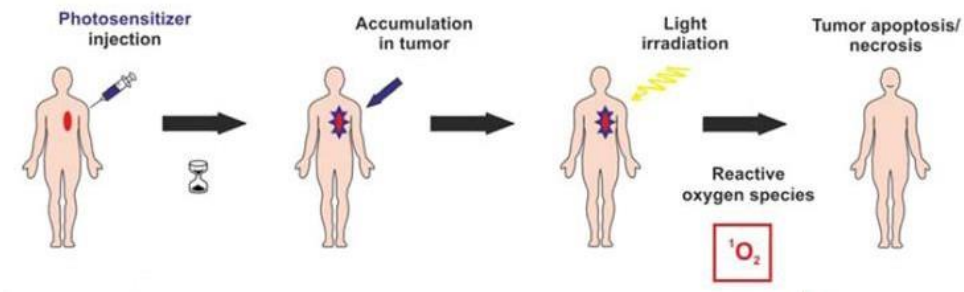

***Figure 14**: Schematic mechanism of how PDT works*

When the photosensitizer absorbs the radiation, it is excited from its singlet ground state (S_0) to one of its singlet excited states (S_n): in a really short time (10^{-12} sec) all the molecules pass from S_n to the first electronic singlet excited state (S_1), according to a process of vibrational relaxation or internal conversion (non-radiative decay). The most likely process, according to Kasha rule, is the emission of a photon with a lower energy with respect to that of the absorbed one: this is what is called fluorescence. Some molecules, like porphyrins, have a specific structure that allows them to undergo a non-radiative decay to a triplet excited state (T_1) with a lower energy with respect to S_1: this process is called intersystem crossing. Triplet state T_1 has a relatively long lifetime (10^{-2} sec) because the transition $T_1 \rightarrow S_0$ is forbidden. At this point, the molecule can decay according to a mechanism of phosphorescence or a non-radiative decay (Figure 15).

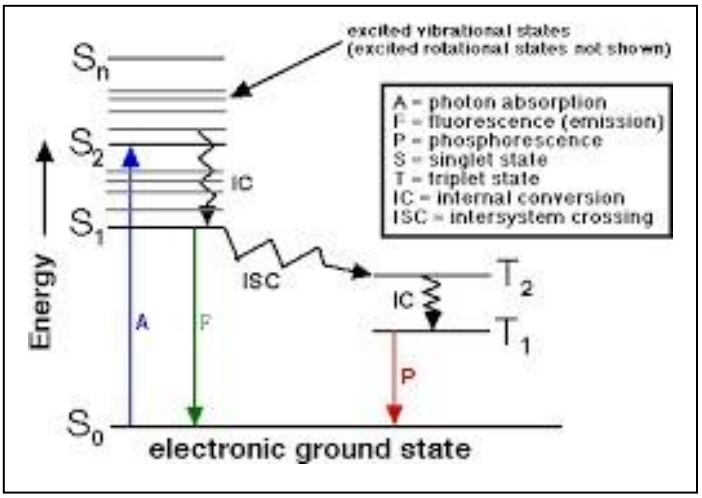

Figure 15*: Possible paths for a photosensitizer after excitation*

Another possible mechanism is an energy transfer process or a photoinduced electron transfer, if a suitable acceptor is nearby.
If the acceptor is a biological substrate (e.g. unsaturated lipids, steroids, aromatic aminoacids), this can undergo an electron transfer process, with the

formation of radicals that can interact with oxygen in tissues, thus generating reactive oxygen species (ROS), like superoxide anion ($\cdot O_{2-}$). These, in turn, can form other reactive species, like H_2O_2 e $\cdot OH$, which can consequently damage cancerous cells, according to what is called *type I reaction*.
In addition, the photosensitizer in its T_1 state can interact directly with molecular oxygen, according to an energy transfer process: molecular oxygen, an inert species in its triplet state ($^3O_2$), is so turned into singlet oxygen ($^1O_2$), a very reactive and cytotoxic species. This other process is named *type II reaction*.
Furthermore, according to type II reaction, the cytotoxic species is restored, thus repeating the process many times.
Singlet oxygen is a strong oxidizing species and can react with a plethora of biomolecules, like proteins and DNA: it causes an irreversible cellular damage, then its death according to apoptosis or necrosis mechanisms.
Singlet oxygen has a very short lifetime in water (1-3 μsec), even shorter in the biological medium (about 100 nsec in lipophilic membrane and 250 nsec in cytoplasm): for this reason it's not likely that it can spread far from the point in which it is generated, thus damaging only this region.

Photodynamic therapy is not employed to treat widespread or not enough localized diseases. Furthermore, since photoactivation occurs only when the photosensitizer is exposed to light, deep solid tumours can't be treated, unless light can deeply penetrate them[40].
Light, in fact, cannot easily penetrate biological tissues, since it can be scattered or absorbed, according to the kind of tissue and to the employed wavelength.
Light absorption is mostly due to the presence of tissutal endogenous chromophores, like hemoglobin, myoglobin and cytocromes [41]. The main photosensitizers employed in PDT have spectral bands in the red zone: this light, in fact, is able to penetrate tissues and allows a good selectivity of the therapeutic process, since is only slightly absorbed by endogenous chromophores. For these reasons, side effects in healthy tissues are minimized.
Red light in the spectrum is the so called "therapeutic window" for its capability of penetrating biological tissues [42].

3.1.4 Biological effects of PDT

The efficiency of PDT is strictly related to the intratumoural localization of photosensitizers.
However, it is also related to other very important parameters: the total dose of light employed to target a specific tissue, the time between drug introduction and irradiation, the degree of tissue oxygenation, the kind of cells involved and, last but not least, the formation of ROS.
PDT can destroy a tumour mass with three main mechanisms: by directly damaging cells, by damaging vascular system and by activating immune response.

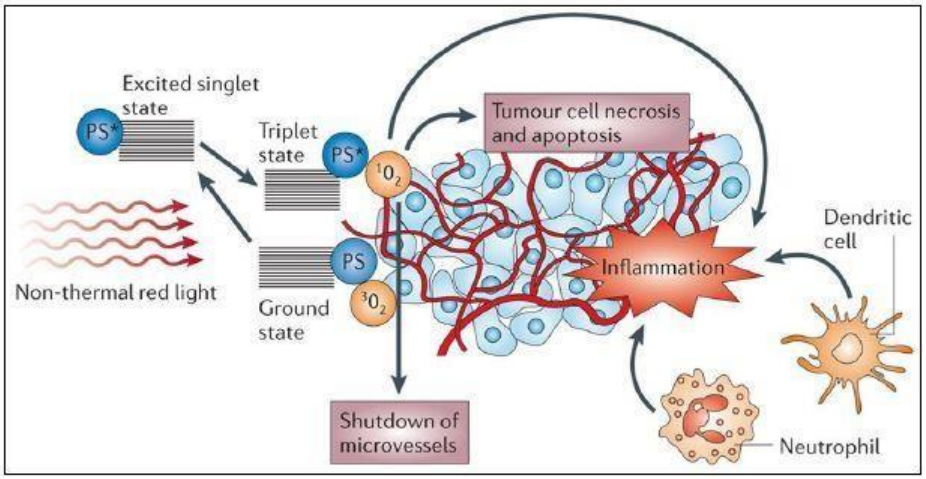

Figure 16: *The mechanism of action on tumours in photodynamic therapy* [43]

Long term control over tumour reduction relies on a synergistic effect due to the combination of the three mechanisms named above, even if the contribution of each single process is still unknown [44].

Direct cellular damage

ROS induced death of tumoural cells can be achieved via necrosis or apoptosis. The latter is not able to completely destroy a tumour mass on its own, since photosensitizer distribution is not homogeneous in a tissue: it lowers while increases the distance from a blood vessel.
In this frame the uptake of a photosensitizer is a fundamental element: if it accumulates in mitochondria or in endoplasmic reticulum it can induce apoptosis. On the other hand, if it is located in membranes or lysosomes, it can impede apoptosis, while favoring necrosis.
The extent of ROS induced oxidative damage confirm the intracellular localization of a photosensitizer, since short lifetime of ROS allows them to spread only for few nanometers [45].
Molecular oxygen has a short range of action, since it cannot spread for more than 0,02 μm; this is an advantage, since it is possible to generate oxidative stress only in target cells, thus leaving healthy tissues undamaged.
The mechanism of cellular death depends on various elements: the targeted cellular line, the injected dose and where the photosensitizer accumulates. Most important factors, however, concern the photosensitizer itself: chemical reactivity, molecular weight, charge, lipophilic and hydrophilic equilibria, aggregation state and its ability to bind proteins [46].
Photodynamic therapy does not lead to mutagenic effects, since most photosensitizers are not likely to damage DNA[47].

Vascular damage

Blood vessels in a tumoural tissue are a difficult issue in antitumoural therapies: first of all they are the main vehicle to spread tumoural cells to other tissues, then they provide neoplastic cells with nutrients and oxygen. Photodynamic therapy causes vascular damages after irradiation: neoplastic tissues can react in the short term, showing an initial vasoconstriction, and in the long term, with the formation of thrombi [48].
Subsequent hypoxia/anoxia in the tissue delays necrosis [49].

Immunitary response

Photodynamic therapy, differently from conventional antitumoural treatments, can stimulate immune response, thus leading to the complete destruction of a tumour mass [43].
Immune response is a consequence of direct cellular damage and inflammatory response. In fact, after irradiation, necrotic and apoptotic cells express proteins attracting macrophages, which in turn expose antigens to T lymphocytes: these migrate towards the tumour to destroy its cells, thus activating the so called cell-mediated immunity. Also leucocytes are involved in this mechanism, but, most important, neutrophil accumulate, that are responsible for tumoural reduction.

3.1.5 Photosensitizers and PDT

A photosensitizer is usually a molecule with usually a polycyclic structure, whose delocalized electrons
favor the absorption of light with a wavelength in the red or near infrared spectral zone.
Designing a good photosensitizer is quite difficult, since it must fulfil some specific and important requirements.
The features of an ideal photosensitizer for PDT are well described in the literature:

- well-defined composition and easily reproducible
- chemical purity and high yield
- low trend to aggregate with other molecules
- high molar extinction coefficient ε
- generation of $^1O_2$ with a high quantum yield (e.g. a ^3T excited state with a relatively long lifetime)
- no toxicity in the dark
- good dispersion in biological medium
- selective accumulation in the tumour

- fast and easy removal from healthy organs

Photosensitizers can be both hydrophilic and hydrophobic: the first ones cannot easily penetrate into cells, whereas the latter do, especially into neoplastic tissues.
Lipophilic photosensitizers, once introduced intravenously, associates with plasmatic lipoproteins, especially with low density lipoproteins (LDL), whose receptors are more overexpressed on tumoural cells membranes, with respect to healthy cells [50]. These receptors favor photosensitizer internalization by endocytosis: here the photosensitizer, once photoactivated, can trigger both apoptotic and necrotic processes [51].
On the other hand, hydrophilic photosensitizers are carried into blood mainly by albumin, but also by other whey proteins, and accumulate into vascular stroma or into interstitial spaces in neoplastic tissues, even if they don't easily spread through plasmatic membrane.
Once irradiated, they can damage the vascular system, causing tumour ischemia and hypoxia for an arterial constriction.
The pH is another important factor in the accumulation of porphyrin-like photosensitizers: a pH decrease, in fact, increases lipophilicity and thus cellular accumulation of porphyrins.
Selective accumulation of porphyrins in tumoral tissues can be achieved with two different strategies: in the active transport mechanism the photosensitizer is conjugated to a selective ligand, which is recognized by an overexpressed receptor.
Passive transport, instead, relies on the difference in permeability and retention between healthy and cancerous cells: the latter, in fact, proliferate fast and continuously, so that they need more cholesterol to synthetize cellular membranes. Furthermore, they overexpress LDL receptors, which are good carriers of lipophilic molecules in the bloodstream, like porphyrins: these compounds are well retained in the tumoural cells, since their membrane is more hydrophobic than that in healthy ones.

In experimental and clinical PDT first generation photosensitizers, like porphyrins, and second generation photosensitizers can be both employed.

Among first generation compounds we can mention Hematoporphyrin (Hp), its derivative (Hpd), *Foscan*® (Temoporfin) and *Photofrin*® (Porfimer sodium): they all have the typical porphyrinic structure, consisting of four pyrroles linked by methine bridges [44].

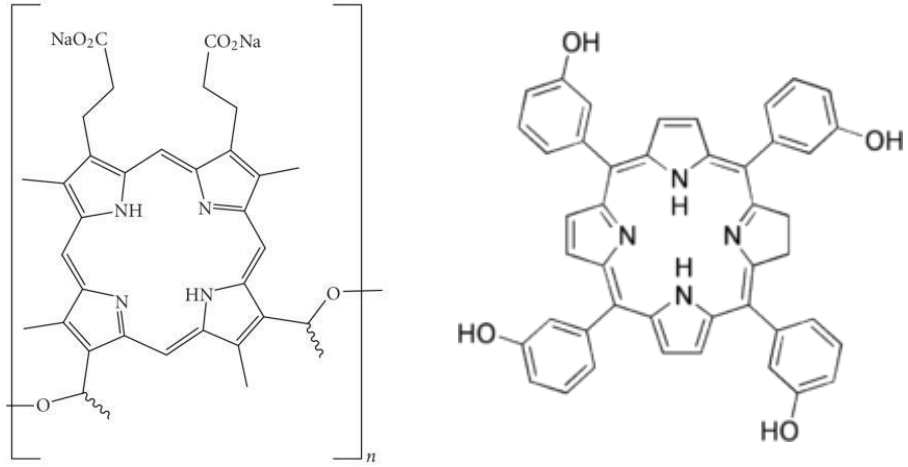

***Figure 17**: Photofrin® (left) and Foscan® (right)*

The latter in 1995 was approved by FDA as photosensitizer for PDT and gained success in treating different kind of tumours, even if it does not fulfil many features proper of an ideal photosensitizer: in fact, *Photofrin*® has a low absorption band at 650 nm, so light of such a wavelength cannot deeply penetrate tissues, thus limiting the treatment only to superficial tumours [52]. Then *Photofrin*® does not consist of a single and well-defined molecule, whereas is a mixture of several components, due to the hydration of C=C double bonds and oligomerization processes. Its administration can lead to a lot of side effects, first of all prolonged light sensitivity (until to 4-6 weeks after the treatment).

To overcome this problems, a new series of molecules, the so called second generation photosensitizers, are now being studied. These molecule have

improved properties with respect to Photofrin: chemical purity, a high molar extinction coefficient in the red zone of spectrum, high absorption peaks at wavelengths greater than 630 nm, to allow a deeper light penetration into tissues [40], and a reduced skin sensitivity to solar light[53].
Some second generation photosensitizers are: tin ethilethiopurpurine (SnET2) and n-aspartil chlorin e6 (Npe6) (Figure 18), both activated with light at 664 nm; phtalocyanines and naphtalocyanines, respectively excited with radiations at 670-680 nm and 750-780 nm; hypericin and benzoporphyrine monoacidic derivative (BPD-MA) excited with light at 689 nm, and aminolevulinc acid (ALA).

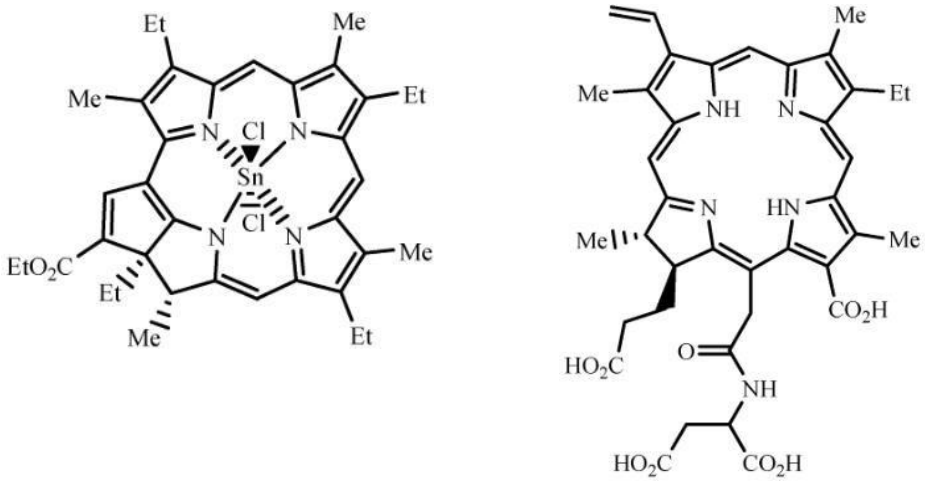

Figure 18: *Left: Tin ethyl ethiopurpurine (SnET2)*
Right: N-aspartil chlorin e6 (Npe6)

3.1.6 Self-lighting photodynamic therapy and BioNiMED project

Traditional photodynamic therapy (PDT), as explained in the previous paragraphs, employs a molecule, named photosensitizer, that is excited by a

radiation in the UV-VIS field. When it undergoes a de-excitation process, it can transfer its energy to a substrate, which can be molecular oxygen.
Therefore, PDT can explicate its cytotoxic effect only with these three elements: photosensitizer agent, light and oxygen. For this reason, treated tissues must be oxygenated and reached by a radiation capable of exciting the photosensitizer: such a radiation is often in the UV or, at least, in the visible field. Radiation with a lower energy (e.g. in the infrared region), instead, are not capable of inducing electronic transitions. Biological tissues, on the contrary, are transparent only in the near infrared (NIR): radiations in this spectral zone, unfortunately, are incapable of exciting a photosensitizer and reaching inner tissues.
Traditional photodynamic therapy employs a laser radiation as excitation source, with a wavelength ranging from 600 to 900 nm: such a radiation is able to excite the photosensitizer, but can't penetrate target tissues deeply: this kind of therapy is useful only for the treatment of superficial tumours. BioNiMED project, on the other hand, aims to develop nanosystems for the treatment of deep solid tumours, diseases that nowadays can't be treated with conventional clinical approaches, like chemotherapy or radiotherapy.
These novel nanosystems are able to generate singlet oxygen, a very reactive and cytotoxic species, after being exposed to a source of X-ray, a deep and penetrating radiation, capable of reaching also inner tissues: this mechanism is the basis of *Self Lighting Photodynamic Therapy* (SLPDT).
In BioNiMED project we are interested in developing hybrid inorganic-organic nanosystems made up of core-shell nanowires covalently linked with various porphyrins.
Core shell nanowires, the inorganic component of our nanosystem, have a special structure consisting of a SiC core in its cubic phase and a shell of silica.
SiC is known to be a biocompatible material, a semiconductor capable of emitting light at 525 nm, when hit by a X-ray radiation. SiOx coating, on the other hand, is functional to increase the emission intensity of SiC at 430-450 nm, a wavelength at which porphyrins absorb light. Furthermore, silica coating is able to widen this emission range and allow an easy functionalization of the nanowire, due to the presence of free hydroxy groups on the surface.
In self lighting photodynamic therapy SiC core in the nanowires is excited with a X-ray radiation and, once excited, de-excites, thus inducing

porphyrin excitation: this process can be described as a radiative or Forster like energy transfer (FRET). In such a mechanism the photosensitizer is not directly excited by an external source, but with an energy transfer process. In this framework the nanowire is said to work as a scintillator.
Using X-ray as an excitation source is advantageous and makes possible to treat also deep solid tumours: this is the aim of *Self Lighting Photodynamic Therapy* and it is what distinguish the latter from traditional PDT, which employs visible laser as light source, thus treating only superficial tumours.

3.2 Important applications of porphyrins in other fields

3.2.1 Porphyrins and energy transfer

Porphyrins are highly versatile organic compounds, since they are useful for many applications: besides their employ in photodynamic therapy, porphyrins are interesting in other fields, as catalysts in oxidation reaction or in electronics, for instance.
Porphyrins show outstanding electronic properties, which make them interesting also for functionalizing electrodes on metal oxides surfaces: electronic devices based on organic-inorganic hybrid systems are now being intensely studied, especially in the field of organic photovoltaic, to turn solar energy into electric one, and in the field of photoelectrochemical cells (DSSC, Dye Sensitized Solar Cells) for water splitting, to turn solar energy into fuel [54].
The specific properties of an electronic device can be tuned according to the functionalization. For example TiO_2, ZnO, SnO_2 and other hybrid oxides metal surfaces can be functionalized with photosensitizers like porphyrins or phtalocyanines attached through carboxy or phosphonic acid groups.

Porphyrins and related materials show a number of intrinsic features that render their use interesting in organic photovoltaic. They have strong absorption (high extinction coefficients ε, allowing reduction of the active layer thickness and thereby reducing charge transport losses) in both the blue (Soret or B-band) and red (Q-bands) part of the visible spectrum, high (thermal) stability and their photo- and electrochemistry can readily be adapted through functionalization of the periphery (*meso* and β-positions) and variation of the metal center. The large structural degree of freedom also allows optimization of the processability (from solution) and the interactions with the electron acceptor component.
Recently, it was demonstrated that the efficiency of an energy transfer process largely relies in orientation and distance between electron donor and electron acceptor: the efficiency of this process, in fact, depends on how fast is holehopping between adjacent chromophores and on how fast is holes recombination. Moreover, the presence of a metal showed an improvement in the electron transmission from the porphyrin to the electron withdrawing acceptor.

Despite these intrinsic benefits, porphyrinoid materials have remained underexposed in the organic photovoltaic domain, in particular in comparison with their phthalocyanine cousins. A remarkable exception is the field of dye-sensitized solar cells (DSSCs), in which specifically designed porphyrin photosensitizers recently afforded top efficiencies, outperforming the classical Ru-based dyes.

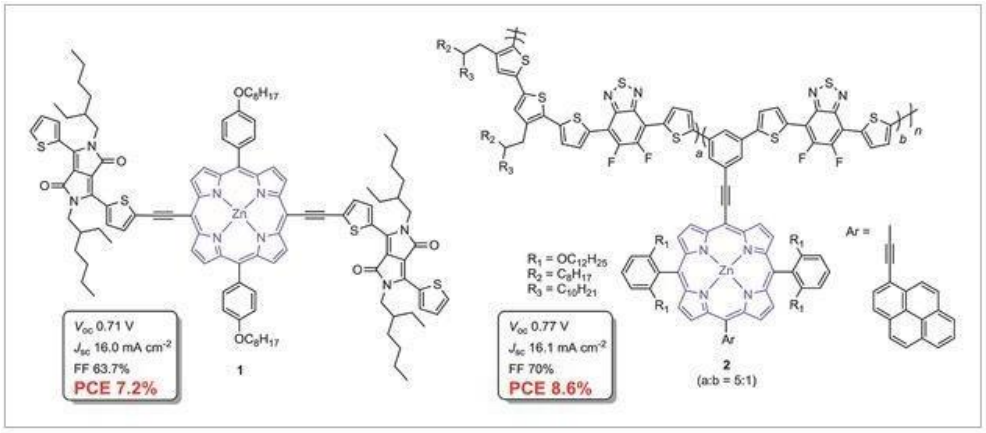

***Figure 19**: Porphyrin-based small molecule (left) and polymer material (right) currently showing highest efficiencies in BHJ OSCs, with their respective I-V parameters*

The intense absorption bands in the visible region, versatile modifications of their core, and facile tuning of the electronic structure make attractive the porphyrin application in the field of Dye Sensitized Solar Cells (DSSCs).
Dye-sensitized solar cells (DSSCs) have drawn much attention as an alternative to silicon-based solar cells because of their low-cost production and high power conversion efficiency (η).
The typical DSSC consists of a dye-sensitized photoanode (TiO_2) and a platinum counter electrode sandwiching an electrolyte that contains a redox mediator.

The efficiency of DSSCs strongly relies on sensitizers. Ruthenium complexes, such as N3 and N719, are the best known photosensitizers employed in this field, as well as the most efficient, showing more than a power conversion efficiency (η) of 11%.
However, the high cost of ruthenium prevented their widespread application. In this frame, it seemed convenient to shine light on organic dyes with no metal or inexpensive metal complexes: these compounds are nowadays being intensively explored, owing to their potential low-cost production and easy tailoring of their structure and basic properties including HOMO−LUMO levels and absorption profiles.
A wide variety of organic dyes exhibiting a relatively high cell performance have been reported so far.
Recently, a series of meso-tetraphenylporphyrins with a β-oligoalkenyl anchoring group were synthetized and employed in DSSCs, showing an η-value of 5.6%.
Furthermore, in 2007 it was noticed that a Zn-1-based DSSC showed a higher η-value of 7.0%.

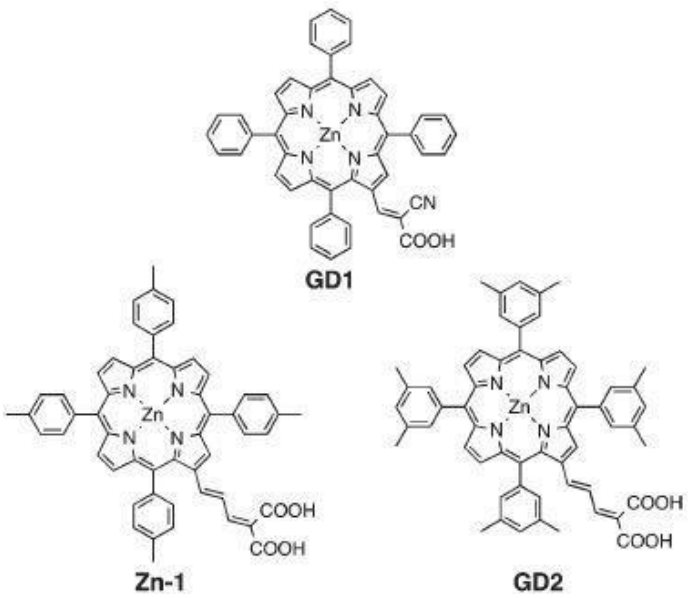

Figure 20: *β-functionalized porphyrin sensitizers*

In the following years, various porphyrins characterized by a push–pull structure and/or π-conjugated elongation have been synthesized.
Furthermore, it was noticed that porphyrins anchoring by phosphonic acid groups turned out to be one of the most efficient in the field of photoelectrochemical cells. Phosphonic groups can be introduced in various positions on the macrocycle: on β-positions, on phenyl rings, when present, or in meso positions.
The orientation of a sensitizer on TiO_2 surface in a DSSC can vary according to the positions of its substituents: thus, it is very important to introduce substituents in convenient positions on a porphyrin. Since energy transfer (ET) rates are a function of electronic coupling between the adsorbed dye and the TiO_2 surface, the cell performance is influenced by adsorption structures of the dye on TiO_2.
D'Souza et al. studied how the effect of dye-orientation on TiO_2 could affect the photovoltaic properties in meso-carboxyphenylporphyrins in which the carboxy group was attached to the para, meta or ortho position [54].
The cell performance was reduced by varying the substituents positions from para to ortho, which reflects the faster charge recombination.
Furthermore, it was noticed that the presence of a metal in the porphyrin core was able to optimize electron transmission from the porphyrin to the electron withdrawing acceptor.

3.2.2 Porphyrin and photocatalysis

A completely different field of porphyrin application is photocatalysis.
A wide variety of inorganic-and organic-based structures are emerging as new building blocks to construct photocatalytic systems [55]. However, if compared to inorganic compounds, the organic counterparts present numerous advantages, due to their good flexibility in molecular design, excellent tunability of the optoelectronic properties and their good solution processability. Among the various organic building blocks, porphyrins are of great interest for their outstanding photophysical, photochemical, electrochemical and structural properties.

Porphyrins, as already described, are macrocycles of particular importance owing to their 18-π-electron aromatic structure, which is responsible for some of their stunning features: small singlet−triplet splitting, high quantum yield for intersystem crossing, and long triplet state lifetime: these properties make them perfectly suited for being robust electron mediators. Upon light irradiation, in fact, porphyrins can absorb photons, and, once in the excited state, they are able to transfer energy (photosensitization) or electrons (photoredox catalysis).
The advantage of a porphyrin catalyst is that its efficiency can be optimized by varying substituents at the periphery of the macrocycle at both the β and meso positions.
This allows to tune optical and electrochemical properties of the catalyst and thus its catalytic activity.
Metalloporphyrins are nowadays being widely studied as bioinspired models of cytochrome P-450 (hemoproteins), which in nature catalyzes the aliphatic C−H hydroxylation reaction.
Other reactions of interest include amination, alkylation, olefin epoxidation, cyclopropanation, olefination, oxidative amine coupling, oxidative Mannich reaction, Diels−Alder reactions, and functional group transformations.

Metalloporphyrins are well known in the literature, as artificial photosynthesis models and enzyme mimics, as well as in catalyzing chemical reactions.
It was noticed that, in catalytic C–H oxidation reactions, metalloporphyrins with no substituents on their meso positions are not useful because they undergo fast oxidative degradation. The degradation process (the catalase reaction) leads to hydroxylation at the meso position, followed by other processes that occur in natural heme degradation, to form meso-hydroxyporphyrin derivatives which then inhibit the catalytic activity.
Therefore, it has been proved that the introduction of phenyl or related groups at the meso positions is mandatory to achieve efficient catalytic oxidations.
Free base porphyrins, instead, are well-known as photosensitizers to generate singlet oxygen: upon irradiation, porphyrins are excited to a singlet state, then they can undergo ISC to produce a triplet state, and, by means of an energy transfer process, singlet oxygen is formed or reactive oxygen species are generated.

This process is at the base of Photodynamic Therapy, as described in paragraph 3.1.1, but it is also important in the catalytic domain: using this methodology various compounds including olefins, aromatic compounds, amines, enamines, and aldehydes can be oxidized.
For example, Nagata and co-workers reported photooxidation of alcohols to aldehydes via photoinduced electron transfer from a porphyrin (free base or zinc) to the quinone.
Moreover, free base porphyrins are able to catalyze photooxidative hydroxylation of arylboronic acids.
Recently, it was reported that free-base porphyrins bearing phenyl groups on meso positions were able to promote α-alkylation of different aldehydes reacting with diazocompounds [56].

References

[1] E. Drexler and C. Peterson, "Unbounding the future-The Nanotechnology Revolution", **1991**

[2] V. Wagner, A. Dullaart, A.-K. Bock, and A. Zweck, "The emerging nanomedicine landscape", *Nat. Biotechnol., 24* (10), pp. 1211–1217, **2006**

[3] A. Kumar, F. Chen, A. Mozhi, X. Zhang, Y. Zhao, X. Xue, Y. Hao, X. Zhang, P. C. Wang, and X.-J. Liang, "Innovative pharmaceutical development based on unique properties of nanoscale delivery formulation", *Nanoscale, 5*, (18), pp. 8307–8325, **2013**

[4] J. Evans, "Five big ideas for nanotechnology", *Nat. Med., 15*, (4), p. 348, **2009**

[5] V. Sanna, N. Pala, and M. Sechi, "Targeted therapy using nanotechnology: focus on cancer", *Int. J. Nanomedicine, 9*, pp. 467–483, **2014**

[6] F. Rossi, E. Bedogni, F. Bigi, T. Rimoldi, L. Cristofolini, S. Pinelli, R. Alinovi, and M. Negri, "Porphyrin conjugated SiC/SiOx nanowires for X-ray-excited photodynamic therapy", *Sci. Rep., 5*, p. 7606, **2015**

[7] L. K. Bogart, G. Pourroy, C. J. Murphy, V. Puntes, T. Pellegrino, D. Rosenblum, D. Peer, and R. Lévy, "Nanoparticles for imaging, sensing, and therapeutic intervention", *ACS Nano, 8*, (4), pp. 3107-3122, **2014**

[8] M. J. Dalby and M. J. Biggs, "Special focus on nanoscale regeneration," *Nanomedicine, 10,* (5), pp. 677-680, **2015**

[9] F. Patolsky and C. Lieber, "Nanowire nanosensors", *Mater. Today, 8* (4), pp. 20-28, **2005**

[10] http://www.nano.gov/nanotech-101/what/nano-size

[11] Charles R M., "Welcome to Nanomedicine", *Nanomedicine, 1* (1), p. 5, **2006**

[12] K. H. Miller, J. Kulkarni, M. Motskin, A. Goode, P. Winship, J. N. Skepper, M. P. Ryan, and A. E. Porter, "pH-Dependent Toxicity of High Aspect Ratio ZnO Nanowires Due to Intracellular Dissolution", *ACS Nano, 4* (11), pp. 6767–6779, **2010**

[13] E.J. Park, G.H. Lee, H.W. Shim, J.H. Kim, M.H. Cho, and D.W. Kim, "Comparison of toxicity of different nanorod-type TiO_2 polymorphs in vivo and in vitro", *J. Appl. Toxicol., 34* (4), pp. 357-366, **2014**.

[14] A. Magrez, L. Horváth, R. Smajda, V. Salicio, N. Pasquier, L. Forró, and B. Schwaller, "Cellular toxicity of TiO_2-based nanofilaments.," *ACS Nano, 3* (8), pp. 2274–2280, **2009**

[15] J. Lee, B. S. Kang, B. Hicks, T. F. Chancellor Jr., B. H. Chu, H.-T. Wang, B. G. Keselowsky, F. Ren, and T. P. Lele, "The control of cell adhesion and viability by zinc oxide nanorods", *Biomaterials, 29* (27), pp. 3743-3749, **2008**

[16] S.H. Monnink, A.J. Van Boven, H.O. Peels, I . Tigchelaar, P.J. De Kam, H.J. Crijns and W. Van Oeveren, "Silicon-carbide coated coronary stents have low platelet and leukocyte adhesion during platelet activation" *J. Investig. Med., 47* (6), pp. 304–310, **1999**

[17] X. Li, X. Wang, R. Bondokov, J. Morris, Y.H. An and T.S. Sudarshan, "Micro/nanoscale mechanical and tribological characterization of SiC for orthopedic applications", *J. Biomed. Mater. Res. B. Appl. Biomater. 72* (2), pp. 353–361, **2005**

[18] M. Katsuno, N. Ohtani, J. Takahashi, H. Yashiro and M. Kanaya, "Mechanism of Molten KOH Etching of SiC Single Crystals: Comparative Study with Thermal Oxidation" *Jpn. J. Appl. Phys., 38* (8), pp. 4661–4665, **1999**

[19] S.E. Saddow, "Silicon Carbide Materials for Biomedical Applications" *Silicon Carbide Biotechnology* (Elsevier Inc.) pp. 1–15, **2012**

[20] J.B. Casady and R.W. Johnson, "Status of silicon carbide (SiC) as a wide-bandgap semiconductor for high-temperature applications: A review" *Solid. State. Electron., 39* (10), pp. 1409–1422, **1996**

[21] P. Colombo, E. Bernardo and L. Biasetto, "Novel Microcellular Ceramics from a Silicone Resin" *J. Am. Ceram. Soc., 87* (1), pp. 152–154, **2004**

[22] P. Du, X. Wang, I.K. Lin and X. Zhang, "Effects of composition and thermal annealing on the mechanical properties of silicon oxycarbide films", *Sensors and Actuators, A:Phys., 176*, pp. 90-98, **2012**

[23] A. Tamayo, J. Rubio, F. Rubio, J.L. Oteo and R. Riedel, "Texture and micronanostructure of porous silicon oxycarbide glasses prepared from hybrid materials aged in different solvents" *J. Eur. Ceram. Soc., 31* (9), pp. 1791–1801, **2011**

[24] S. Onclin, B.J. Ravoo and D.N. Reinhoudt, "Engineering silicon oxide surfaces using self-assembled monolayers". *Angew. Chem. Int. Ed. Engl. 44*, pp. 6282–6304, **2005**

[25] F. Fabbri, F. Rossi, M. Melucci, I. Manet, G. Attolini, L. Favaretto, M. Zambianchi and G. Salviati, "Optical properties of hybrid T_3Pyr/SiO_2/3C-SiC nanowires". *Nanoscale Res. Lett, 7: 680*, **2012**

[26] F. Rossi, E. Bedogni, F. Bigi, T. Rimoldi, L. Cristofolini, S. Pinelli, R. Alinovi and M. Negri
"Porphyrin conjugated SiC/SiOx nanowires for X-ray-excited photodynamic Therapy" *Sci. Rep. 5: 7606*, pp. 1–6, **2015**

[27] S.E. Saddow, "Silicon Carbide Materials for Biomedical

Applications", *Silicon Carbide Biotechnology (Elsevier Inc.),* pp 311-316, **2012**

[28] F. Fabbri, F. Rossi, G. Attolini, G. Salviati, S. Iannotta, L. Aversa, R. Verucchi, M.V. Nardi, N. Fukata, B. Dierre, T. Sekiguchi. "Enhancement of the core near-band-edge emission induced by an amorphous shell in coaxial one-dimensional nanostructure: the case of SiC/SiO_2 core/shell self-organized nanowires". *Nanotechnology*, *21* (34), **2010**.

[29] F. Fabbri, F. Rossi, G. Attolini, G. Salviati, B. Dierre, T. Sekiguchi, N. Fukata "Luminescence properties of SiC/SiO_2 core–shell nanowires with different radial structure". *Mater Lett, 71*, pp. 137-140, **2012**

[30] D. Dolphin, T.G. Traylor, L.Y. Xi "Polyhaloporphyrins: unusual ligands for metals and metal-catalyzed oxydations", *Acc. Chem. Res.*, *30* (6), pp. 251-259, **1997**

[31] A) R. Bonnett. "Photosensitizers of the porphyrin and phtalocyanine series for photodynamic therapy", *Chem. Soc. Rev., vol 24*, (1), pp. 19-33, **1995**; B) O. Gaud, R. Granet, M. Kaouadji, P. Krausz, J. C. Blais, G. Bolbach. "Synthesis and structural analysis of novel glycosylated meso-arylporphyrins for application to cancer phototherapy", *Canadian Journal of Chemistry, vol. 74,* (4), pp. 481-499, **1996**; C) K. Driaf, R. Granet, P. Krausz, M. Kaouadji, F. Thomasson, A. J. Chulia, B. Verneuil, M. Spiro, J. C. Blais, G. Bolbach, "Synthesis of glycosylated cationic porphyrins as potential agents in photodynamic therapy", *Can. J. Chem., 74* (8), pp. 1550-1563, **1996**

[32] D.K. Chatterjee, L.S. Fong, Y. Zhang, "Nanoparticles in photodynamic therapy: An emerging paradigm", *Adv. Drug Deliv. Rev. 60* (15), 1627-1637**, 2008**

[33] T. J. Dougherty, C. J. Gomer, B. W. Henderson, G. Jori, D. Kessel, M. Korbelik, J. Moan, Q. Peng, "Photodynamic therapy", *J. Natl. Cancer Inst., 90* (12), pp. 889-905, 1998

[34] D. Russel & J. Gavrilovic, "Intracellular photodynamic therapy with

photosensitizer-nanoparticle conjugates: cancer therapy using a “Trojan horse”, *Photochem. Photobiol. Sci., 5* (8), pp. 727- 734, 2006,.

[35] D.E.J.G.J. Dolmans, A. Kadambi, J.S. Hill, C.A. Waters, B.C. Robinson, J.P. Walker, D. Fukumura, R.K. Jain, “Vascular accumulation of a novel photosensitizer, MV6401, causes selective thrombosis in tumor vessels after photodynamic therapy”, *Cancer Res., 62* (7), pp. 2151-2156, **2002**

[36] M. Zeisser-Labouèbe, A. Vargas, F. Delie, “Nanoparticles for Photodynamic Therapy of Cancer”, *Nanomaterial for Cancer Therapy*, Challa Kumar Ed., pp. 40-86, **2007**

[37] W.M. Sharman, C.M. Allen, J.E. Van Lier, “Photodynamic therapeutics: basic principles and clinical applications”, *Drug. Discov. Today, 4* (11), pp. 507-517, **1999**

[38] W.E. Grant, P.M. Speight, C. Hopper, S.G. Bown, “Photodynamic therapy: an effective, but non-selective treatment for superficial cancers of the oral cavity”, *Int. J. Cancer, 71* (6), pp. 937-942, **1997**

[39] Zhang, Tang Liu, Zhihong Li, Xiangsheng Zhang, “Progress of photodynamic therapy applications in the treatment of musculoskeletal sarcoma”, *Oncol. Lett., 8* (4), pp. 1403–1408, **2014**

[40] G. Palumbo, “Photodynamic therapy and cancer: a brief sightseeing tour” *Expert Opin. Drug Deliv., 4* (2), pp. 131-148, **2007**

[41] A. Juzeniene & J. Moan, “The history of PDT in Norway. Part oneidentification of basic mechanisms of general PDT”, *Photodiag. Photodyn. Ther., 4*, pp. 3-11, **2007**

[42] L.O. Svaasand, E. Martinelli, C.G. Gomer, A.E. Profio, “Optical characteristics of intraocular tumours in the visible and near-infrared” *Photodynamic Therapy: Mechanisms II (1 July 1990)*, Proceedings Volume 1203 *SPIE*, OE/LASE '90, 1990, Los Angeles, CA, United States

[43] A. P. Castano, P. Mroz, M.R. Hamblin, "Photodynamic therapy and anti-tumour immunity", *Nat. Rev. Cancer, 6* (7), pp. 535-545, **2006**

[44] D. E. J. G. J. Dolmans, D. Fukumura, R. K. Jain, "Photodynamic therapy for cancer", *Nat. Rev. Cancer, 3* (5), pp. 380-387, **2003**

[45] Q. Peng, J. Moan, J.M. Nesland, "Correlation of subcellular and intratumoral photosensitizer localization with ultrastructural features after photodynamic therapy" *Ultrastruct. Pathol. 20* (2), pp. 109-129, **1996**

[46] B. C. Wilson, M. Olivo, G. Singh, "Subcellular localization of Photofrin and aminolevulinic acid and photodynamic cross-resistance in vitro in radiation-induced fibrosarcoma cells sensitive or resistant to Photofrin-mediated photodynamic therapy", *Photochem. Photobiol., 65* (1), 166-176, **1997**

[47] T. J. Dougherty, C. J. Gomer, B. W. Henderson, G. Jori, D. Kessel, M. Korbelik, J. Moan, Q. Peng, "Photodynamic therapy", *J. Natl. Cancer Inst., 90* (12), pp. 889-905, **1998**

[48] D.E.J.G.J. Dolmans, A. Kadambi, J.S. Hill, C.A. Waters, B.C. Robinson, J.P. Walker, D. Fukumura, R.K. Jain, "Vascular accumulation of a novel photosensitizer, MV6401, causes selective thrombosis in tumor vessels after photodynamic therapy", *Cancer Res., 62* (7) pp. 2151-2156, **2002**

[49] Q. Chen, H. Chen, F.W. Hetzel, "Tumor oxygenation changes post photodynamic therapy", *Photochem. Photobiol., 63* (1), pp. 128-131, **1996**

[50] B.A. Allison, P.H. Pritchard, J.G. Levy, "Evidence for low- density lipoprotein receptor-mediated uptake of benzoporphyrin derivative", *Br. J. Cancer, 69* (5), pp. 833-839, **1994**

[51] S.I. Zaidi, N.L. Oleinick, M.T. Zaim, H. Mukhtar, "Apoptosis during

photodynamic therapy-induced ablation of RIF-1 tumors in C3H mice: electron microscopic, histopathologic and biochemical avidence" *Photochem. Photobiol., 58* (6), pp. 771-776, **1993**

[52] J.G. Levy, "Photodynamic therapy", *Trends in Biotechnology, 13* (1), 14-18, **1995**

[53] C.J. Gomer, "Preclinical examination of first and second generation photosensitizers used in photodynamic therapy", *Photochem. Photobiol., 54* (6), 1093- 1107, **1991**

[54] A.S. Hart, C.B. KC, H.B. Gobeze, L.R. Sequeira, F. D'Souza, "Porphyrin-sensitized solar cells: effect of carboxyl anchor group orientation on the cell performance", *ACS Appl. Mater. Interfaces, 5* (11), pp. 5314−5323, **2013**

[55] Hsiao-Chu Lin, Gordon A. MacDonald, Yanrong Shi, Nathan W. Polaske, Dominic V. McGrath, Seth R. Marder, Neal R. Armstrong, Erin L. Ratcliff, and S. Scott Saavedra (2015) "Influence of Molecular Orientation on Charge-Transfer Processes at Phthalocyanine/Metal Oxide Interfaces and Relationship to Organic Photovoltaic Performance", *J. Phys. Chem. C, 119* (19), pp. 10304−10313, **2015**

[56] K. Rybicka-Jasinska, W.Shan, K. Zawada, K.M. Kadish, D. Gryko, "Phorphyrins as Photoredox Catalysts: Experimental and Theoretical Studies", *JACS, 138* (47), pp. 15451-15458, **2016**

Chapter 1

Synthesis of novel hybrid nanosystems composed by core-shell SiC/SiO_x nanowires conjugated with porphyrins for X-ray-excited PDT

Introduction

This chapter reports the synthesis of a novel hybrid nanosystem, based on cytocompatible inorganic SiC/SiO_x *core shell* nanowires ($1.8<x<2$) conjugated with an organic photosensitizer, a tetra(4-carboxyphenyl) porphyrin derivative. This idea was first proposed in 2011 by Dott. Salviati in the framework of BioNiMed Project, with the aim of preparing a new tool exploitable in nanomedicine and especially in anticancer therapy of deep tumors: the photosensitizer, in fact, is activated by the emission of the inorganic component under highly energetic X-Ray irradiation.

This kind of process can be well described introducing the concept of **Self Lighted Photodynamic Therapy** (**SLPDT**), which was named for the first time in a paper published in 2006 by Chen and Zhang [1][2]: they described that scintillating nanoparticles can potentially be used to activate a photosensitizer for photodynamic therapy as a promising approach for deep cancer treatment.

As states US-National Cancer Institute, traditional Photodynamic therapy (PDT) is successfully employed to treat superficial tumours (e.g. under the skin or on the lining of internal organs or cavities) through the generation of an active form of oxygen (singlet oxygen) that destroys nearby cancer cells. The limit of traditional PDT arises from its inability to treat deep solid tumours: this is due to the fact that traditional PDT employs a laser radiation to excite the photosensitizer: such a radiation is not penetrating enough to reach inner tissues into human body.

In SLPDT, instead, the light is generated by a scintillator functionalized with photosensitizers when it is irradiated by X-Ray, a deep penetrating radiation. The photosensitizer in the tumor adsorbs the light and produces singlet oxygen, a cytotoxic species [3].

As X-Ray can penetrate through tissues, with this approach also deep tumors can be reached and treated. Previous studies carried out in our lab shed light on the preparation of hybrid nanosystems composed of SiC/SiO_x nanowires conjugated via *click* chemistry, that turned out to be active in in vitro studies. The efficiency of these nanosystems in producing singlet oxygen ($^1O_2$) was tested by exposing the nanowires in water solution to 6 MeV X-Ray in a clinical Linac Varian setup for radiation therapy of Parma Hospital [Dr. Benecchi].

A dish containing the sample solution is put on the couch and irradiated from the bottom, then it is transferred to a spectrophotometer to acquire the fluorescence spectrum of the SOSG marker.

The amount of toxic oxygen that was produced by this nanosystem was revealed by using the SOSG (Singlet Oxygen Sensor Green) kit. This kit shows a green fluorescence activated by interaction with $^1O_2$, showing high selectivity for this species.

Further, a different functionalization approach, via amide bond, was started to be studied, employing derivatives of *tetrakis*(N- carboxylphenyl)porphyrin (H_2TCPP).

Here I describe the preparation of novel hybrid nanosystems based on biocompatible SiC/SiO_x nanowires (NWs) functionalized via amide bond formation with *tetrakis*(N-carboxyphenyl)porphyrin (H_2TCPP). We designed to introduce in the porphyrin moiety also different short PEG chains to increase the dispersion of the nanosystem in the biological medium, with respect to those previously prepared. Two different short PEG chains (with the same length, but ending with different functional groups) were synthetized and bound to the porphyrin, to check an improvement in the dispersion of our nanosystem in the biological medium. Indeed. It is well known that PEG chains are hydrophylic and increase the solubility of a compound in water.

In addition, aiming to increase the thickness of the photosensitizer single layer on the NWs, we designed to link *tetrakis*(N-carboxyphenyl)porphyrin (H_2TCPP) with *tetrakis*(N-aminophenyl)porphyrin with an amide bond, under mild conditions. This was thought to increase the porphyrin loading, so that singlet oxygen production would be increased too. The properties of these novel nanosystems are here presented and discussed.

Synthesis and characterization of a hybrid nanosystem consisting of SiC/SiO_x nanowires conjugated with PEGylated tetrakis(N- carboxyphenyl)porphyrin (H_2TCPP) via amide bond

Core-shell SiC/SiO_x nanowires were grown on silicon substrates with a VPE reactor (1100 °C), from a thin layer of Si(100), CO (g) and an iron catalyst at IMEM CNR. They are composed by a cubic SiC core (~20 nm) covered by an amorphous silica layer (~20 nm).

The 3C-SiC/SiO_x nanowires present an increased optical luminescence, with respect to pure SiC nanowires, that matches well the absorption bands of porphyrins photosensitizers.

The SiO_x shell, in addition, can be easily functionalized with organic molecules as well as with inorganic crystals. Among the various photosensitizers, porphyrins have a well-known application in photodynamic therapy and are also approved by the U.S. Food and Drug Administration. In this work we planned to link porphyrins to the SiC/SiO_x NWs exploiting the formation of covalent amide bonds under mild conditions.

A previous PhD thesis carried out in our lab focused the attention on the conjugation of H_2TCPP porphyrin to the nanowires via alkyne-azide 1,3-dipolar cycloaddition and presented preliminary results on conjugation via amide bond formation.

H_2TCPP porphyrin was chosen as best due to the presence of four identical phenyl rings ending with carboxylic functions on its skeleton: these groups permit the anchorage through more than one linkage and, in addition, can be easily functionalized and turned into other functional groups. In order to conjugate H_2TCPP to the inorganic counterpart, amino groups were previously introduced on the nanowires surface by reacting them with a silane ending with an amino function, 3-(aminopropyl)triethoxysilane (APTES).

Then, the carboxylic groups on H_2TCPP porphyrin were turned into active esters by means of condensing agents: their reaction with N-(3-dimethylaminopropyl)-N'-ethylcarbodimide (EDC) produces an active intermediate (PE), that can further react with 1-hydroxybenzotriazole (HOBt) forming the intermediate PH.

This compound can react directly with an alkyl amine or can form a further intermediate salt with 4-dimethylaminopyridine (DMAP) before reacting with the alkylamine. (*Scheme 1*)

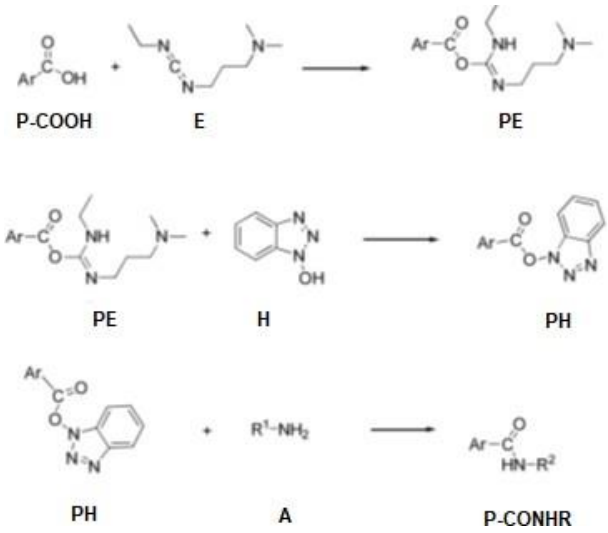

Scheme 1*: Formation of an amide bond in the presence of condensing agents EDC and HOBt*
P-COOH=acid porphyrin; E=1-ethyl-3-(3-dimethylaminopropyl)carbodiimide (EDC); PE=intermediate 1; H=hydroxybenzotriazole (HOBt), PH=intermediate 2; P-CONHR=amide porphyrin

Propargylamine was then chosen as an amine with short chain to react with the remaining active esters on porphyrin H_2TCPP. This nanosystem was prepared under milder conditions with respect to those employed in the thermal Huisgen 1,3-dipolar cycloaddition, previously used in our lab to decorate the NWs by "click" reactions.
The multistep procedure is reported in the following scheme (Scheme 2a and 2b).

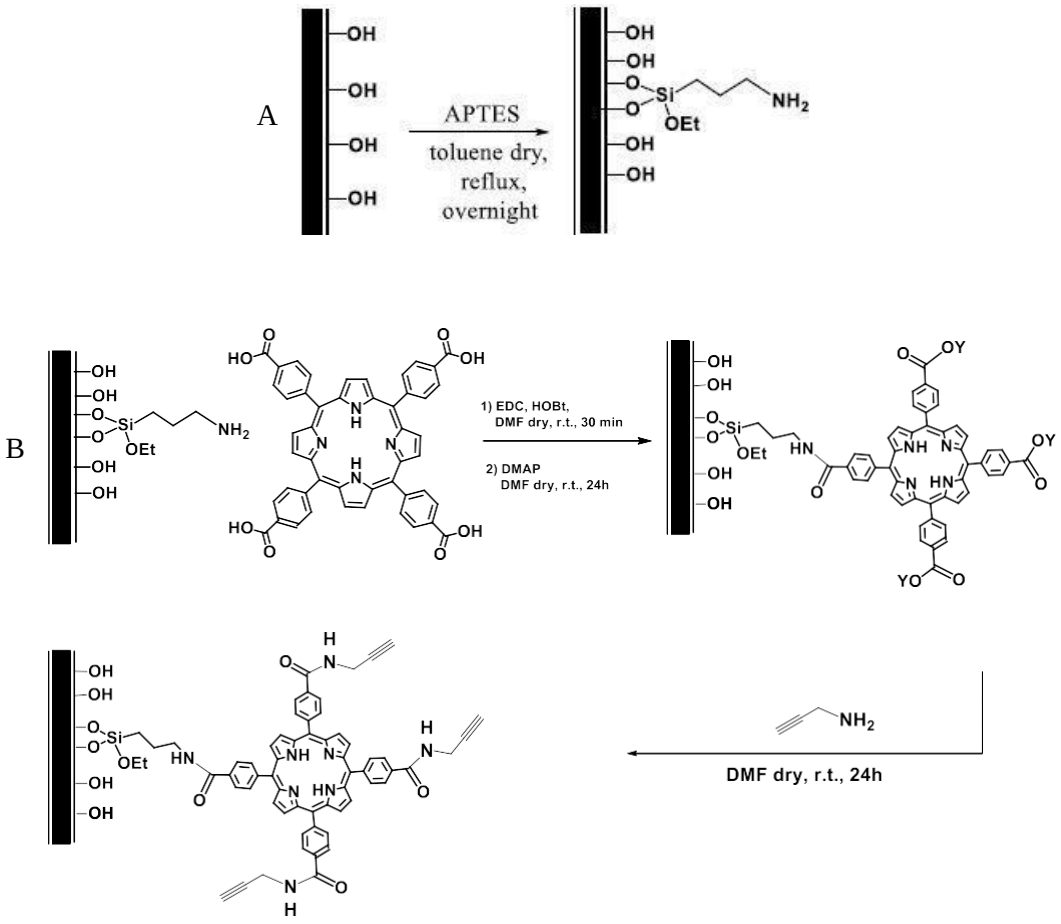

***Scheme 2a and 2b**: Reaction of free hydroxyl groups on silica with 3-(aminopropyl)triethoxysilane (APTES).*

Nanosystem consisting of SiC/SiO_x nanowires functionalized with H_2TCPP porphyrin and propargylamine via amide bonds.

During my PhD work, we planned to introduce short PEG chains, aiming to increase the dispersion of the nanosystem in aqueous medium. Two short amino PEG chains with a similar length but different polarity were synthetized and inserted into the nanosystem, in order to evaluate their effect on the dispersion. Indeed, in the literature it is reported that strong linkages

are preferred for hydrolytically stable conjugates[4] and amide bonds between PEG and photosensitizers are reported to be stable under physiological conditions[5].

In particular, one chain ending with three carboxy acid groups and the other ending with hydroxy groups were prepared.
First, starting from commercially available PEG-6, it was possible to prepare a PEG-6 chain bearing at one side an amino function and at the other side a carboxylic group by a multistep process.

All the reactions involving the nanowires were carried out leaving them on the Si supporting plate where they were grown. The silica shell surface of the nanowires was activated by refluxing the wafers in concentrated HCl for 2 hours: this activation is useful to expose a larger number of free hydroxyl groups on the NWs surface. The sample was then washed with water to neutral pH, then with acetone, and finally dried in the air.
The amino groups were introduced on the nanowire surface by reacting the free hydroxy groups with (3-aminopropyl)triethoxysilane (APTES). This reaction was carried out at reflux in dry toluene, under inert atmosphere of nitrogen to avoid large hydrolysis of the reagent and consequent gelation process. This functionalization with APTES occurs by partial hydrolysis of the ethoxy groups and subsequent condensation with surface hydroxy groups, giving Si-O-Si bond formation with alcohol elimination. The reaction was repeated twice to increase the nanowire coverage, washing the wafer with dry toluene and acetone between the first treatment and the second one. In the third step the carboxy groups on H_2TCPP, previously activated with condensing agents (EDC, HOBt and DMAP), were conjugated to the amino functions on the nanowires, affording the amide bond formation between the two partners.
After this step, the residual carboxy groups on the porphyrin, still in the form of active esters, were reacted with an excess of amino PEG-6 (**Compound 4**). Finally, deprotection of the *tert*-butyl ester with trifluoroacetic acid (TFA) in dichloromethane gave free acid carboxylic functions at the end of the PEG- chains (Scheme 3).

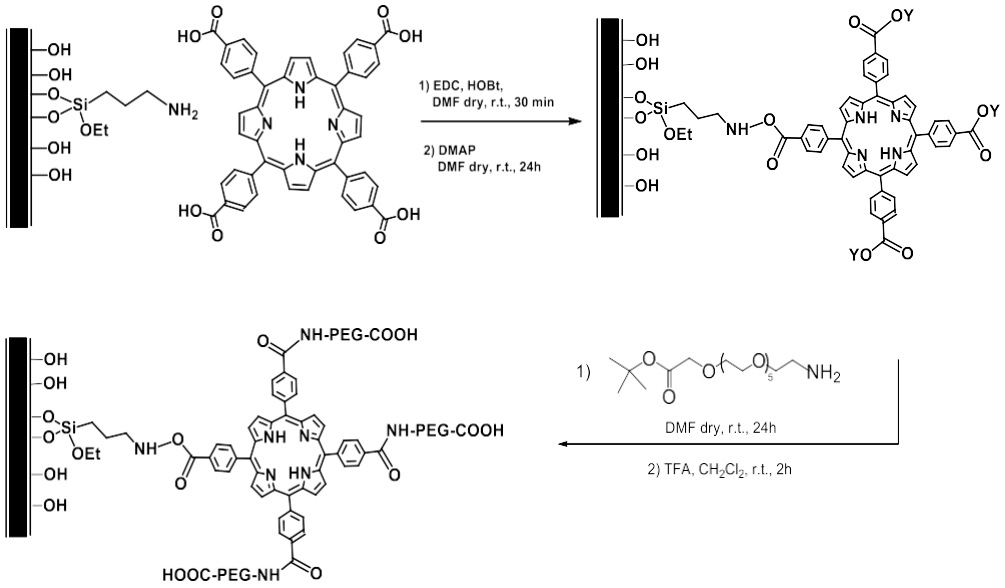

Scheme 3: *Synthesis of a nanosystem consisting of SiC/SiO_x nanowires functionalized with H_2TCPP porphyrin and an amino PEG-6 chain ending with a carboxylic group.*

The hybrid nanosystem was characterized by fluorescence spectroscopy, as can be seen in Figure 1. A laser with a wavelength emission at 473 nm was employed as excitation source. This radiation excites both the nanowires and the porphyrin fluorescence, being completely absorbed by the NWs but only partly absorbed by the porphyrin. As a consequence the observed fluorescence, which has indeed a direct contribution from porphyrin (as it can be deduced by its spectral shape, consisting of the typical $Q_x(0,0)$ and $Q_x(0,1)$ emission bands[6]), must be due to an energy transfer process from the SiC core in the nanowires to the porphyrin. Two possible energy transfer processes can take place:

- a radiative energy transfer, in which the porphyrin absorbs the light emitted by the nanowires, and then it re-emits on her typical Q(0,0) emission [6]
- a Forster resonance energy transfer, in which the nanowires, acting as the donor chromophore, transfer energy to the porphyrin, the acceptor, through non-radiative dipole–dipole coupling [7] [8]

We can instead rule out the hot electrons transfer mechanism from the inorganic NW to the organic molecule, due to the presence of the wide band-gap oxide shell.

This is supposed to be in the form of Foster resonance energy transfer between inorganic donor and organic acceptor.

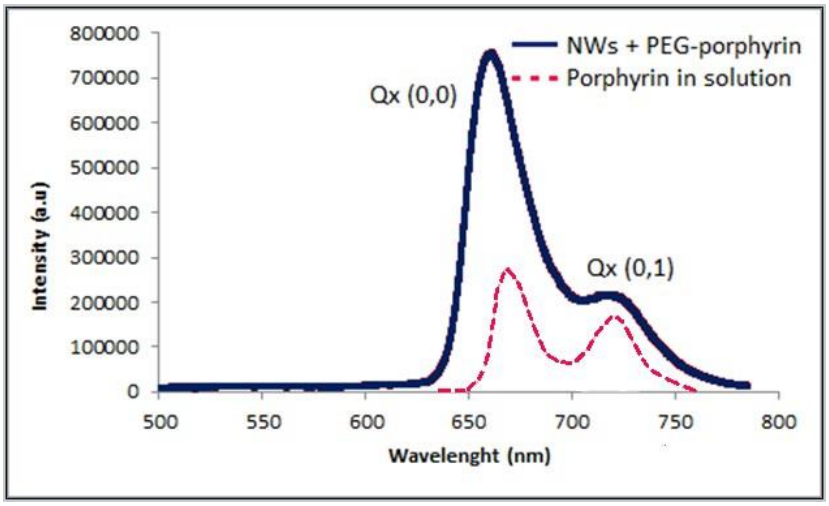

Figure 1: *Fluorescence spectrum of the hybrid nanosystem consisting of SiC/SiO_x nanowires functionalized with H_2TCPP porphyrin and amino-PEG-6 chain (blue line). It is noteworthy that the SiC fluorescence is negligible with respect to the porphyrin fluorescence, due to the high degree of functionalization achieved. Red dashed line shows the fluorescence of free H_2TCPP porphyrin in a DMF solution, to prove that the emission properties of porphyrins in the nanosystem are not altered.*

The emission from bare NWs usually consists of a single large peak centered at λ = 523 nm**,** in excellent agreement with the near band-edge emission (NBE) of 3C-SiC. The spectrum of the hybrid system contains both the signals, due to both the inorganic and organic components. The SiC NBE transition in the hybrid nanosystem is red shifted to 545 nm, as reported by other authors [9], but is negligible with respect to the typical porphyrin fluorescence signals, as can be seen in the figure above

(Figure 1). Nanowires functionalized *via* amide bonds, in fact, show a higher fluorescence intensity than that observed in NWs functionalized with the previously employed 'click' chemistry method (Figure 2). This result is attributed to an increase of porphyrin loading, due to the higher degree of silica shell functionalization with APTES. This result was expected due to the known higher reactivity of alkoxysilane bearing amino groups.

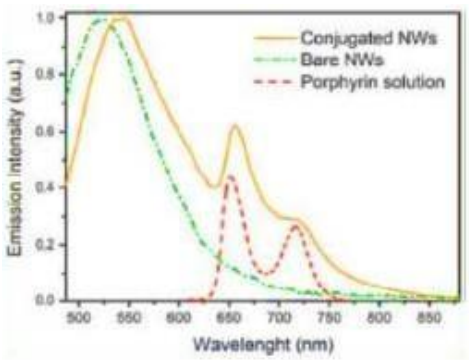

Figure 2: *Fluorescence spectra acquired at room temperature over as-grown NWs (dashed-dotted line) and NW-H_2TPACPP (solid line). The porphyrin emission (red dashed line) is also shown for sake of clarity.*
It is noteworthy that the SiC fluorescence here is not negligible with respect to the porphyrin fluorescence (see yellow solid line). This is due to the lower loading of porphyrin that is achieved in nanowires functionalized with the "click" chemistry approach.

In vitro study on the activity of the hybrid nanosystem

The activity of the prepared nanosystem was studied carrying out in vitro experiments on tumoural cell lines, in particular lung tumoural cell. Thus, clonogenic assays were performed after incubating A549 and IL45 cell lines. A cell biology technique employed to study the activity of specific agents on the survival and proliferation of cells is called clonogenic assay. It is frequently used in cancer research laboratories to evaluate the effect of drugs or radiation on rapidly proliferating tumour cells.[10]

It was developed for the first time by T.T. Puck and Philip I. Marcus at the University of Colorado in 1955.[11]
The word "clonogenic" is related to the fact that these cells are clones of one another.
A clonogenic assay can be divided into three major steps:

1. The treatment is applied to a sample of tumoural cells.
2. The cells are "plated" in a tissue culture vessel and allowed to grow.
3. The colonies produced are fixed, stained, and counted.

At the end of the experiment, the percentage of cells that survived the treatment is measured. A graphical representation of survival *versus* drug concentration or dose of ionizing radiation is called a *cell survival curve*.[12] Another possible graphical representation of surviving fraction of cells is given by histograms. The cells either come from prepared "cell lines," whose general characteristics are known, or from a biopsy of a tumor in a patient.[13] The cells are put in petri dishes or in plates which contain several circular "wells." A specific number of cells are plated according to the kind of experiment; for a radiotherapy experiment it is usual to plate larger numbers of cells with increasing dose of radiation. The treatment is usually a drug, ionizing radiation, or a combination of the two.[14] Nowadays some research works are studying the enhancement of drug effects by concurrent irradiation—a kind of synergistic effect—and in this situation two groups are studied: a control group, which is not treated with the drug; and a treatment group, which is treated with the drug. Both groups are irradiated. If the slopes of their survival curves differ significantly, then an additional effect may be evident and could be studied further.

Human lung adenocarcinoma

A549 cells are adenocarcinomic human alveolar basal epithelial cells. The A549 cell line was first discovered in 1972 by D. J. Giard, et al. by removing and culturing of cancerous lung tissue in the explanted tumor of a 58-year-old caucasian male.[15][16][17] In nature, these cells are normally squamous and responsible for the diffusion of some substances, such as water and electrolytes, across the alveoli of lungs.

These cells are able to synthesize lecithin and contain high level of unsaturated fatty acids, which are crucial to maintain phospholipidic membranes in cells.[15] A549 cell line are widely used as an in vitro model for a type II pulmonary epithelial cell model for drug metabolism and as a transfection host.[18][19]

Malignant pleural mesothelioma

Malignant pleural mesothelioma is an extremely aggressive neoplasia, related to the exposition to asbestos fibers. Even if it is an uncommon tumour, pleural mesothelioma is the most frequent primitive tumour that affects pleura, a thin lubricating membrane that covers lungs and thoracic wall. The importance of this tumour increased in the last few years for the increasing incidence in people exposed to asbestos fibers. It has a long time latency, about 46 years, and a clinical median course of 1-2 years.
This tumour originates into pleura, but can rapidly spread out, thus damaging thoracic wall, abdomen and heart.

In vitro studies

To study the effect of the nanosystem on cells for a possible application in X-ray excited photodynamic therapy, *in vitro* experiments were performed [Prof. Mutti's, Prof. Cacchioli's and Dr. Benecchi's groups]. In particular, adenocarcinoma human alveolar basal epithelial cells were examined. It was already published the cellular uptake of the nanowires as grown[20] as well as of nanowires conjugated with H_2TPAPP via thermal click reaction[21]. In Figure 3 some published SEM and TEM images are reported. In the present study the conjugated nanowires were detached from the support using an ultrasound microtip in ethanol (Misonix Sonicator S4000, 5W) and were recovered from the solvent by ultracentrifugation (14000 Hz).

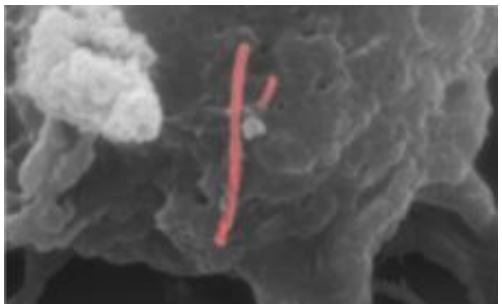

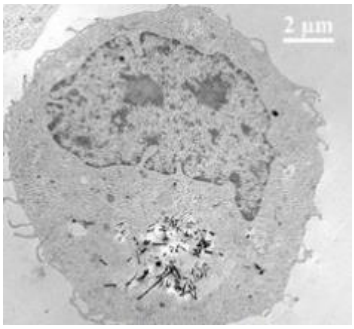

Figure 3: *Left: SEM image showing cellular internalization of as grown nanowires (50 µg/ml for 24 hours) by A549 cells.*[19]

.

Right: TEM image showing the uptake of porphyrinated nanowires (50 µg/ml for 24 hours) by A549 cells. [20]

A549 cells were incubated with H_2TCPP-conjugated NWs and after 24h they were irradiated with 6 MV X-Ray at the dose of 2Gy using the linear accelerator at the Parma Hospital (Figure 4). The dose was chosen accordingly to the standard conditions of clinical radiotherapy (only one session).

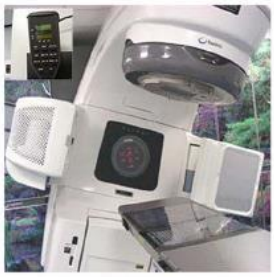

Figure 4:*. Linac Varian DHX @ Parma Hospital*

After that, the clonogenic survival assay was performed. Cells were cultured for 12 days and stained to evaluate the proliferation.

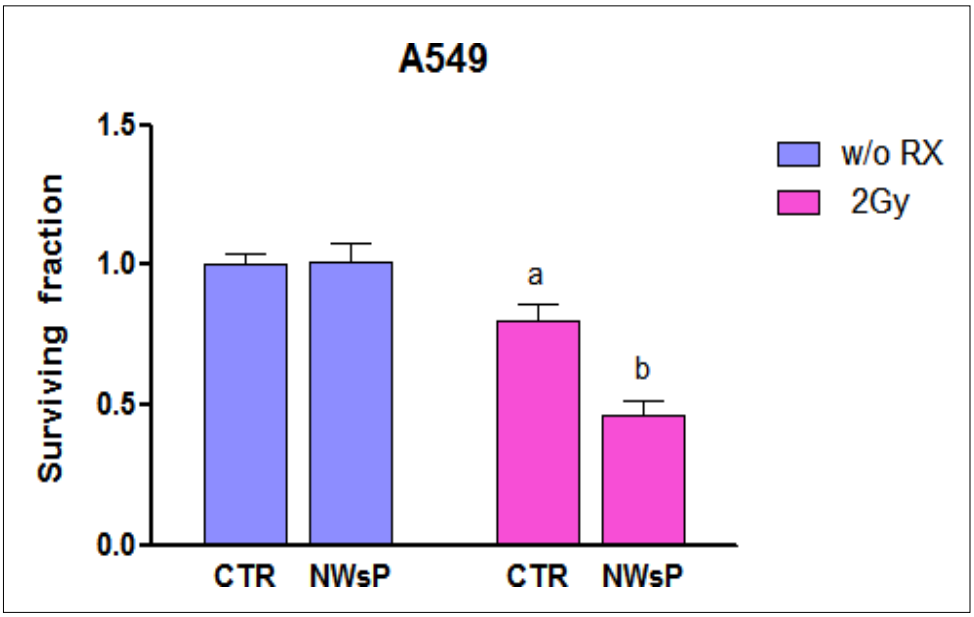

Figure 5: *Clonogenic survival assay of A549 cells treated with nanowires functionalized with PEG_6-COOH-H_2TCPP porphyrin*

The most striking result is that the cell plating efficiency after the radiation treatment is significantly lower for cultures incubated with the NWs than for control cells. Further, the best result is that this effect came from a lower total dose than that it is usually employed in radiotherapy.

This study demonstrates that our novel nanosystem has an additive antiproliferative effect compared to irradiation alone at the selected dose. In addition, the irradiation time used is significantly shorter than that required by traditional radiotherapy. Indeed, the treatment time is usually 40 seconds

or 90 seconds, and it is usually necessary to repeat the treatment several times.

The clonogenic assay was performed also on IL45 Malignant pleural mesothelioma cell line. A lower effect was obtained, but it was not surprising taking into account that this cancer cell line is more resistant, since mesothelioma is a tumor very difficult to treat. Figure 6 shows TEM images of IL45 cells treated with nanowires functionalized with PEGylated H_2TCPP porphyrin, after radiotherapy treatment.

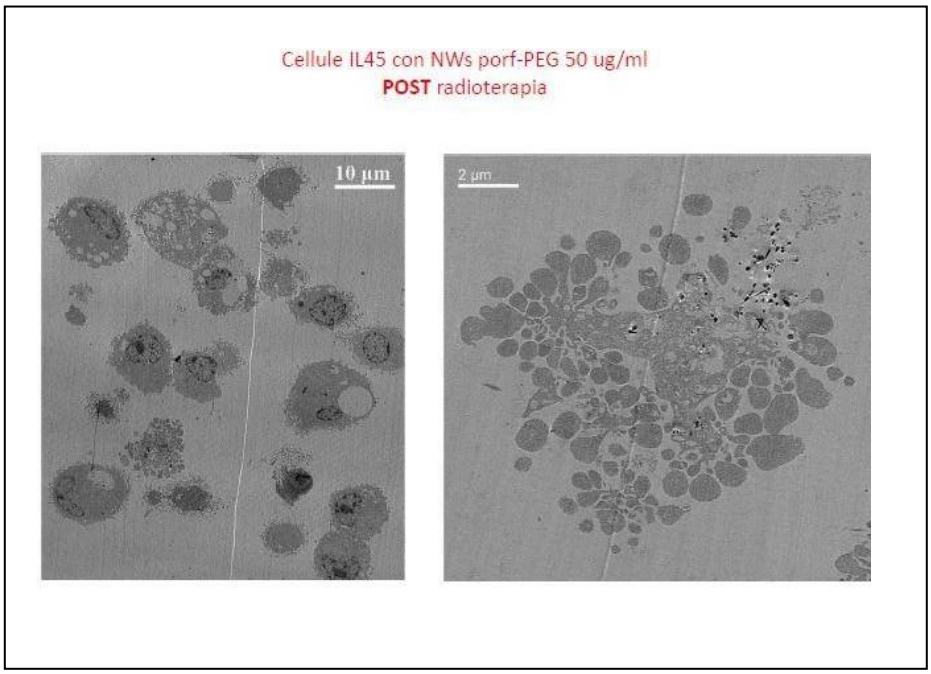

Figure 6: *IL45 cells treated with porphyrinated NWs 50 µg/mL after radiotherapy treatment.*

The present nanosystem, however, shows also some drawbacks, mostly related to its dispersion in the biological medium, which is not the same as in distilled water or physiological solution. As previously stated, we designed to introduce a PEG_6-COOH chain to increase the dispersion in aqueous medium.

During the clonogenic test it was observed the tendency of nanowires to aggregate in the biologic medium where the cells are grown, forming

bundles. This could cause minor uptake due to the minor biological availability. Therefore, we verified this behavior by adding the nanowires to a culture broth. As shown in Figure 7, the formation of bundles was observed in a relatively short time.

We rationalized that the presence of -COOH groups, even if positive for nanosystem dispersion in water, could facilitate the formation of complex salts in the culture broth since the carboxylic acid is partially deprotonated at physiological pH and may interact with the components of the culture broth, which is a complex mixture of salts, amino acids and other organic molecules, to which glutamine and bovine serum albumin (10%) are added.

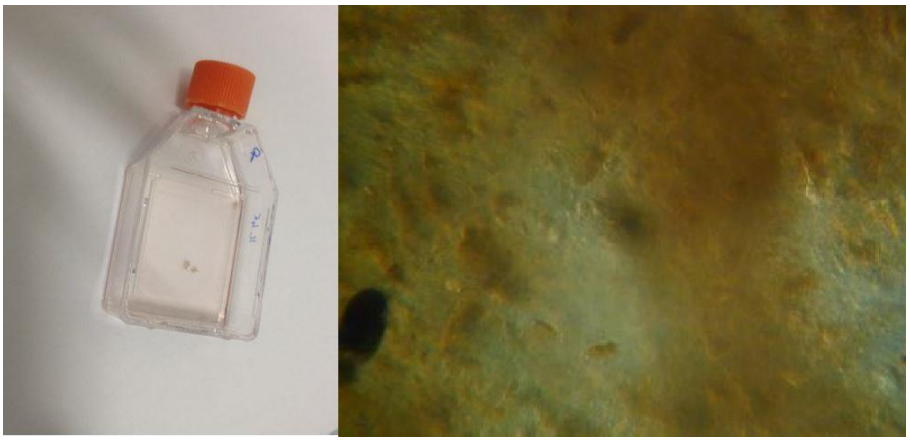

Figure 7*: Left: Nanowires dispersed in a flask containing the culture broth: it is possible to observe the formation of bundles.*
Right: Microscope magnification of the bundles

To overcome this trouble, we planned to synthesize a new PEG_8-chain with the same length as the previous one, but ending with a hydroxyl group instead of a carboxylic one (Figure 8).

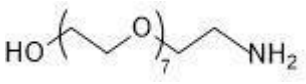

***Figure 8**: PEG$_8$NH$_2$(OH) chain (Compound **5**)*

Such a chain is supposed to be functional in order to increase the dispersion of the nanosystem in the biological medium, since it is hydrophilic and the terminal hydroxyl group should not interact with the culture broth as a carboxylic group does.

To synthetize this compound, we started from tetraethylene glycol (PEG_4). The present chain was then incorporated into the nanosystem, according to the same procedure described above. After functionalization of the NWs surface with amino groups, these were reacted with the carboxy groups of H_2TCPP previously converted in activated esters by means of condensing agents. Then, after removal of the excess unreacted porphyrin, a solution of compound **5** was added (Scheme 4).

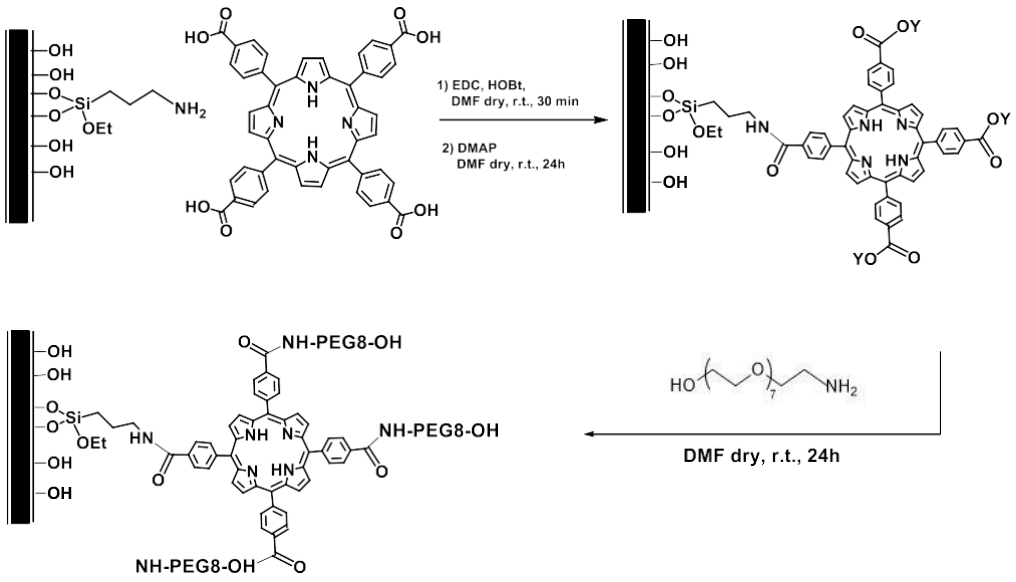

***Scheme 4**: Synthesis of a nanosystem consisting of SiC/SiO$_x$ nanowires conjugated with H$_2$TCPP porphyrin and an amino PEG-8 chain ending with hydroxy group.*

The nanosystem was characterized with solid state fluorescence spectroscopy, leaving the nanowires on their support, using a laser at 473 nm as excitation source (Figure 9).

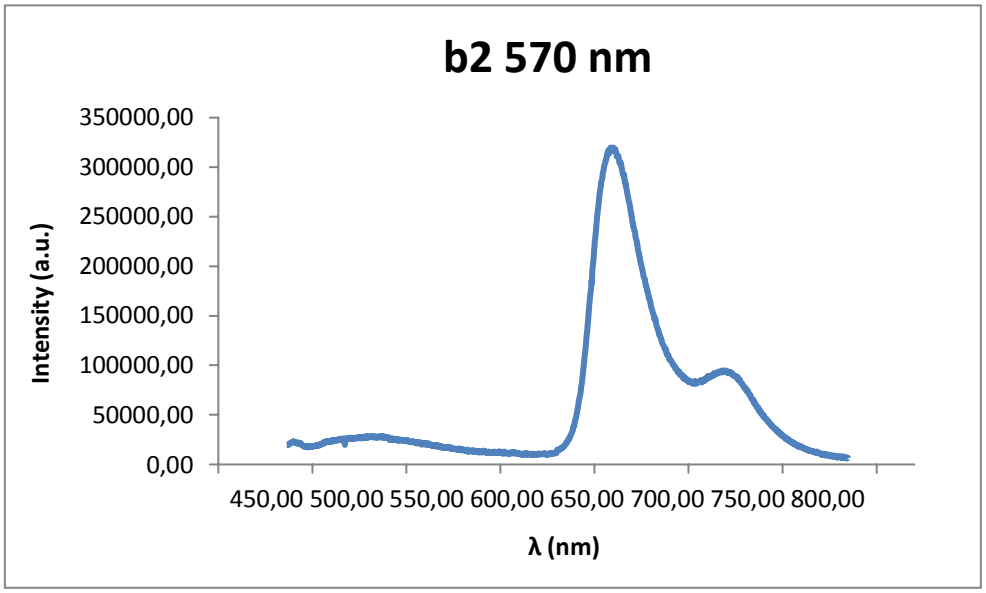

***Figure 9**: Fluorescence spectrum of a nanosystem consisting of SiC/SiO_x nanowires functionalized with H_2TCPP porphyrin and an amino PEG_8 chain ending with hydroxy groups.*

It is noteworthy the high degree of functionalization that is possible to achieve with the porphyrin conjugation to the nanowires via amide bond. Also in this case the fluorescence of the inorganic nanowire is very low with respect to that of porphyrin. This confirms that the functionalization was carried out successfully and that the procedure is reliable and repeatable.

The conjugated nanowires were detached from their support by sonication in ethanol, using an ultrasound microtip, then recovered by ultracentrifugation (14.000 rpm, 15 min).

The dispersion of the nanowires was checked both in physiological solution and culture broth, in order to observe some differences in their behavior, according to the medium which they are dispersed in.
Unexpectedly, also this new nanosystem showed the similar drawback as the previously described, even if in lower extent. The nanowires turned out to be quite dispersible in physiological solution, after sonication with an ultrasound microtip. On the contrary, they originated hanks floating over the cells in culture broth (Figures 10 and 11).

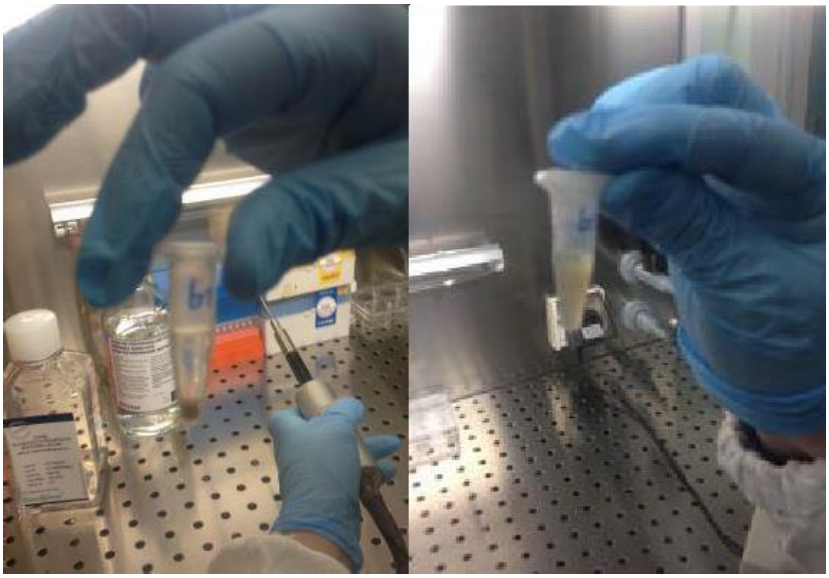

Figure 10: *Suspension of ammino-PEG$_8$-OH functionalized nanowires in physiological solution before (left) and after (right) sonication*

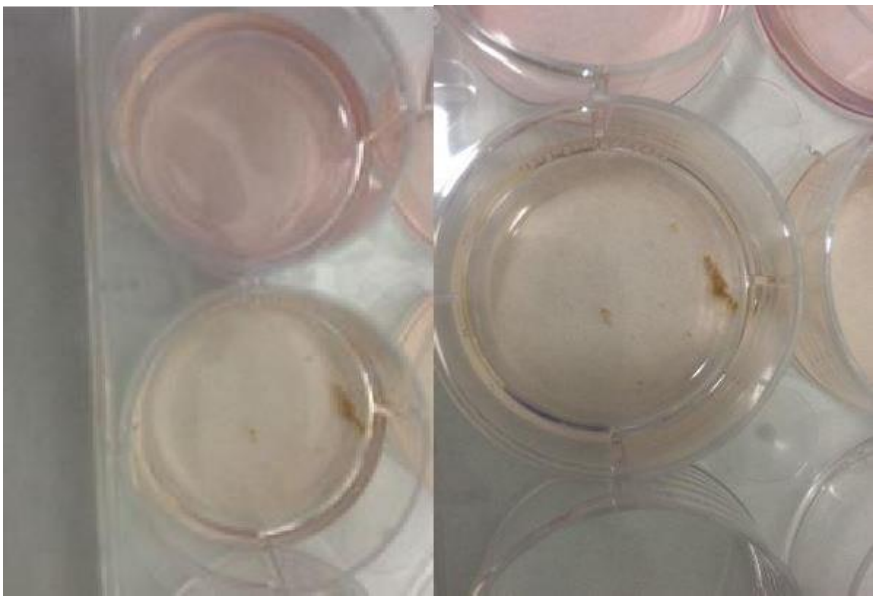

Figure 11*: Hanks observed in the flasks during the preparation for clonogenic survival assay*

In vitro tests were carried out to test the antiproliferative activity of the nanosystem on A549 cellular line: the cells were incubated with porphyrinated nanowires (50 μg/ml) for 24 hours. After that they were irradiated with 6 MeV X-ray at the dose of 4 Gy for 20 seconds. The suspension of nanowires in the flask was monitored and, after 10 days, survival of cells was evaluated by clonogenic assay (Figure 12).

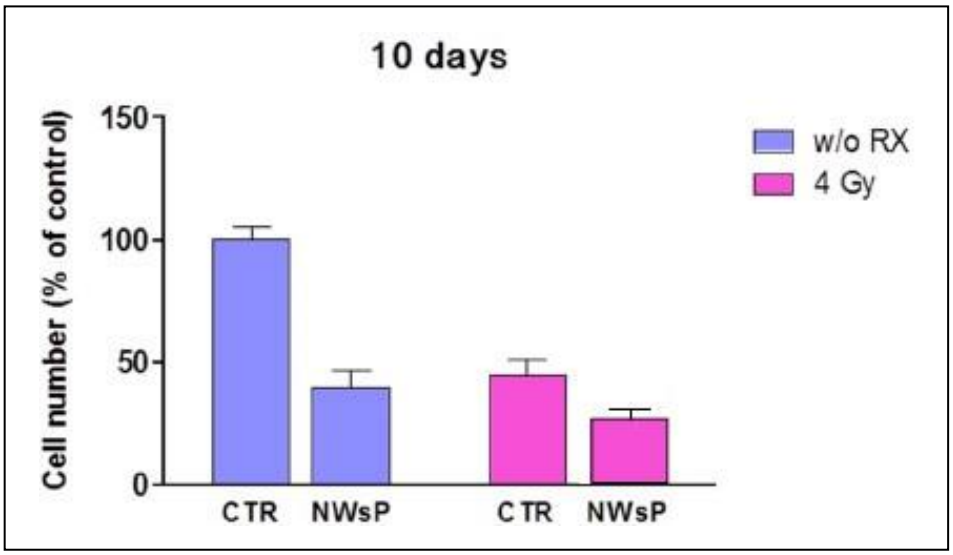

***Figure 12**: Histograms evidencing the results of clonogenic assays 10 days*

It was chosen to increase the dose to 4 Gy to observe a possible additional effect. Clonogenic assay evidenced that, after 10 days, the antiproliferative activity of the nanowires was not remarkable under irradiation, at 4 Gy dose; it seems that the antiproliferative activity of the nanowires is overcasted by that of irradiation. This result could be explained considering the published data [19] regarding the production of singlet oxygen that reached a plateau at a 2Gy dose. The results obtained using the nanosystem without irradiation deserve further studies.

Synthesis of Compound 4 [^{t}Bu-OOCCH$_2$(OCH$_2$CH$_2$)$_6$NH$_2$]

According to a procedure reported in the literature[22], starting from hexaethylene glycol a short PEG chain was synthetized containing an amino group at one end and at the other end a tert-butyl ester function, able to easy generate a terminal carboxylic acid function.

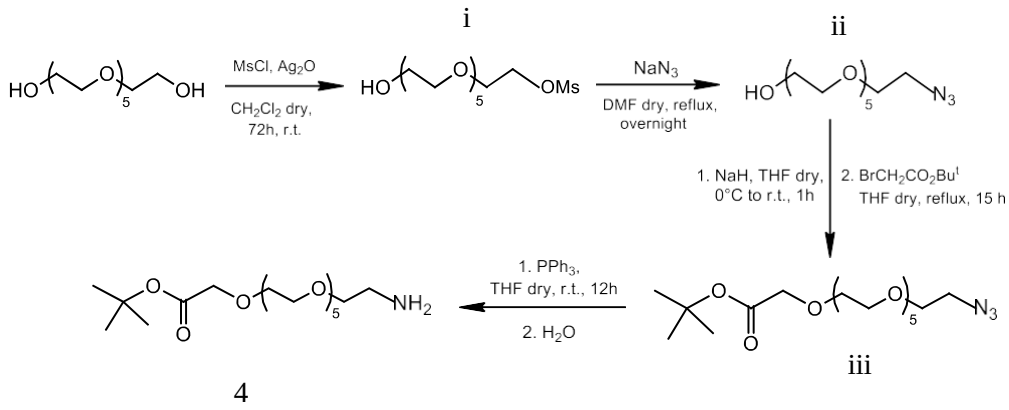

In the first step hexaethylene glycol was reacted with methanesulfonyl chloride in dichloromethane at room temperature, in the presence of Ag_2O as promoter, to turn one of the terminal –OH in a sulfonic ester, a good leaving group useful in the next step.

The reaction is not selective for the monosubstitution because of the symmetry of the starting molecule: the raw consists of unreacted reagents, monosubstituted product and disubstituted product. After purification by flash chromatography the monosubstitution compound was isolated in low yield (30 %). Analysis by ^{1}H NMR spectroscopy confirmed that the monosubstituted product was obtained pure. Figure 13 is a zoom of the most diagnostic region in the spectrum, consisting of two peaks: one is the broad singlet of the OH at one end of the PEG chain, and the other is the CH_3 sharp singlet of methanesulfonate, at the opposite end of the chain.

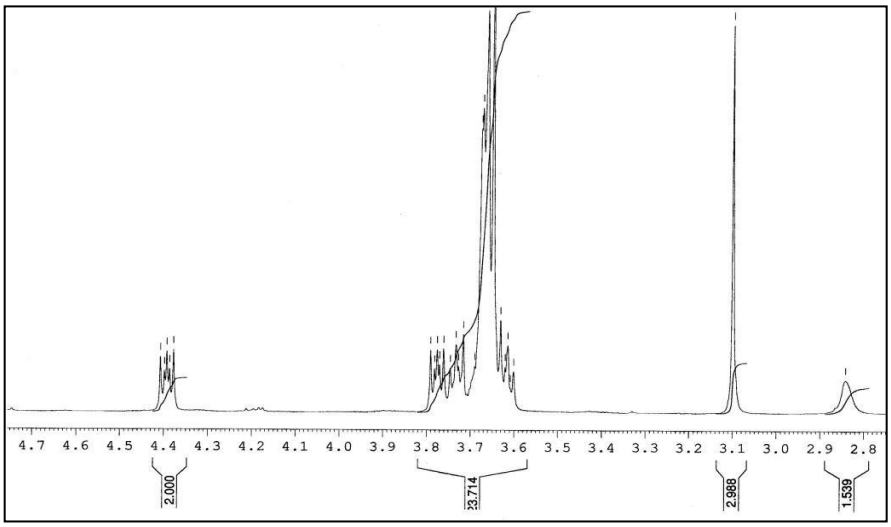

Figure 13**: Zoom of the most diagnostic region in the ^{1}H NMR spectrum of Compound **i

Higher yields (about 55%) were obtained using para-toluenesulfonyl chloride, instead of methanesulfonyl chloride. In the second step the monosubstituted sulfonic ester was reacted with sodium azide to give a terminal azido group (Compound **ii**).

Purification of the crude by flash chromatography gave the desired product in ~80 % isolated yield. However, if the starting sulfonic ester is that containing paratoluenesulfonate, the conversion is complete and there is no need of chromatographic purification. The crude was dried to remove DMF, then re-dispersed in ethyl acetate and centrifugated three times, to yield the pure product. In the third step the remaining –OH on the other side of the PEG chain was reacted with tert-butyl bromoacetate, after salification of the hydroxy group with NaH to increase the nucleophilicity.
After flash chromatography (AcOEt:MeOH=9:1) the product was isolated in modest yield (about 50 %), since competitive reactions occurred: tert-butyl bromoacetate, in fact, can undergo a self-condensation reaction. Another competitive reaction is due to the condensation of the alcoholate (generated on the PEG chain by NaH) with the ester group in tert-butyl bromoacetate (instead of the S_N2 reaction). In ^{1}H NMR spectrum pure product was easily identified by two diagnostic peaks: the singlet at δ=1.48 ppm, associated to

the tert-butylester, and the singlet at δ=4.03 ppm, attributable to the CH_2 in α position with respect to the ester carbonyl (Figure 14).

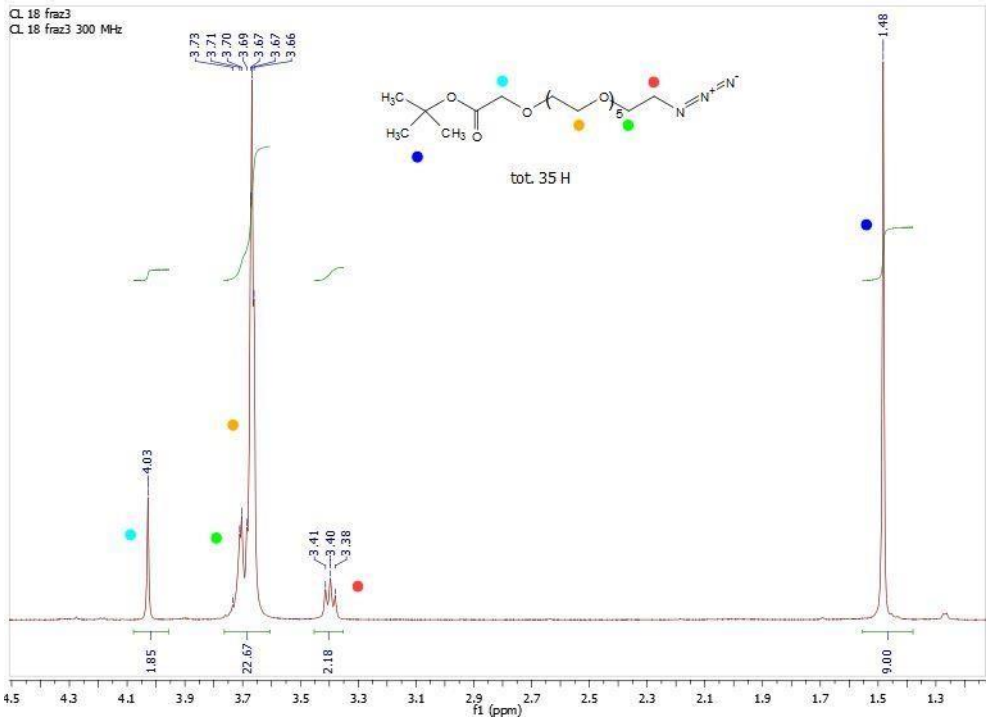

Figure 14**: Zoom of the most diagnostic region in ^{1}H NMR spectrum of Compound **iii

The last step consisted in the reduction of the azido group into a primary amine (Scheme 5).

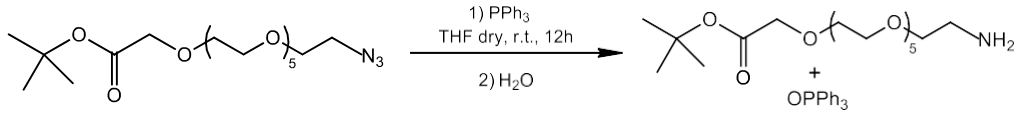

Scheme 5**: Staudinger reduction of Compound **iii** to the desired product Compound **4

Two approaches were used for this purpose: the Staudinger reduction and a catalytic hydrogenation. The first one turned out to be the most efficient: it employs triphenylphosphine in dry THF as reducing agent and the reaction is carried out under very mild conditions, leading to the pure product in quite high yield (80 %) by treating the crude with toluene many times. The product was characterized by ^{1}H NMR spectroscopy (Figure 15). It is possible to observe the absence of the triplet at 3.40 ppm (due to CH_2-N_3 protons) and the presence of the triplet at 2.88 ppm attributed to CH_2-NH_2 methylene protons.

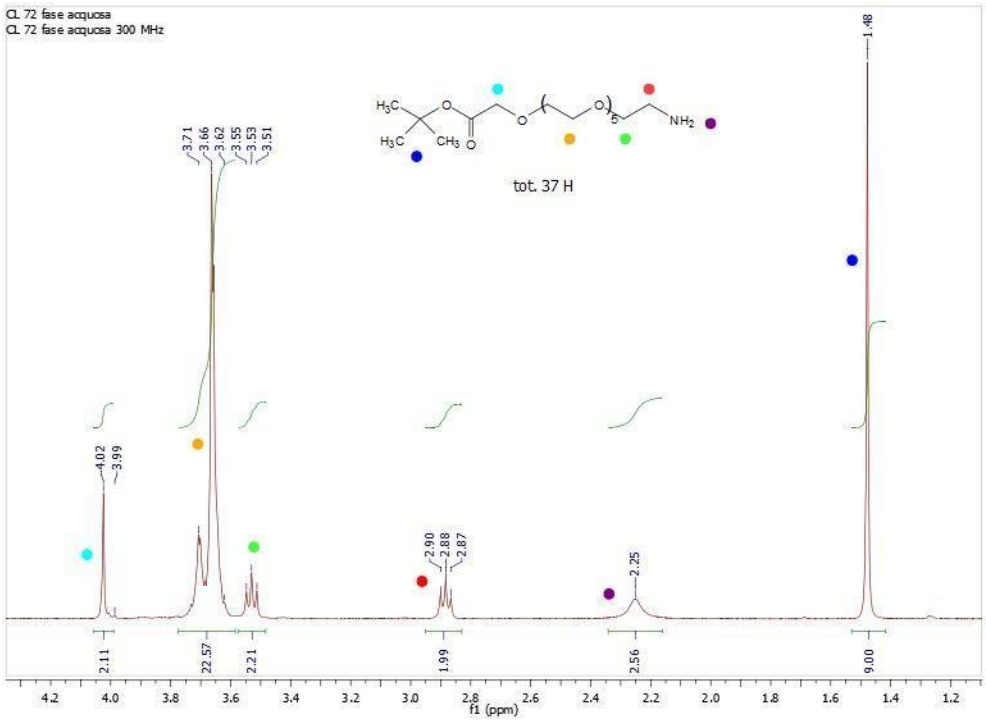

Figure 15*: Zoom of the most diagnostic region in the ^{1}H NMR spectrum of Compound* ***4***

The other approach, a catalytic hydrogenation with Pd/C, can be also useful, but the control of the reaction conditions (temperature and concentration of the reagents) is more complex: changes of temperature and concentration of the starting azide can lead to a by-product, which was identified as a

secondary amine due to a reductive dimerization process. This compound was identified with ESI-MS analysis (Figure 16a and 16b). In particular, this by-product is favored with increasing temperature and concentration. This secondary reaction can be partially avoided keeping the concentration of the reagent (Compound **iii**) at the constant value of 0.02 M. The yield of the reaction, however, is lower than that achieved with the Staudinger reaction (Scheme 6). In addition, we observed that silica chromatography separation did not afforded pure compound **4**.

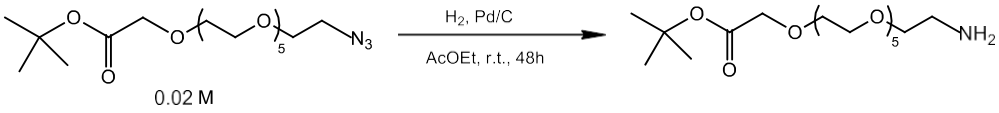

Scheme 6**: Catalytic hydrogenation of Compound **iii** to the desired product Compound **4

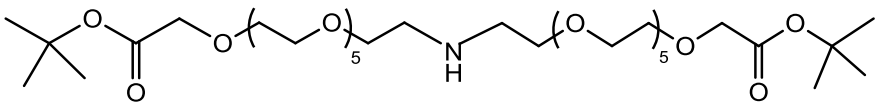

***Figure 16a**: Secondary amine due to a reductive dimerization process*

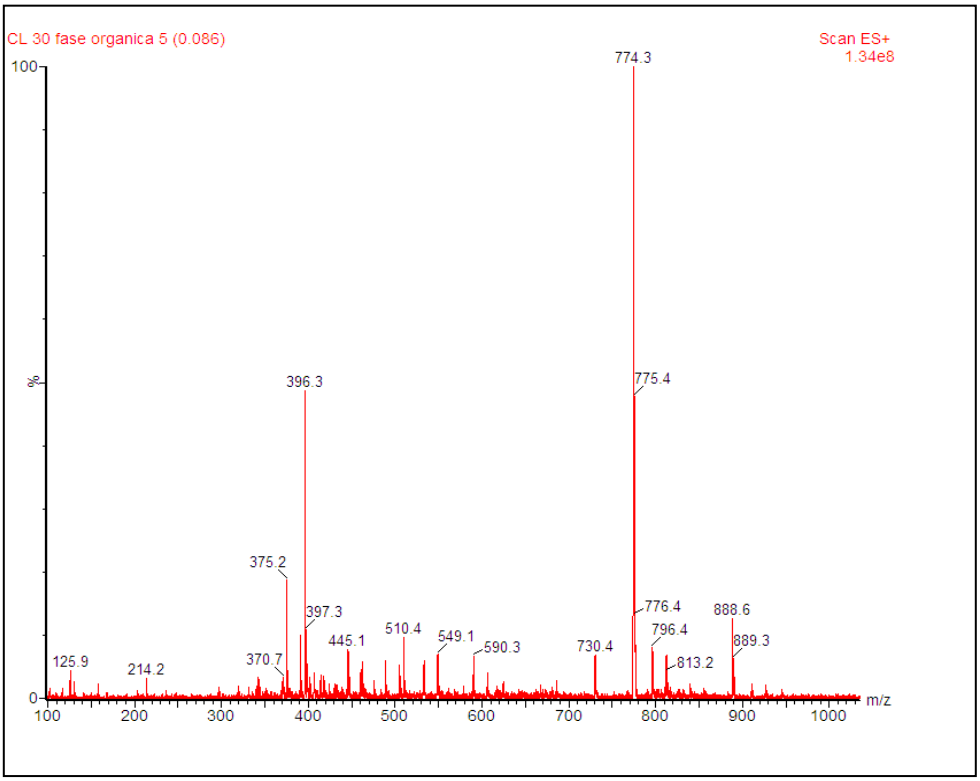

***Figure 16b**: ESI-MS spectrum showing the presence of the by-product secondary amine, due to a reductive dimerization process*

Synthesis of Compound 5 [$HOCH_2CH_2(OCH_2CH_2)_7NH_2$]

Starting from tetraethylene glycol I synthetized another short PEG chain bearing an amino group at one end and a OH group at the other side of the chain. We planned to synthetize a compound with a chain length similar to the previous one, but without the carboxylic function. The scheme shows the overall multistep procedure I accomplished conveniently modifying the experimental procedures reported in the literature.[23]

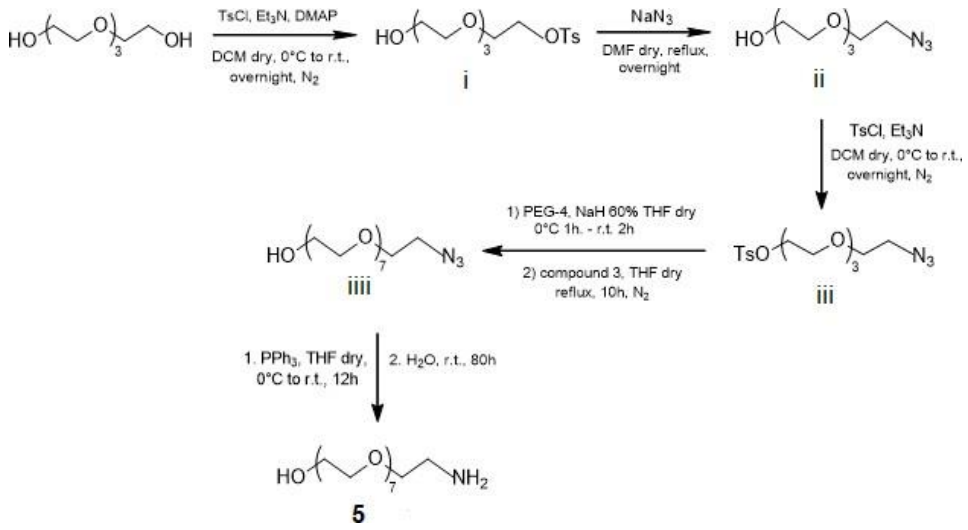

In the first step tetraethylene glycol was reacted with paratoluenesulfonyl chloride in the presence of DMAP and triethylamine, to turn one of the terminal OH into a sulfonic ester.

The reaction is not selective for the monosubstitution because of the symmetry of the starting molecule. The crude consists of unreacted reagents, monosubstituted product and disubstituted product. After purification by flash chromatography the monosubstituted compound was isolated in moderate yield (60 %). Analysis by ^1H NMR spectroscopy confirmed that the monosubstituted product was obtained pure.

In the second step the monosubstituted sulfonic ester was reacted with sodium azide to introduce a terminal azido group.
The conversion of this reaction was complete and there was no need of chromatographic purification. The crude was dried to remove DMF, then redissolved in ethyl acetate and centrifugated three times, to yield the pure product (92 %).

In the third step compound **ii** was reacted again with paratoluenesulfonyl chloride, to turn the OH at the other end of the chain into a sulfonic ester.
The crude reaction was purified with flash chromatography to yield pure product **iii** in a good yield (84%).
In the fourth step compound **iii** was coupled with another unit of PEG-4 to get a PEG-8 chain bearing at one side an azido group.

The reaction occurs in two steps. In the first one, PEG-4 is reacted with NaH to generate an alcoholate at one end of the chain. In this step an ice-bath is needed for the first hour, because the reaction is quite exothermic; then, the mixture is stirred for other two hours at room temperature. After that, in the second step compound **iii** is added and the mixture is refluxed for ten hours.

Following the procedure reported in the literature, water was added to quench the reaction. The crude reaction required a laborious purification via flash chromatography due to the presence of by-products and unreacted PEG-4.
The main by-products are due to the reaction of glycolic hydroxyl groups with ethyl acetate, used to extract the product in the work-up. ^{1}H NMR spectra below report some by-products generated by the transesterification reaction with ethyl acetate during the work-up procedure (Figures 17 and 18).

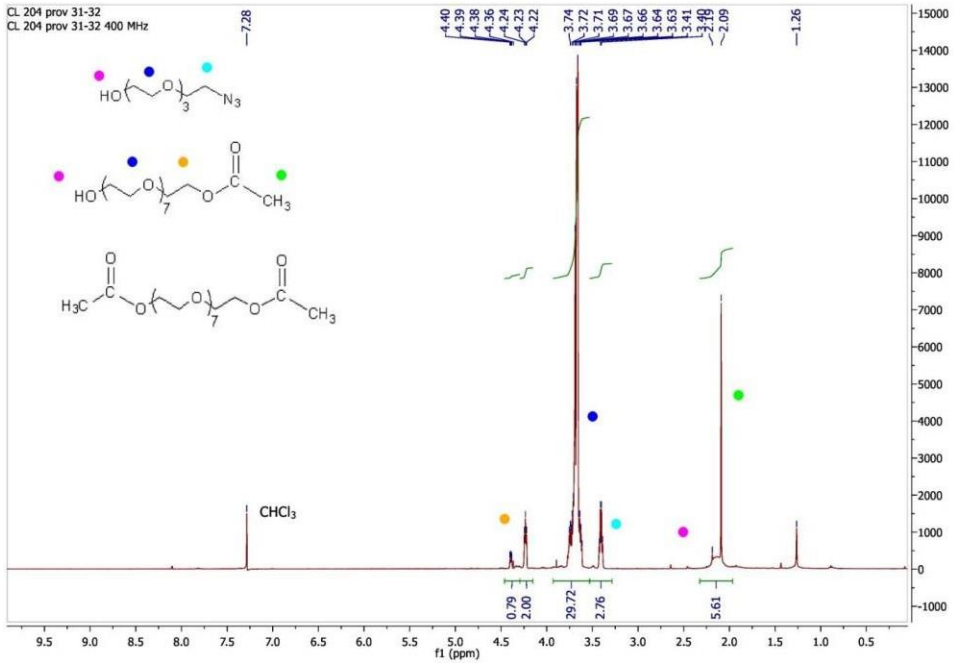

***Figure 17**: [1]H NMR spectrum showing by-products generated by the transesterification reaction with ethyl acetate*

We attributed the formation of these by-products to the presence of not re-protonated alcoholate. Therefore, we deduced that it is important to check the pH of the solution while adding acid to quench the reaction.

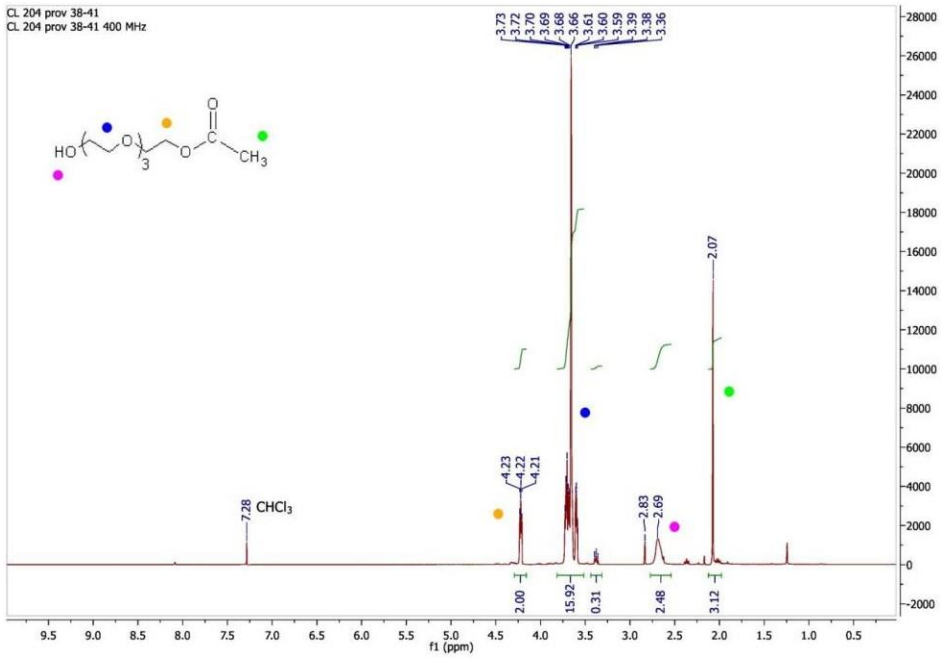

***Figure 18**: [1]H NMR spectrum showing by-products generated by the transesterification reaction with ethyl acetate*

The diagnostic peaks for the transesterification reaction between ethyl acetate and the alcoholate on PEG-4 (or PEG-8) are that related to CH_3CO (2.08 ppm) and that due to CH_2O (4.24 ppm). Then, for the next reactions, I decided to modify the quenching procedure, by adding hydrochloric acid until I reached an acidic pH. To completely avoid the formation of trasesterification by-products, I also formulated an alternative work-up procedure, which doesn't employ ethyl acetate: the reaction mixture is transferred into a falcon and, after centrifugation (10 min, 5000 rpm, x 3), the supernatant is separated from a white solid, then is collected in a flask. This liquid is dried and purified through flash chromatography, to yield pure compound **iv** in a satisfactory yield (66%), as confirmed by ^{1}H NMR spectrum.

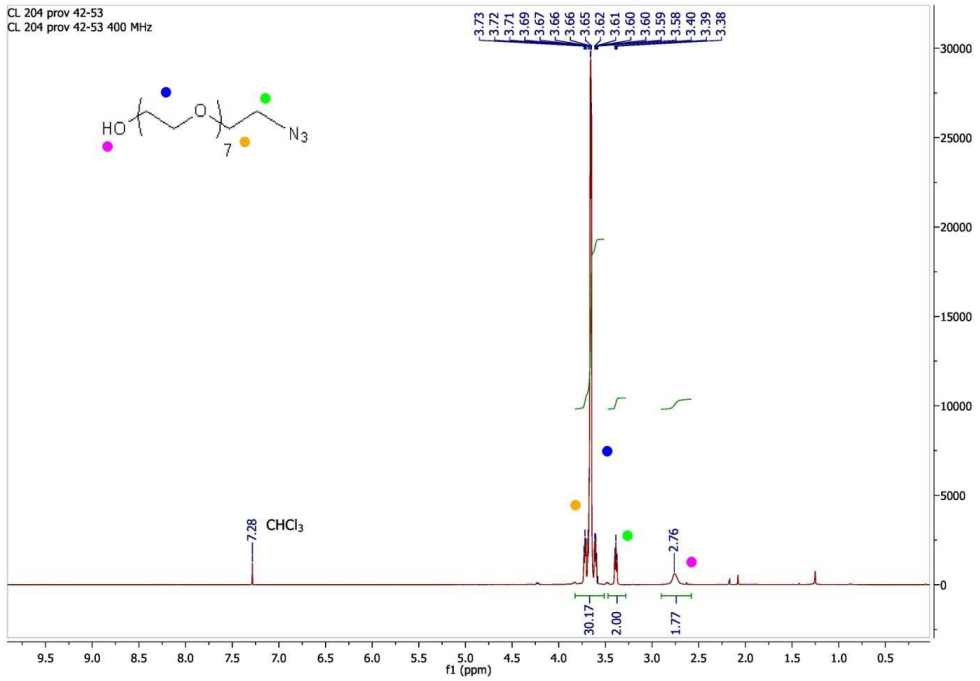

Figure 19**: [1]H NMR spectrum of compound **iv

In the last step Compound iiii was reduced into a primary amine with triphenylphosphine, according to Staudinger reaction approach.
This procedure requires no chromatographic purification and the product is obtained pure with a good yield (80 %) after washing the crude (soluble in water) with toluene at least three times.
^{1}H NMR spectrum proved that the desired product was obtained pure (Figure 20). Indeed, the triplet at 3.39 ppm (due to CH_2-N_3) is substituted by the triplet at 2.87 ppm due to CH_2-NH_2 methylene protons.

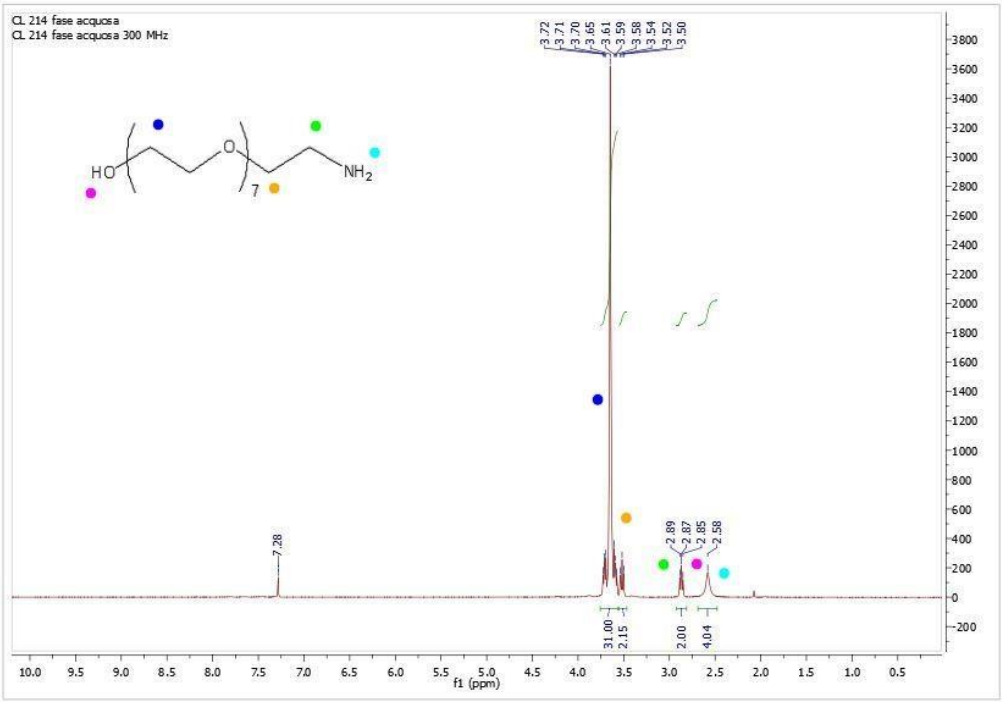

Figure 20**: [1]H NMR spectrum of compound **5

Experimental section

Synthesis of amino PEG-6 chain ^{t}Bu-20-amino-3,6,9,12,15,18-exaoxaeicosanoate [^{t}Bu-$OOCCH_2(OCH_2CH_2)_6NH_2$]

Synthesis of 17-[(Metansulfonyl)oxa-3,6,9,12,15-pentaoxaheptadecanol [$H(OCH_2CH_2)_6OMs$] (Compound ia)

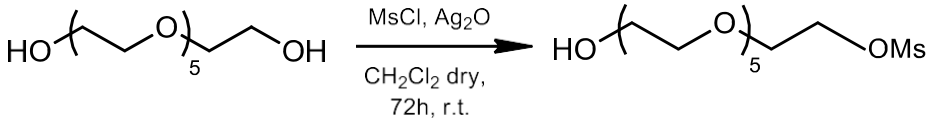

Hexaethyleneglycol (203 mg, 0.719 mmol), dissolved in dry DCM, methanesulfonyl chloride (97.41 mg, 0.850 mmol), dissolved in dry DCM and Ag_2O (183.1 mg, 0.790 mmol) were introduced in a Schlenck tube, previously anhydrifyed with 3 vacuum/nitrogen cycles. The reaction was carried out under inert atmosphere of nitrogen for 72 hours at room temperature and periodically monitored with TLC. The mixture was filtered over celite and the crude was dried at the rotary evaporator, then at the vacuum pump. The crude was purified through flash chromatography with AcOEt:MeOH 10:1 as eluent to yield the product (colorless oil, 396.36 mg, 30% yield). The pure product was characterized with ^{1}H NMR.

^{1}H NMR (300 MHz $CDCl_3$) δ(ppm)=4.29 (2H, t, CH_2OMs); 3.69-3.29 (22H, m, CH_2CH_2O); 3.18 (1H, s, OH); 3.01 (3H, s, CH_3 in OMs)

Synthesis of 7-[(Para-toluensulfonyl)oxa-3,6,9,12,15-pentaoxaheptadecanol [H(OCH$_2$CH$_2$)$_6$OTs] (Compound ib)

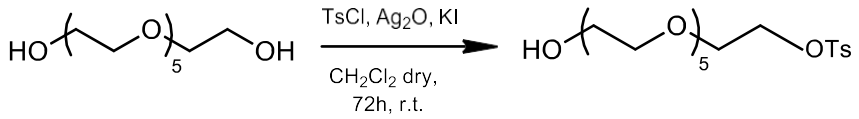

Hexaethylene glycol (684 mg, 2.420 mmol), dissolved in dry DCM, was introduced in a two-necked round bottom flask under nitrogen. The system was put into an ice bath, then Ag_2O (897 mg, 3.870 mmol), KI (88.4 mg, 0.533 mmol) and p-toluene sulfonyl chloride (623 mg, 3.27 mmol) were added under nitrogen and stirring. The reaction was carried out under inert atmosphere for 72 hours and monitored with TLC. The mixture was filtered over celite and the raw, after drying, was purified with flash chromatography using AcOEt:MeOH=85:15 as eluent to yield the product (colorless oil, 614.5 mg, 60% yield). The pure product was analyzed with ^{1}H NMR.

^{1}H NMR (300 MHz CDCl$_3$) δ(ppm)=4.29 (2H, t, CH_2OMs); 3.69-3.29 (22H, m, CH_2CH_2O); 3.18 (1H, s, OH); 3.01 (3H, s, CH_3 in OMs)

Synthesis of 17-[Azido]-3,6,9,12,15-pentaoxaheptadecanol [H(OCH$_2$CH$_2$)$_6$N$_3$] (Compound ii)

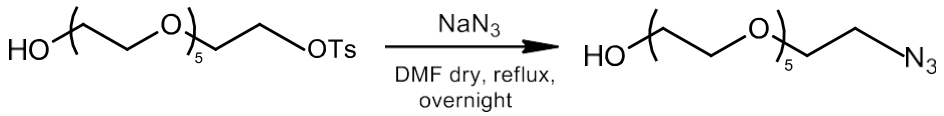

Compound **2** (614.5 mg, 1.41 mmol), dissolved in dry DMF, was introduced in a Schlenck tube under nitrogen. Sodium azide (210 mg, 3.23 mmol) was added under nitrogen and the reaction was refluxed overnight.

At completion, the mixture was dried at the vacuum pump to remove DMF. Ethyl acetate was then added and the crude was centrifugated three times to remove the salt. The product was obtained pure with no need of chromatographic purification (pale yellow oil, 406.5 mg, 94% yield).

^{1}H NMR (300 MHz $CDCl_3$)

δ(ppm)=3.73-3.59 (22H, m, $CH_2\underline{CH_2}O$); 3.40-3.38 (2H, t, $CH_2\underline{CH_2}N_3$); 2.87 (1H, s, OH)

Synthesis of ^{t}Bu-20-azido-3,6,9,12,15,18-hexaoxaeicosanoate [^{t}Bu-$OOCCH_2(OCH_2CH_2)_6N_3$] (Compound iii)

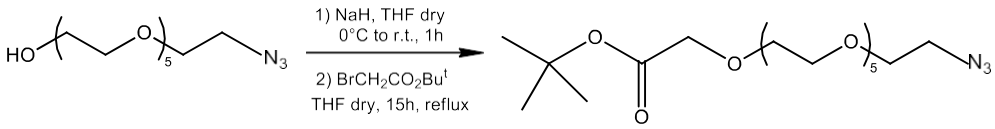

Compound **2** (352.5 mg, 1.147 mmol), dissolved in dry THF, was introduced in a Schlenck tube, previously dried with 3 cycles vacuum/nitrogen. The system was put into an ice bath, then NaH (60% dispersion in paraffin oil) (0.0688 mg, 1.7205 mmol) was added and the mixture was stirred for 20 minutes under nitrogen. Then, the ice bath was removed and the mixture was stirred for an additional hour at room temperature. $BrCH_2CO_2{}^tBu$ (335.6 mg, 1.7205 mmol) was finally added under nitrogen and the reaction was refluxed for 15 hours. The crude was purified through flash chromatography (AcOEt:MeOH=9:1) to yield the pure product (pale yellow oil, 228.3 mg 48% yield).

^{1}H NMR (300 MHz $CDCl_3$)

δ(ppm)=4.03 (2H, s, $CO\underline{CH_2}O$); 3.73-3.66 (22H, m, $CH_2\underline{CH_2}O$); 3.41-3.38 (2H, t, $CH_2\underline{CH_2}N_3$); 1.48 (9H, s, $(\underline{CH_3})_3CO$)

Synthesis of ^{t}Bu-20-amino-3,6,9,12,15,18-exaoxaeicosanoate [^{t}Bu-$OOCCH_2(OCH_2CH_2)_6NH_2$] (Compound 4)

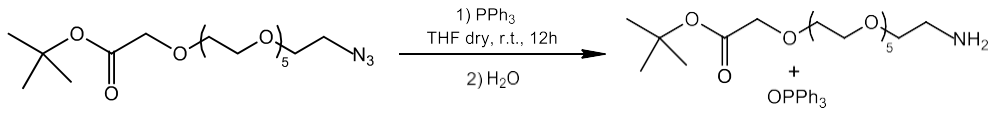

Compound **3** (246.2 mg, 0.5829 mmol), dissolved in dry THF, was introduced in a Schlenck tube, previously dried with 3 vacuum/nitrogen cycles. The system was put into an ice bath and triphenylphosphine (198.5 mg, 0.7577 mmol) was added. The mixture was then stirred at room temperature for 12 hours, under nitrogen. After that, H_2O (27.2 mg, 1.51 mmol) was added and the mixture was stirred for additional 10 hours. The reaction was quenched by adding water. At completion (monitoring via TLC), the mixture was transferred into a separator funnel and washed four times with toluene. The product was obtained pure without any further purification (pale yellow oil, 180.22 mg, 78% yield).

^{1}H NMR (300 MHz $CDCl_3$)

δ(ppm)=4.03 (2H, s, $CO\underline{CH_2}O$); 3.73-3.66 (22H, m, $CH_2\underline{CH_2}O$); 3.4 (2H, t, $O\underline{CH_2}CH_2NH_2$); 3.55-3.52 (2H, t, $O\underline{CH_2}CH_2NH_2$); 2.90-2.87 (2H, t, $OCH_2\underline{CH_2}NH_2$); 2.50 (2H, s, NH_2) 1.48 (9H, s, $(\underline{CH_3})_3CO$)

Experimental section

Synthesis of amino PEG-8 chain (compound 5) (23-Amino-3,6,9,12,15,18,21-heptaoxatricosan-1-ol) [$H(OCH_2CH_2)_8NH_2$]

Synthesis of (2-(2-(2–(2-hydroxyethoxy)ethoxy)ethoxy)ethyl-l4-methylbenzene sulfonate) [$H(OCH_2CH_2)_4OTs$] (Compound i)

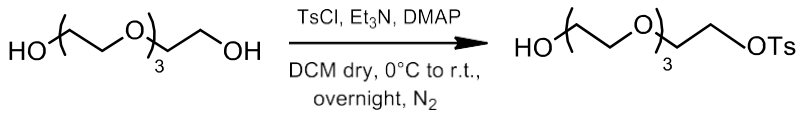

Tetraethyleneglycol (5.625 g, 28.96 mmol), dissolved in dry DCM, was introduced in a Schlenck tube, previously dried with three vacuum/nitrogen cycles. The system was cooled to 0°C with an ice bath, then triethylamine (21.72 mmol), paratoluenesulfonyl chloride (2.761 g, 14.48 mmol) and DMAP (0.1769 g, 1.448 mmol) were added. The reaction was stirred at room temperature overnight, under nitrogen atmosphere. After that, the mixture was monitored via TLC (DCM:MeOH=20:1), then 60 ml of distilled water were added and the reaction was stirred again.
The organic phase was washed with water three times, then dried over anhydrous Na_2SO_4.
The crude was purified with flash chromatography (DCM:MeOH=20:1) to yield pure compound **1** (3.02 g, 60% yield).
^{1}H NMR spectrum showed that the isolated product **1** was pure.

^{1}H NMR (300 MHz, $CDCl_3$)

δ(ppm) = 7.815 (2H, d, CH in OTs, J = 9 Hz); 7.36 (2H, d, CH in OTs, J = 6 Hz); 4.18 (2H, t, CH_2OTs, J = 6 Hz); 3.69 (14H, m, CH_2CH_2O) ; 2.46 (3H, s, CH_3 in OTs); 2.31 (1H, s, OH);

Synthesis of (2-(2-(2-(2-Azidoethoxy)ethoxy)ethoxy)ethanol) [$H(OCH_2CH_2)_4N_3$] (Compound ii)

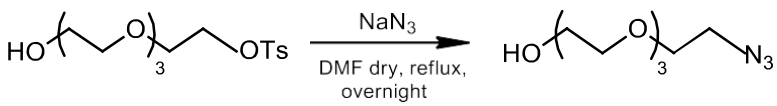

Compound **1** (1.25 g, 3.956 mmol), dissolved in dry DMF, was introduced in a Schlenck tube, previously dried with three vacuum/nitrogen cycles. Sodium azide (2.338 g, 10.79 mmol) was then added slowly and the mixture was refluxed overnight under nitrogen.
The reaction was monitored via TLC (DCM:MeOH=20:1).
DMF was removed through azeotropic distillation with toluene, then the crude was dissolved in ethyl acetate and centrifugated three times to remove the residue salt. The liquid was dried at the rotary evaporator to yield pure product compound **2** as a pale yellow oil (0.24 g, 92% yield).

^{1}H NMR (300 MHz CDCl3)

δ(ppm) = 3.665 (14H, m, CH_2CH_2O); 3.39 (2H, t, CH_2N_3, J = 6 Hz); 2.67 (1H, s, OH);

Synthesis of (2-(2-(2-(2-Azidoethoxy)ethoxy)ethoxy)ethyl-4-Methylbenzensulfonate) [$Ts(OCH_2CH_2)_4N_3$] (Compound iii)

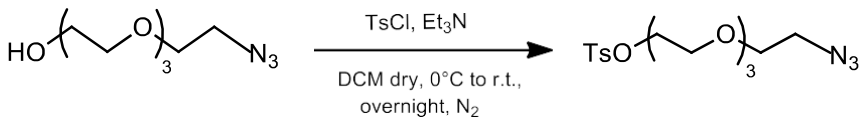

Compound 2 (0.4601 g, 2.103 mmol), dissolved in dry DCM, was introduced into a 50 ml two necked round bottom flask, previously dried with three

vacuum/nitrogen cycles. Triethylamine (0.300 g, 2.965 mmol) was added, then the system was cooled to 0°C in an ice bath. Paratoluenesulfonyl chloride (0.5613 g, 2.944 mmol) was finally added and the mixture was stirred overnight at room temperature, under nitrogen atmosphere.
The reaction was monitored via TLC (AcOEt:hexane=1:1), then, at completion, was quenched by addition of 10 ml of distilled water. The organic phase was washed three times with water and dried over anhydrous $MgSO_4$.
The crude was purified through flash chromatography (AcOEt:hexane=1:1) to yield pure product as a light yellow oil (0.659 mg, 84% yield).

^{1}H NMR (300 MHz $CDCl_3$)

δ(ppm) = 7.81 (2H, d, CH in OTs, J = 8 Hz); 7.36 (2H, d, CH in OTs, J = 8 Hz); 4.15 (2H, d, CH_2OTs, J = 4 Hz); 3.68 (13H, m, CH_2CH_2O); 3.39 (2H, t, CH_2N_3, J = 8 Hz); 2.46 (3H, s, CH_3 in OTs);

Synthesis of (23-Azido-3,6,9,12,15,18,21-heptaoxatricosan-1-ol) [$H(OCH_2CH_2)_8N_3$] (Compound iv)

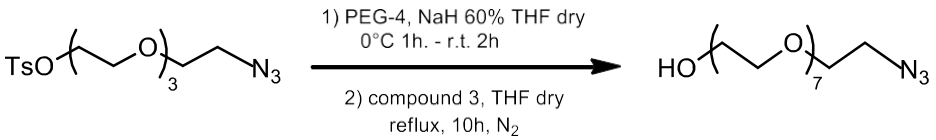

A solution of tetraethyleneglycol (0.3232 g, 1.6962 mmol) in dry THF was introduced in a 25ml Schlenck, previously dried with three vacuum/nitrogen cycles. The system was cooled to 0°C with an ice bath, then NaH (0.0433 g, 1.828 mmol, 60% dispersion in paraffin) was added. The mixture was stirred at 0°C for one hour, then at room temperature for further two hours. After that, a solution of Compound 3 (0.3100 g, 0.8320 mmol) in dry THF was added dropwise and the mixture was refluxed for 15 hour under nitrogen.

This reaction was carried out following two different work-up procedures.

Work up 1:

The reaction was quenched by adding HCl 0.1 M and a small amount of HCl 1 M dropwise, under stirring at room temperature: the final pH must be acidic (about 4,5-5). The mixture was then dried at the rotary evaporator. The crude was dissolved in ethyl acetate and centrifugated three times to remove residue salts.

The supernatant was then put into a separator funnel, adding further ethyl acetate and washing twice with water and once with a saturated solution of NaCl. The organic phase was dried over anhydrous Na_2SO_4 and filtered, whereas the aqueous phase was dried at the rotary evaporator. Both the organic and aqueous phases were checked with TLC (DCM:MeOH=10:1). A great part of the product was in the aqueous phase, whereas the organic one contained a lot of unreacted compound **3**. The two phases were then reunified, dried and the resulting crude purified by flash chromatography (DCM:MeOH=15:1).

Pure product was obtained as a pale yellow oil (0.1082 g, 33% yield) and analysed with ^{1}HNMR.

Work up 2:

The reaction mixture (which is heterogeneous for the presence of salts) was transferred into a falcon tube and centrifugated three times (10 min, 5000 rpm, x 3). The supernatant, a light brown solution, was put into a flask and dried at the rotary evaporator. In this way the crude was obtained as a light brown oil.

Meanwhile, the salt was introduced into another flask and dissolved in water: this strongly basic solution was acidified with HCl 0.1 M and HCl 1 M until an acidic pH (4.5-5) was reached. A TLC of the aqueous phase confirmed that this didn't contain the product. The crude obtained from the supernatant was purified by flash chromatography (DCM:MeOH=12:1)

Pure product was obtained pure (0,217 g, 66% yield) and analyzed with ^{1}H NMR.

^{1}H NMR (300 MHz $CDCl_3$)

δ(ppm) = 3.645 (30H, m, CH_2CH_2O); 3.39 (2H, t, CH_2N_3, J = 4 Hz); 2.76(1H, s, OH)

Synthesis of (23-Amino-3,6,9,12,15,18,21-heptaoxatricosan-1-ol) [$H(OCH_2CH_2)_8NH_2$] (Compound 5)

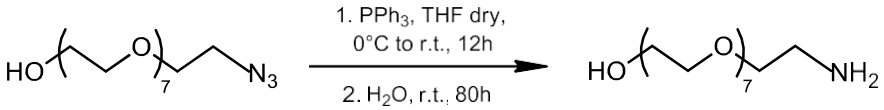

Compound **4** (0.1082 g, 0.2739 mmol) was dissolved in dry THF and introduced in a 25 ml two-necked round bottom flask, which was previously anhydrified with three vacuum/nitrogen cycles. The flask was put into an ice/water bath and the mixture was kept at 0°C. PPh_3 (1.4369 g, 5.4785 mmol) was then added and the mixture was stirred at room temperature for 20 hours, under nitrogen. Water (8.88 μl, 0.4931 mmol) was added and the mixture was stirred for further 80 hours at room temperature. The reaction was monitored via TLC (i-PrOH : NH_3 : H_2O = 6:3:1). Other water was added and the crude was transferred into a separator funnel. Then it was washed four times with toluene. The aqueous phase, containing the product, was dried at the rotary evaporator and at the vacuum pump. Compound **5** was obtained pure (0.0736 g, 73% yield) as confirmed by ^{1}H NMR.

^{1}H NMR (300 MHz $CDCl_3$)

δ(ppm) = 3.65 (30H, m, CH_2CH_2O); 3.52 (2H, t, $\underline{CH_2}CH_2NH_2$); 2.87 (2H, t, CH_2NH_2); 2.58(4H, br s, OH and NH_2)

Functionalization of the nanowires with H_2TCPP porphyrin and amino PEG-6 chain
^{t}Bu-20-amino-3,6,9,12,15,18-exaoxaeicosanoate
[^{t}Bu-OOCCH$_2$(OCH$_2$CH$_2$)$_6$NH$_2$]

Activation of the nanowires surface

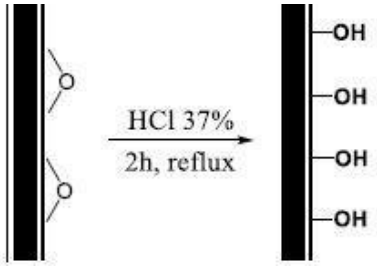

The nanowires were activated by refluxing the wafers in 20 ml of HCl 37% for two hours. Then, the wafers were washed with a lot of distilled water till neutral pH and finally with acetone, to let them dry more quickly.

Functionalization of nanowires with 3-aminopropyl triethoxysilane

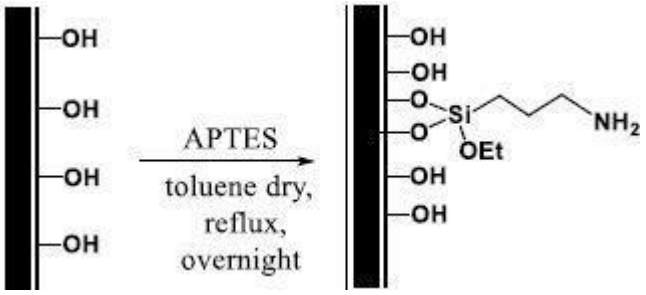

In the second step of functionalization, the previously activated nanowires were reacted with an excess of 3-aminopropyl triethoxysilane (APTES) to introduce an amino group.

The wafers were introduced in a 50 ml two-necked round bottom flask, previously anhydrified with three vacuum/nitrogen cycles, and were covered with 10 ml of dry toluene. APTES (2 µl of a 5mM solution in toluene) was added and the reaction was refluxed overnight. After cooling, the nanowires were thoroughly washed with dry toluene, with acetone and dried in the air.

Functionalization of nanowires with porphyrin (H_2TCPP)

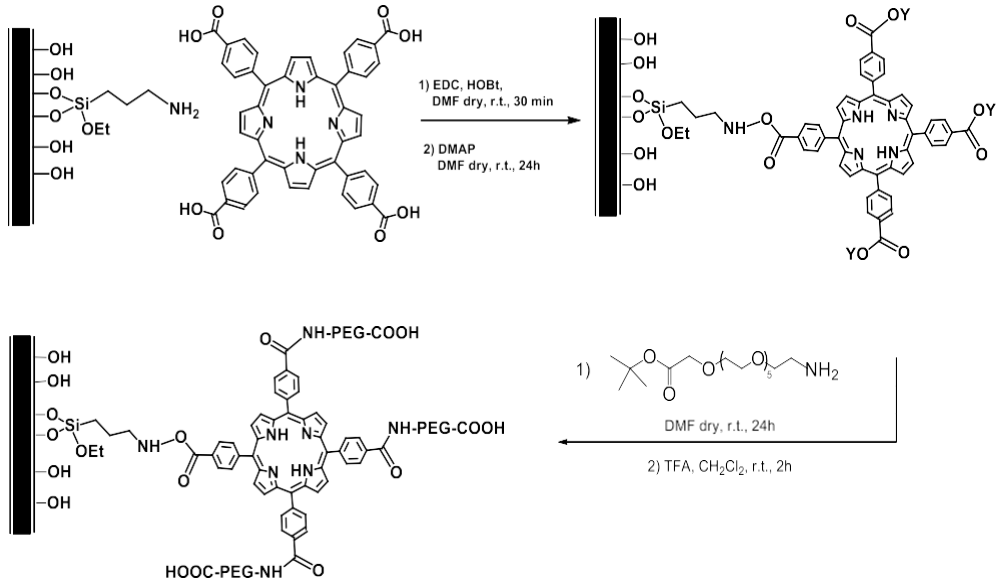

H_2TCPP porphyrin (10.4 mg, 0.0132 mmol) was introduced in a 50 ml two-necked round bottom flask, previously dried with three vacuum/nitrogen cycles, and dissolved in 3 ml of dry DMF. EDCI (15 mg, 0.0787 mmol) and HOBt (10 mg, 0.0740 mmol) were added and the mixture was stirred for 30 minutes under nitrogen. After that, the wafer covered by the nanowires was introduced and DMAP (14 mg, 0.1146 mmol) was added, together with further 4 ml of anhydrous DMF. The reaction mixture was stirred at room temperature for 24 hours under nitrogen flux. After that time, the solution

was completely removed from the flask and a solution of compound **4** in 7 ml of DMF dry was added to cover the wafer. The reaction was stirred at room temperature overnight.
Then, the wafer was washed several times with distilled water, DMF, acetone and dried in the air.
In the last step, the wafer bearing porphyrinated nanowires was put into a 50 ml round bottom flask. A solution of trifluoroacetic acid in dichloromethane (1:4) was added and the mixture was stirred for two hours in the air. The wafer was then washed with dichloromethane, diethyl ether and finally with acetone.
The nanowires were detached from the support by sonicating the wafers in acetone with an ultrasound microtip (Misonix Sonicator): the suspension of nanowires in acetone was then divided into many Eppendorf tubes and was centrifugated (14.000 rpm, 10-15 min). The precipitated nanowires were finally recovered and collected, then dried in the air.

Functionalization of the nanowires with H_2TCPP porphyrin and amino PEG-8 chain (23-Amino-3,6,9,12,15,18,21-heptaoxatricosan-1-ol) [$H(OCH_2CH_2)_8NH_2$]

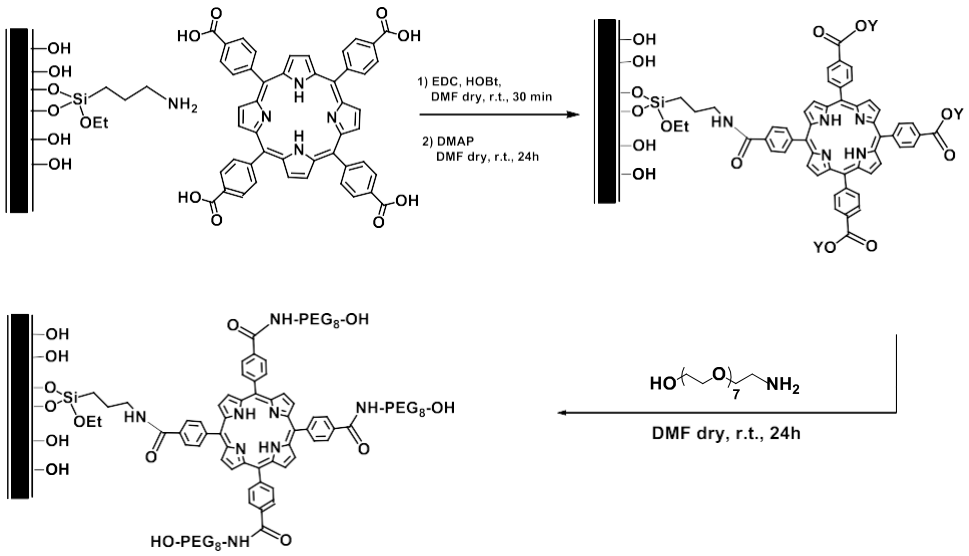

As described above, the previously activated nanowires were reacted with APTES in dry toluene to introduce amino functions.

In the third step of functionalization, H_2TCPP porphyrin (10.4 mg, 0.0132 mmol) was introduced in a 50 ml two-necked round bottom flask, previously dried with three vacuum/nitrogen cycles, and dissolved in 3 ml of dry DMF. EDCI (15 mg, 0.0787 mmol) and HOBt (10 mg, 0.0740 mmol) were added and the mixture was stirred for 30 minutes under nitrogen. After that, the wafer covered by the nanowires was introduced and DMAP (14 mg, 0.1146 mmol) was added, together with further 4 ml of anhydrous DMF. The reaction mixture was stirred at room temperature for 24 hours under nitrogen flux. After that time, the solution was completely removed from the flask and a solution of compound 4 in 7 ml of DMF dry was added to cover the wafer. The reaction was stirred at room temperature overnight.

Then, the wafer was washed several times with distilled water, DMF, acetone and dried in air.
The nanowires were detached from the support by sonicating the wafers in acetone with an ultrasound microtip (Misonix Sonicator): the suspension of nanowires in ethanol was then divided into many Eppendorf tubes and was centrifugated (14.000 rpm, 10-15 min). The precipitated nanowires were finally recovered and collected, then dried in the air.

References

[1] W. Chen, J. Zhang, J., "Using nanoparticles to enable simultaneous radiation and photodynamic therapies for cancer treatment" *Nanosci. Nanotech., 6* (4), pp. 1159-1166, **2006**

[2] Y. Liu, W. Chen, S. Wang, A.G. Joly, "Investigation of water-soluble x-ray luminescence nanoparticles for photodynamic activation", *Appl. Phys. Lett., 92* (4), 043901/1-043901/3, **2008**

[3] M.C. De Rosa, R.J. Crutchley., "Photosensitized singlet oxygen and its applications", *Coord. Chem. Rev., vol. 233-234*, 351-371, **2002**

[4] M. Sibrian-Vazquez et al., "Synthesis and cellular studies of PEG-functionalized meso-tetraphenylporphyrins", *J. Photochem Photobiol B, 86* (1), pp. 9-21, **2007**

[5] M. F. Grahn, et al., "mTHPC Polymer Conjugates: The In Vivo Photodynamic Activity of Four Candidate Compounds", *Lasers Med. Sci., 14* (1), pp. 40-6, **1999**

[6] D. L. Akins, S.Ozcelik, et al., "Fluorescence decay kinetics and structure of aggregated tetrakis(p-sulfonatophenyl)Porphyrin", *J. Phys. Chem., 100* (34), pp. 14390-14396, **1996**

[7] F. Fabbri et al., "Enhancement of the core near-band edge emission induced by an amorphous shell in coaxial one-dimensional nanostructure: the case of SiC/SiO_2 core/shell self-organized nanowires", *Nanotechnology, 21* (34), **2010**

[8] F. Fabbri, F. Rossi, M. Negri, R. Tatti, L. Aversa, S. C. Dhanabalan, R. Verucchi, G. Attolini and G. Salviati, "Carbon-doped SiOx nanowires with a large yield of white emission", *Nanotechnology, 25* (18), 185704, **2014**

[9] A. Wei, X.W. Sun, J.X. Wang, Y. Lei, X.P. Cai, C.M. Li, Z.L. Dong, W. Huang, "Enzymatic glucose biosensor based on ZnO nanorod array grown by hydrothermal decomposition", *Appl. Phys. Lett., 89* (12), 123902, **2006**

[10] Robert M. Hoffman, "In vitro sensitivity assays in cancer: A review, analysis, and prognosis". *Journal of Clinical Laboratory Analysis, 5,* (2), pp. 33–43, **1991**

[11] Puck TT, Marcus PI, "A rapid Method for Viable Cell Titration and Clone Production With HeLa Cells In Tissue Culture: The Use of X-Irradiated Cells to Supply Conditioning Factors", *Proc. Natl. Acad. Sci. USA, **1955** Jul. 15, 41* (7): 432-7. URL: PNASJSTOR

[12] N.A.P. Franken, H.M. Rodermond, J. Stap, J. Haveman, C. Van Bree, "Clonogenic assay of cells in vitro", *Nature Protocols, 1* (5), pp. 2315–9, **2006**

[13] A.W. Hamburger, "The Human Tumor Clonogenic Assay as a Model System in Cell Biology", *The International Journal of Cell Cloning*, *5*, (2), pp. 89–107, **1987**

[14] D.N. Carney, C.F. Winkler, "In vitro assays of chemotherapeutic sensitivity". *Important advances in oncology*, pp. 78–103, **1985**

[15] M. Lieber, G. Todaro, B. Smith, A. Szakal, W. Nelson-Rees, "A continuous tumor-cell line from a human lung carcinoma with properties of type II alveolar epithelial cells", *International Journal of Cancer, 17* (1), pp. 62-70, **1976**

[16] K. A. Foster, C.G. Oster, M.M. Mayer, M. L. Avery, K. L. Audus "Characterization of the A549 Cell Line as a Type II Pulmonary Epithelial Cell Model for Drug Metabolism", *Experimental Cell Research, 243* (2), pp. 359-366, **1998**

[17] D.J. Giard, S.A. Aaronson, G.J. Todaro, P. Arnstein, J.H. Kersey, H. Dosik, W.P. Parks, "In vitro cultivation of human tumors: Establishment of cell lines derived from a series of solid tumors", *Journal of the National Cancer Institute., 51* (5), pp. 1417–23, **1973**

[18] abcam.com. "A549 (Human lung adenocarcinoma epithelial cell line) Whole Cell Lysate (ab7910)". Retrieved 3 January 2012.

[19] ATCC.org. "A549 cell line: CCl-185 Product Description". Retrieved 3 January 2012.

[20] A. Cacchioli, F. Ravanetti, R. Alinovi, S. Pinelli, F. Rossi, M. Negri, E. Bedogni, M. Campanini, M. Galetti, M. Goldoni, P. Lagonegro, R. Alfieri, F. Bigi, and G. Salviati, "Cytocompatibility and Cellular Internalization Mechanisms of SiC/SiO_2 Nanowires", *Nanoletters, 14* (8), pp. 4368−4375, **2014**

[21] F. Rossi, E. Bedogni, F. Bigi, T. Rimoldi, L. Cristofolini, S. Pinelli, R. Alinovi, M. Negri, S.C. Dhanabalan, G. Attolini, et al "Porphyrin conjugated SiC/SiOx nanowires for X-ray-excited photodynamic therapy" *Scientific Reports, 5*, 7606, **2015**

[22] M. Sibrian-Vazquez, et al., "Peptide-Mediated Cell Transport of water Soluble Porphyrin Conjugates", *Journal of Medicinal Chemistry, 49,* (4), pp. 1364-1372, **2006**

[23] X. Yue, Z. Wang, L. Zhu, Y. Wang, C. Qian, Y. Ma, D.O. Kiesewetter, G. Niu, X. Chen, "Novel ^{19}F Activatable Probe for the Detenction of Matrix Metalloprotease-2 Activity by MRI/MRS" *Molecular Pharmaceutics, 11* (11), pp. 4208-4217, **2014**

Chapter 2

Synthesis of a novel hybrid nanosystem composed by core-shell SiC/SiOx nanowires conjugated with H_2TCPP-H_2TAPP porphyrins via amide bond

Introduction

Aiming to increase the efficiency of the nanosystem, we looked for a strategy to increase the thickness of the porphyrin monolayer to produce larger amount of singlet oxygen.

Thus, we designed to link H_2TCPP, conjugated to the nanowires according to the previously procedure, with H_2TAPP [*tetrakis*(4-aminophenyl)porphyrin] exploiting again the formation of an amide bond between the two porphyrins (Figure 1).

This chapter reports the preparation of another hybrid inorganic/organic nanosystem having a thicker porphyrin monolayer, as depicted in Figure 1.

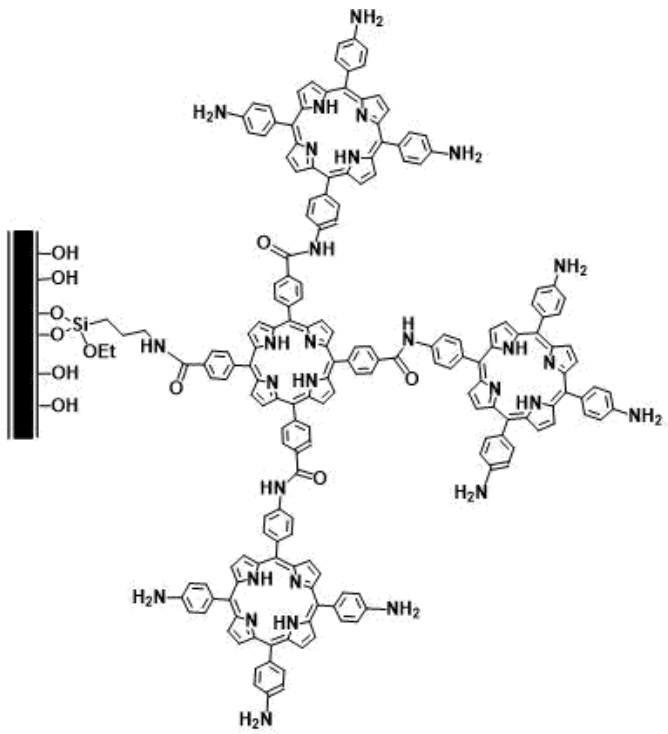

Figure 1*: Hybrid nanosystem based on the conjugation of H_2TCPP-H_2TAPP porphyrins*

As described in the previous chapter, H_2TCPP is a high versatile compound, due to the presence of four carboxylic functions on its phenyl rings, which allows different possibilities of functionalization.

First, H_2TCPP was conjugated to the SiC/SiOx nanowires through amide bond formation. The residual carboxylic functions, in the activated ester form, were reacted with the amino groups of the second porphyrin H_2TAPP. This conjugation strategy, as described in the previous chapter, allows to form stable amide bonds in very mild conditions. Indeed, in the literature it is reported that strong linkages, such as amide bond, are preferred for hydrolytically stable conjugates [102]

The *tetrakis*(4-aminophenyl)porphyrin (H_2TAPP) was chosen for the presence on its skeleton of four aminophenyl groups: even if aromatic amines are less nucleophilic than aliphatic ones, they should be able to react with the active esters on H_2TCPP forming amide bonds. Free remaining amino groups on H_2TAPP, on the other hand, are thought as functional to maintain a certain degree of dispersion of the whole nanosystem in the biological medium.

This novel nanosystem, containing two linked porphyrins conjugated to the nanowires, designed to increase the porphyrin loading on the nanowires and consequently an improved production of cytotoxic singlet oxygen, was successfully prepared.

Before carrying out these reactions on the nanowires, some preliminary studies were carried out in solution and on silica gel: First, preliminary studies were carried out in solution to test the reactivity of aromatic amines with an aromatic carboxylic group in the presence of coupling agents.

Then, the reaction was studied in heterogeneous phase, using silica gel as a substrate quite similar to the nanowires surface, able to be a good 'model' to study what can actually happen once reactions occur on nanowire surface.

Preliminary study 1: analysis of the reactivity of aromatic amines in the formation of a covalent amide bond with an aromatic carboxylic group

This preliminary study was carried out to test if it was possible to form a covalent amide bond between H_2TCPP and H_2TAPP porphyrins.

Alkyl amines are well known to be good nucleophilic compounds in the formation of covalent amide bonds, but it's not possible to state the same for aromatic amines.

In aliphatic amines the lone pair on the nitrogen atom can easily attack an electrophilic centre, like a C=C or carboxylic C=O bond, making them good nucleophilic compounds.

On the contrary, in aromatic amines, the lone pair on nitrogen atoms is involved in the resonance with other π-electrons, so is less likely to react, making them worse bases and nucleophiles with respect to their aliphatic counterpart.

Thus, we first studied the model reaction between benzoic acid and 4-bromo aniline. We choose 4-bromo aniline as amine in this reaction, due to the presence of an electron withdrawing group in its para position, that further reduces the nucleophilicity of the amino group. Such a compound is useful to mimic the reactivity of H_2TAPP, whose amino groups are less nucleophilic for the fact that phenyl rings are directly linked to the porphyrin skeleton, an electron withdrawing unit, on the whole.

On the other hand, benzoic acid was chosen as a model compound to mimic the behavior of carboxylic groups on H_2TCPP porphyrin.

A further study was carried out on H_2TCPP porphyrin itself, which was reacted with 4-bromoaniline to find out the optimal reaction conditions to convert the porphyrin carboxylic groups into amide derivatives.

Preliminary study 1a: synthesis of 4-bromo benzanilide

The first preliminary study that was carried out is the synthesis of the model compound 4-bromo benzanilide (Scheme 1):

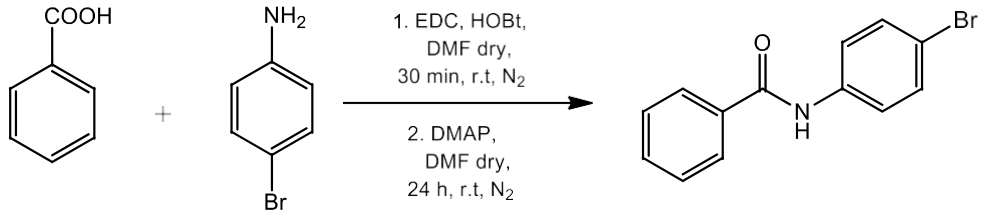

Scheme 1: *Synthesis of 4-bromo benzanilide*

In this reaction the carboxylic groups on benzoic acid were turned into active esters by means of condensing agents (EDC and HOBt). After 30 minutes DMAP and 4-bromo aniline were added. The reaction was carried out under nitrogen atmosphere to protect active esters from hydrolysis.
The crude didn't need a chromatographic purification: the product, a white solid, was obtained pure in good yields by precipitation in dichloromethane. ^{1}H NMR spectrum (400 MHz, DMSO d6) is reported below (Figures 1a and 1b). A zoom on the aromatic region is also showed for the sake of clarity.
The most diagnostic peak is the singlet of the amidic proton (violet circle, 10.37 ppm). On the other hand, COOH broad singlet disappeared, proving that benzoic acid was completely converted into amide. Other diagnostic peaks are those in the aromatic region, especially the doublets belonging to the para system (see orange and red circles, at lower fields since in ortho position with respect to bromine, and yellow and pink circles, more shielded by nearby amidic –NH).

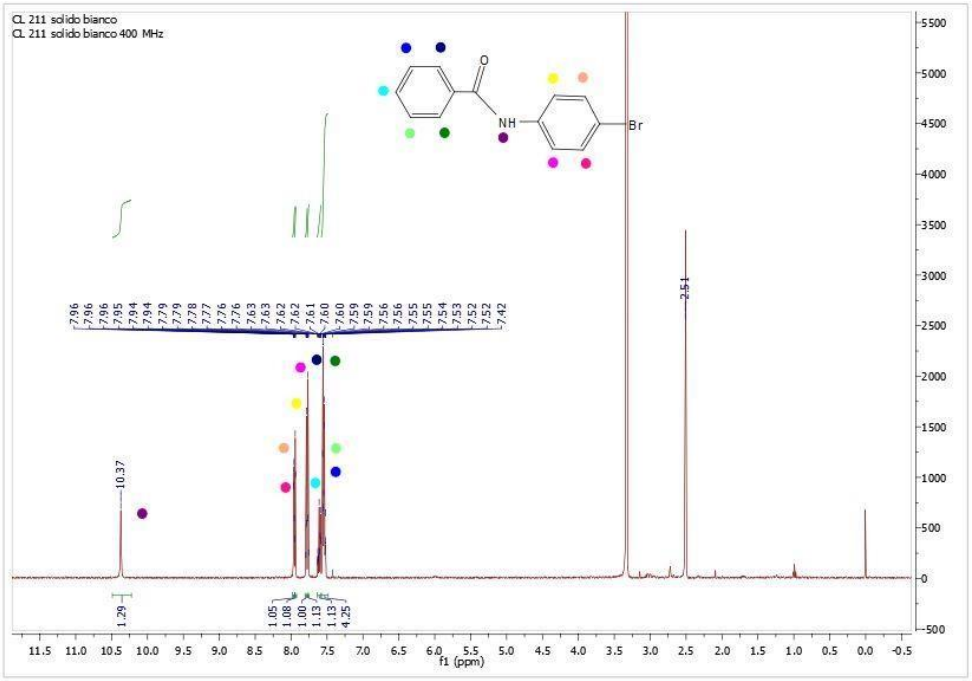

Figure 1a: *^{1}H NMR of 4-bromo benzanilide*

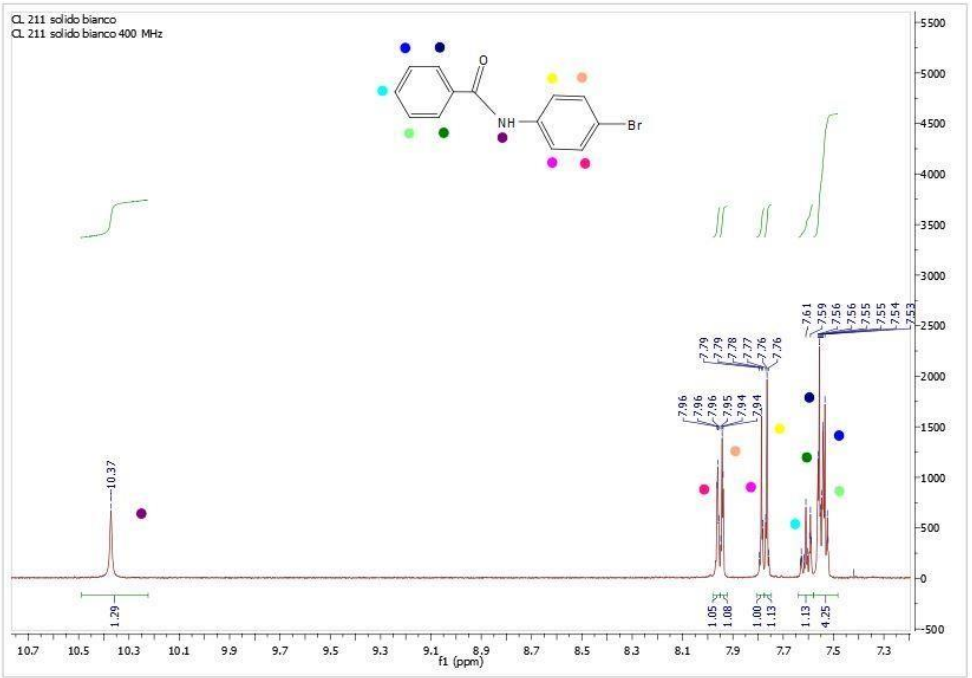

Figure 1a: *^{1}H NMR of 4-bromo benzanilide. Zoom on aromatic region*

Preliminary study 1b: synthesis of 5,10,15,20-Tetrakis[4-(4-bromobenzanilide)phenyl] porphyrin

The subsequent step to carry out the same reaction using H_2TCPP porphyrin to check the reactivity of the real substrate.

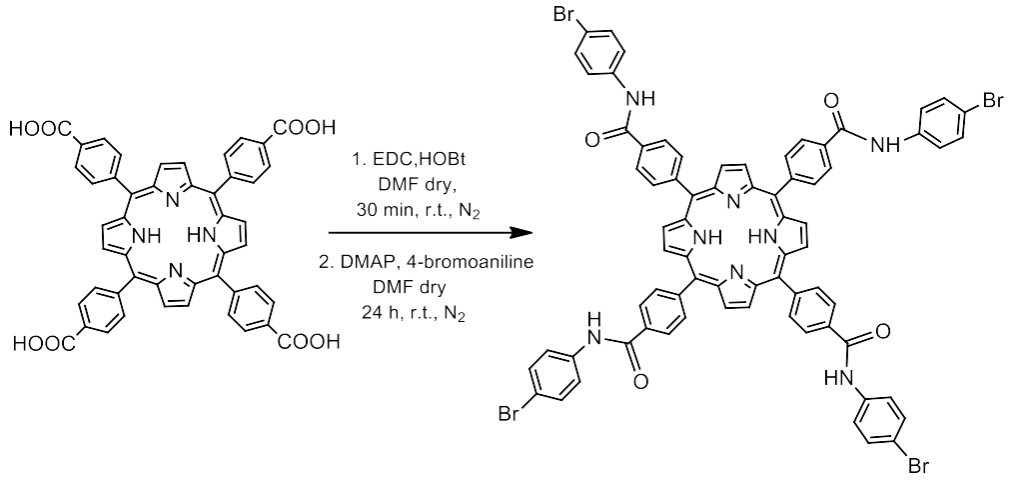

Scheme 2: *Synthesis of 5,10,15,20-Tetrakis[4-(4-bromobenzanilide)phenyl] porphyrin*

The reaction was carried out in the same conditions described above, to check eventual different reactivity of the different substrates. Coupling agents and 4-bromo aniline were employed in a three-fold excess with respect to the porphyrin, so that all its carboxylic functions could be involved in the formation of the amidic bond. Also in this case it was possible to isolate the product pure, although in modest yield (48
%), with no need of chromatographic purification. The crude was purified by multiple extractions with dichloromethane and water.
^{1}H NMR spectrum (400 MHz, DMSO d6) is reported below (Figure 2), showing the presence of the tetra substituted product. It is a quite simple spectrum, since the molecule is symmetric. The signals of porphyrin were

not altered and, at the same time, the signals of 4-bromo benzanilide are evident as two doublets typical of *para*-system (see light green and dark green circles).

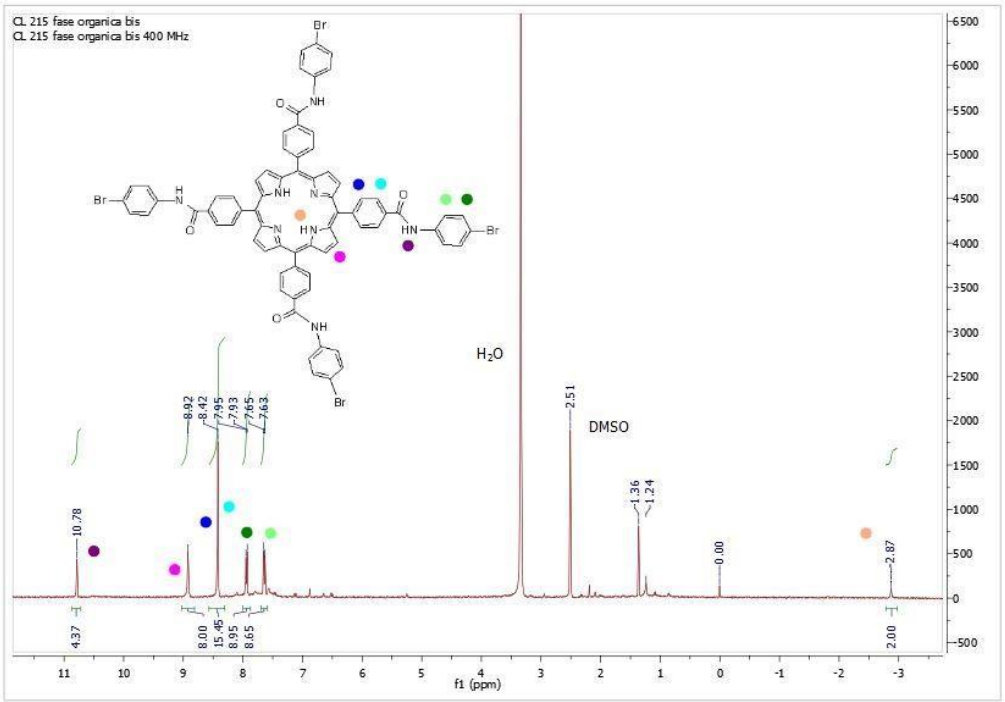

Figure 2: *^{1}H NMR of 5,10,15,20-Tetrakis[4-(4-bromobenzanilide)phenyl] porphyrin*

These preliminary studies encouraged us to try to couple H_2TAPP with H_2TCPP porphyrin exploiting the formation of a covalent and stable amide bond. We excluded the possibility to link the two different porphyrin before conjugation with the nanowires, because the formation of trimers, polymers or dendrimers were expected.

The purification of such a complex mixture of products would be too difficult and laborious. Thus, we designed to work in heterogeneous phase, i.e. first to conjugate the H_2TCPP porphyrins on the SiC/SiOx nanowires and then to link the other porphyrin (H_2TAPP) to the first one.

Before carrying out these reactions on the nanowires, however, we focused on another set of preliminary studies, consisting of reactions on silica gel (the same used for columns and chromatography).

Preliminary study 2: reactions on silica gel

This second set of preliminary studies aims to simulate what happens on the nanowires surface when the planned functionalization will be performed. Silica gel was chosen as a model solid support to mimic the behavior of nanowires. These tests were carried out to check if H_2TCPP and H_2TAPP porphyrins could be conjugated one to another directly on the nanowires surface.

The same reactions described in the previous part were carried out on silica gel with almost the same procedures, varying only some conditions according to each specific case.

As in the case of nanowires, silica gel needs activation to favor the functionalization.

Silica gel was activated by refluxing in concentrated HCl for 2 hours. The solid was then washed with water to neutral pH, then dried in the air and in a oven at 150°C.

The amino groups were introduced on silica gel by reacting the free hydroxy groups with (3-aminopropyl)triethoxysilane (APTES): this reaction was carried out at reflux in dry toluene, under inert atmosphere of nitrogen to avoid hydrolysis and autocondensation of the silane. This functionalization with APTES occurs by hydrolysis of the ethoxy groups and subsequent condensation with surface hydroxy groups, giving Si-O-Si bond formation. In the functionalization step, the carboxy groups on H_2TCPP, previously activated with condensing agents (EDC, HOBt and DMAP), were coupled to the amino functions on silica gel, affording the amide bond formation between the two partners.

After this step, the carboxy groups on the porphyrin, still in the form of active esters, were reacted with H_2TAPP, to form a bilayer of porphyrins on silica gel.

Further, we tested the reactivity of active esters on silica in different reactions: by hydrolyzing them to restore free carboxylic acids, reacting them with a simpler aliphatic amine (we chose butylamine), or with *tetrakis*(N-

carboxyphenyl) porphyrin (H_2THPP) to form esters.

Thermogravimetric analysis were carried out an all the samples prepared in order to evaluate the reaction outcomes by the loss of weight.
The TGA analysis showed that the treatment with water at room temperature to hydrolyze the remaining active ester after H_2TCPP conjugation on nanowires does not cause porphyrin loss, due to amide bond hydrolysis.
Then, it evidenced the successful reaction of linked porphyrin with the H_2TAPP and with H_2THPP (tetra(4-hydroxyphenyl)porphyrin).
Further, we could deduce that the amide bond between H_2TCPP and H_2TAPP
is stable under water treatment and that, on the contrary, the ester bond between H_2TCPP and H_2THPP is partially hydrolyzed.
The samples were also characterized by IR spectroscopy.

These preliminary studies were useful to understand the reactivity of H_2TCPP porphyrin once they it is anchored on a silica support. Basing on reported results, we tried to carry put the same reactions on nanowires.
In particular, this chapter is focused on the preparation of a nanosystem with a thicker porphyrin coating, a bilayer of H_2TCPP and H_2TAPP porphyrins, which were linked together operating directly on the nanowires surface (Figure 3).
Also in this case, all the reactions were carried out leaving the nanowires attached on their Si solid support. The silica shell surface of the nanowires was activated by refluxing the wafers in concentrated HCl for 2 hours. The sample was then washed with water to neutral pH, then with ethanol, and finally dried in the air.
The amino groups were introduced on the nanowires surface by reacting the free hydroxy groups with (3-aminopropyl)triethoxysilane (APTES): the reaction was carried out at reflux in dry toluene, under inert atmosphere of nitrogen to avoid hydrolysis and condensation of the silane. This functionalization with APTES occurs by hydrolysis of the ethoxy groups and subsequent condensation with surface hydroxy groups, giving Si-O-Si bond formation. The reaction was repeated twice, washing the wafer with dry toluene and acetone between the first reaction and the second one. In the third step the carboxy groups on H_2TCPP, previously activated with

condensing agents (EDC, HOBt and DMAP), were coupled to the amino functions on the nanowires, leading to amide bond formation between the two partners. In the last step, remaining active esters on H_2TCPP were reacted with an excess of H_2TAPP porphyrin.

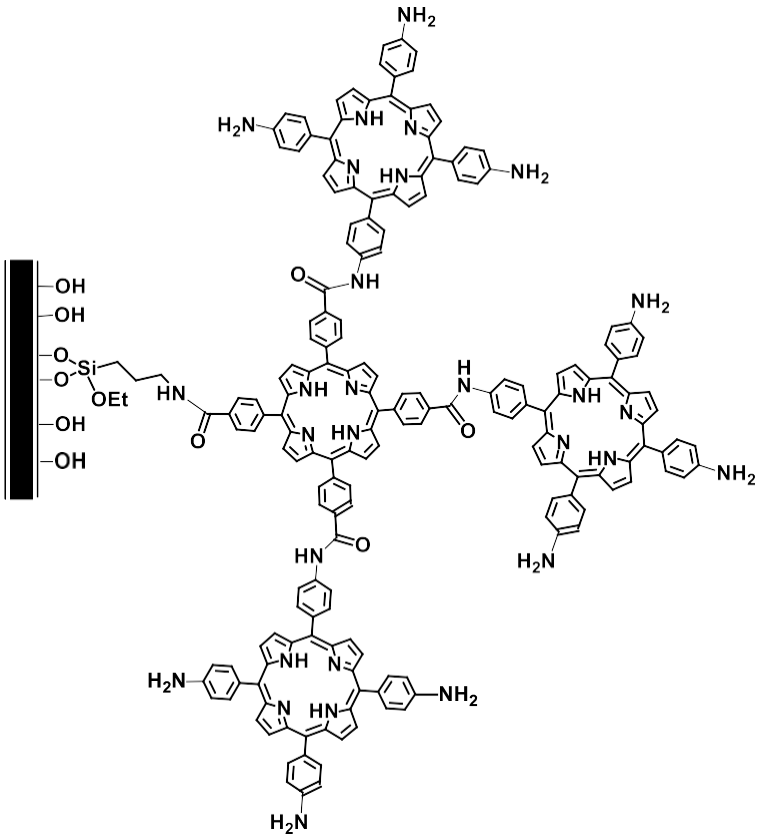

Figure 3: *Nanosystem containing H_2TCPP-H_2TAPP conjugated to SiC/SiOx nanowires*

This novel hybrid nanosystem was characterized by fluorescence spectroscopy, employing a laser at 473 nm as excitation source. This radiation, as stated in the previous chapter, is able to excite both the SiC in nanowires and the porphyrin fluorescence. The high fluorescence of

porphyrin, with respect to that of SiC, indicates that the functionalization occurred successfully (Figure 4).

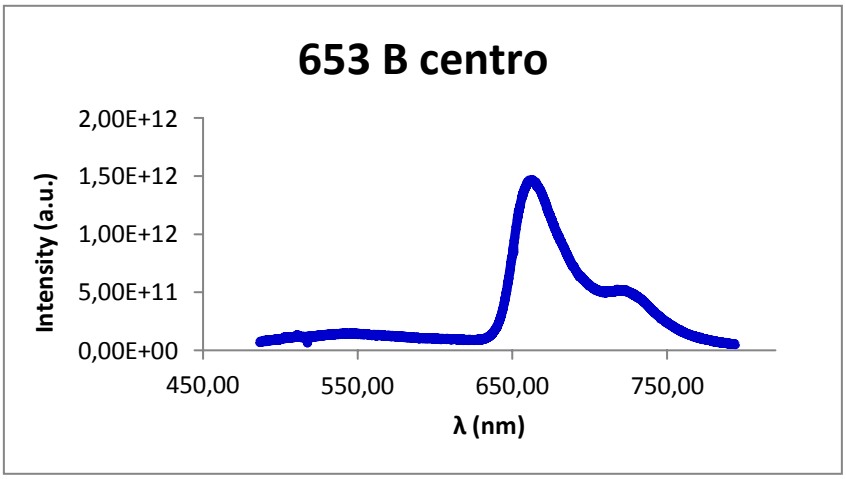

***Figure 4**: Fluorescence spectrum of the nanosystem based on H_2TCPP and H_2TAPP porphyrins*

The cytotoxic activity of this new nanosystem will be examined with *in vitro* tests.

Experimental section-preliminary study 1a

Synthesis of 4-bromo benzanilide

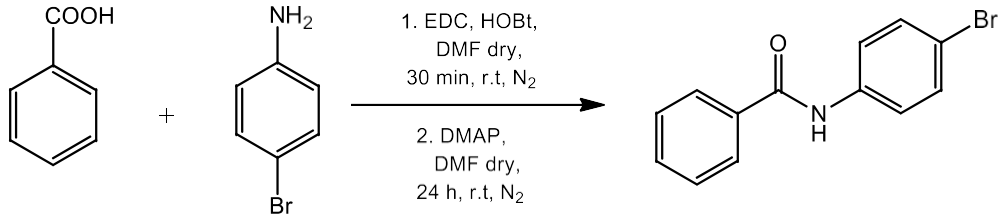

Benzoic acid (200 mg, 1.638 mmol) was introduced in a two-necked 50 ml round bottom flask, previously dried with 3 vacuum-nitrogen cycles, and dissolved in10 ml of dry DMF. Condensing agents EDC (314 mg, 1.638 mmol) and HOBt (221.3 mg,1.638 mmol) were then added and the mixture was stirred for 30 minutes at room temperature, under nitrogen.
After that, DMAP (20 mg, 0.1638 mmol) and 4-bromo aniline (280.4 mg, 1.638 mmol) were added and the mixture was stirred at room temperature for 24 hours.
The reaction was monitored via TLC (DCM:acetone = 9:1). DMF was removed at the vacuum pump and the crude was dissolved in dichloromethane: a white solid precipitated, and it was collected by filtration on a Buchner funnel. The product was obtained as a white solid (284.91 mg, 63 % yield)

^{1}H NMR (400 MHz, DMSO d6)

δ(ppm)= 10.37 (s, 1H, NH), 7.96 (d, 1H, Har, ortho Br), 7.94 (d; 1H, Har, ortho Br), 7.79 (d, 1H, Har, ortho NH), 7.76 (d, 1H, Har, ortho NH), 7.62 (m, 1H, Har), 7.56 (m, 4H, Har)

Synthesis of
5,10,15,20-Tetrakis[4-(4-bromobenzanilide)phenyl] porphyrin

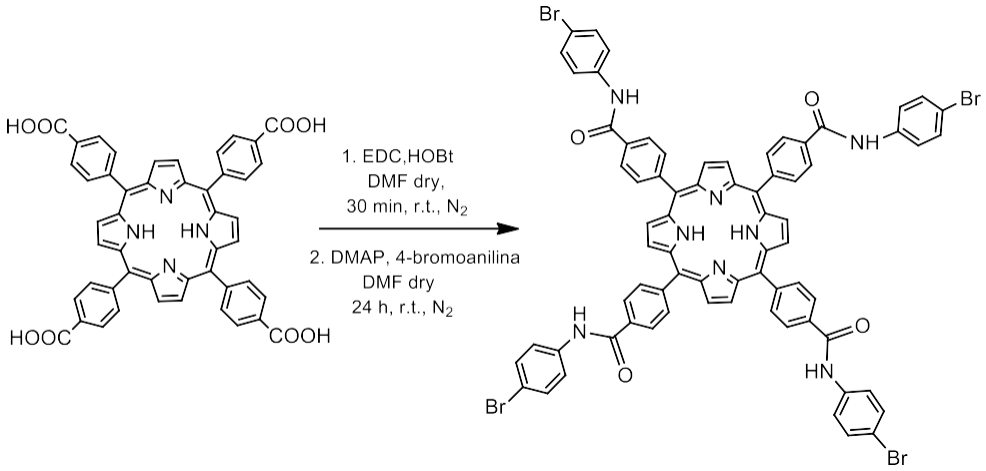

H_2TCPP (300 mg, 0.3729 mmol), was introduced in a 100 ml two-necked round bottom flask, previously dried with three vacuum-nitrogen cycles and dissolved in 25 ml of dry DMF. EDC (872.4 mg, 4.552 mmol) and HOBt (615.1 mg, 4.552 mmol) were added and the reaction was stirred at room temperature for 30 minutes, under nitrogen. DMAP (556.2 mg, 4.552 mmol) and 4-bromo aniline (783.1 mg, 4.552 mmol) were then added and the reaction was stirred at room temperature for 24 hours.
The reaction was monitored via TLC (AcOEt:MeOH = 15:1).
DMF was evaporated at the vacuum pump and the raw was dissolved in DCM, then washed three times with distilled water. The organic phase was dried over anhydrous Na_2SO_4, then filtered and the solvent evaporated at the rotary evaporator. The crude was dissolved in the least amount of THF, then precipitated by addition of distilled water. The solid was collected by filtration over a Buchner funnel, thus yielding the product as a purple solid (258 mg, 48 % yield).

^{1}H NMR (400 MHz, DMSO d6)

δ(ppm) = 10.78 (s, 1H, amidic NH), 8.92 (s, 8H, pyrrolic H), 8.42 (s, 16 H, Har, Ph), 7.94 (d, 8H, Har, ortho Br), 7.64 (d, 8H, Har, ortho NH), -2.87 (s, 2H, pyrrolic NH)

MALDI-TOF MS
Matrix: alpha-cyano-4-hydroxycinnamic acid

m/z calculated: 1407,14
m/z experimental: 1407,17

Experimental section-preliminary studies 2

Activation of silica gel

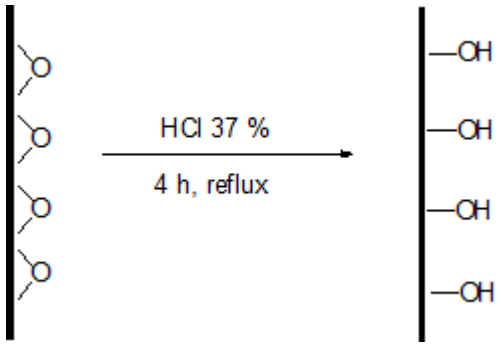

Silica gel (20.4 g, 0.040-0.063 mesh) and hydrochloric acid (70 ml) were introduced in a 250 ml round bottom flask.
The mixture was refluxed at 120°C for four hours under vigorous stirring. The suspension was then cooled to room temperature and filtered on a Buchner funnel. The resulting white solid was washed with distilled water to neutral pH, then it was dried in a crystallizer for two hours and finally in an oven at 150°C for 24 hours.

Functionalization of activated silica gel with 3-aminopropyl triethoxysilane

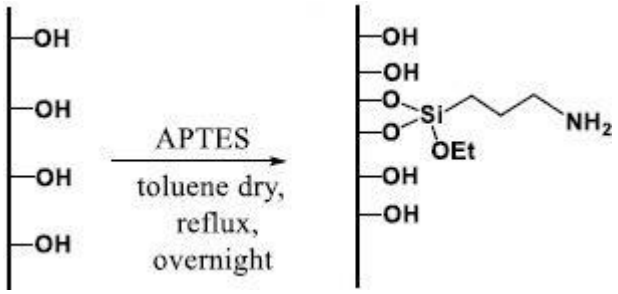

Previously activated silica gel (5 g) and 30 ml of toluene were introduced in a 100 ml flask, equipped with a condenser. The mixture was refluxed for an hour, under stirring. Then, the suspension was cooled and the condenser was quickly changed with a new one. APTES (10 mmol, dissolved in 3-4 ml of toluene) was introduced through the flask and the mixture was refluxed for an hour. After that, the alcoholic product (ethanol) was distilled away, then the suspension was refluxed for another hour. Further 3 ml of alcohol were distilled again and the mixture was refluxed for half an hour.

After that, the resulting suspension was cooled and filtered on a Buchner funnel: the white solid was washed with toluene (2x25 ml) and dichloromethane (2x25 ml), then dried at the vacuum pump.

Functionalization of silica gel with H_2TCPP porphyrin

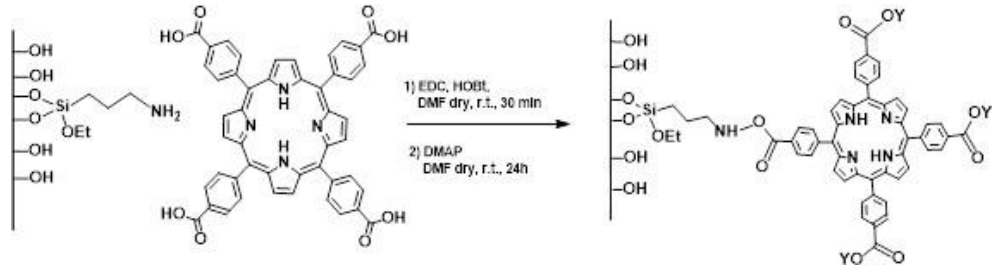

H_2TCPP (296.5 mg, 0.375 mmol) was introduced in a 100 ml two-necked round bottom flask, previously dried with 3 vacuum-nitrogen cycles, and dissolved in 20 ml of dry DMF. Condensing agents EDC (424 mg, 2.123 mmol) and HOBt (283.7 mg, 2.1 mmol) were then added and the mixture was stirred at room temperature for 30 minutes, under nitrogen flux. After that, silica gel functionalized with APTES (500 mg) was added, together with DMAP (398.5 mg, 3.263 mmol).

The mixture was vigorously stirred overnight at room temperature. The suspension was then filtered under nitrogen and washed with dry DMF. The resulting solid was centrifugated three times (5 min x 5000 rpm) under nitrogen, and repeatedly washed with dry DMF. After washing, the solid was immediately employed in the next step and functionalized in different ways.

Functionalization of silica gel with H_2TAPP porphyrin

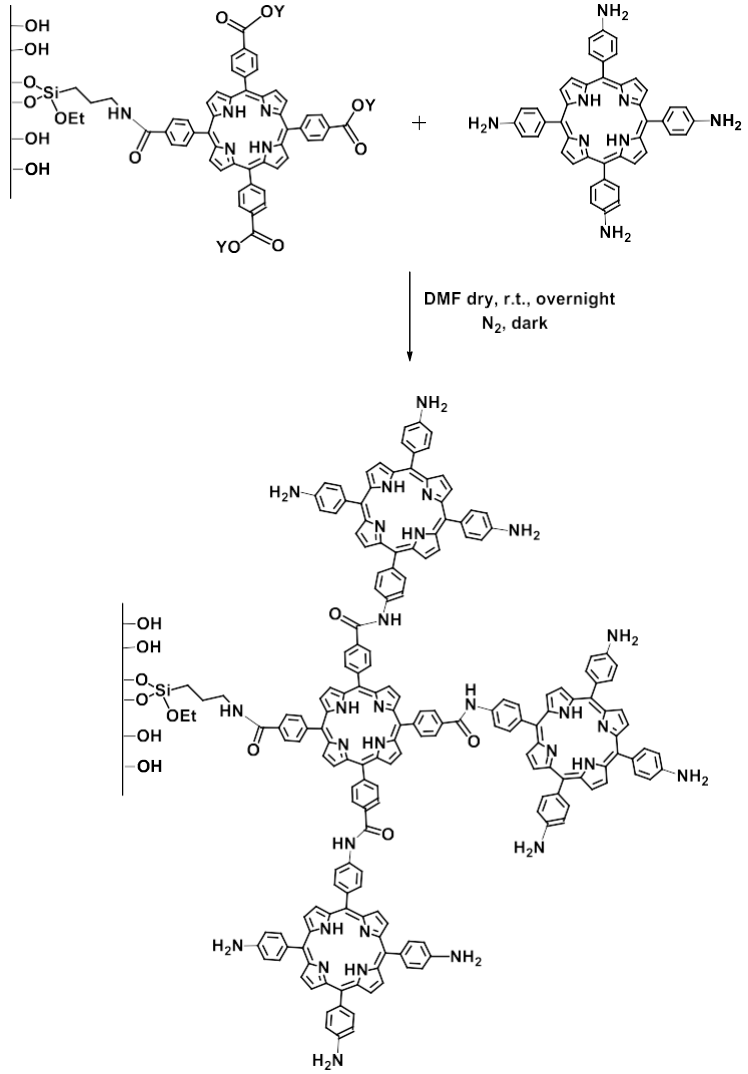

Silica gel functionalized with APTES and H_2TCPP (100 mg) was introduced in a 25 ml two-necked round bottom flask, previously dried with three vacuum-nitrogen cycles, and dispersed in 10 ml of dry DMF. H_2TAPP (5 mg,

0.0074 mmol) was added and the mixture stirred overnight at room temperature, under nitrogen and covered with tinfoils. The resulting solid was centrifugated twice in DMF (5 min x 5000 rpm), twice in water (5 min x 5000 rpm) and twice in acetone (5 min x 5000 rpm).
The solid was then dried and analyzed by TGA analysis.

Functionalization of porphyrin on silica gel with butylamine

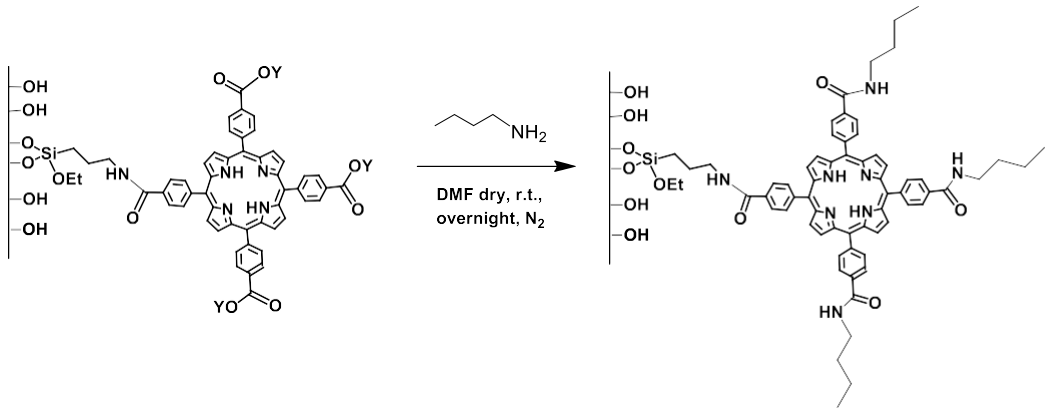

Silica gel functionalized with APTES and H_2TCPP (100 mg) was introduced in a 25 ml two-necked round bottom flask, previously dried with three vacuum-nitrogen cycles, and dispersed in 10 ml of dry DMF. Butylamine (50 μL) was added and the mixture stirred overnight at room temperature, under nitrogen. The resulting solid was centrifugated twice in DMF (5 min x 5000 rpm), twice in water (5 min x 5000 rpm) and twice in acetone (5 min x 5000 rpm).
The sample was then dried and analyzed by TGA.

Hydrolysis of remaining active esters of H_2TCPP on silica

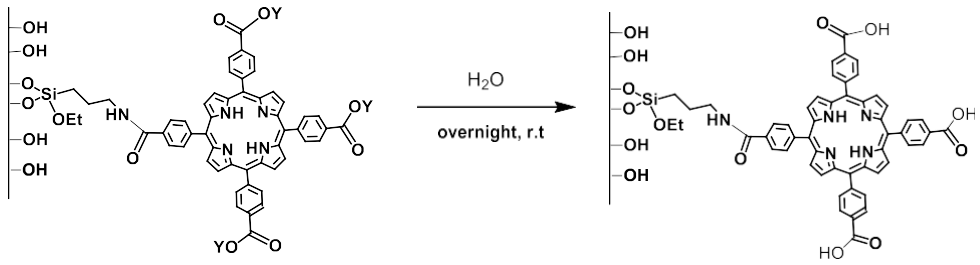

Silica gel functionalized with APTES and H_2TCPP (100 mg) was introduced in a 25 ml two-necked round bottom flask, previously dried with three vacuum-nitrogen cycles, and dispersed in 10 ml of dry DMF. Distilled water (5 ml) was added and the mixture stirred overnight at room temperature. The resulting solid was centrifugated twice in DMF (5 min x 5000 rpm), twice in water (5 min x 5000 rpm) and twice in acetone (5 min x 5000 rpm).
The sample was then dried and analyzed by TGA.

Functionalization with H_2THPP porphyrin

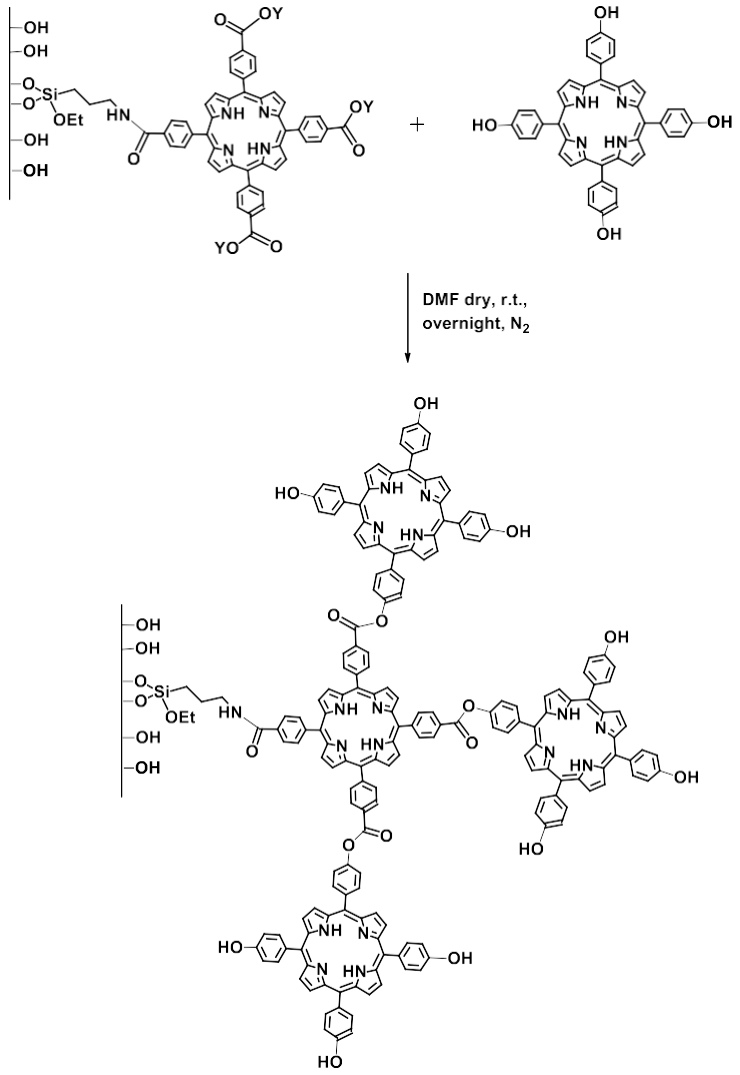

Silica gel functionalized with APTES and conjugated H_2TCPP (100 mg) was introduced in a 25 ml two-necked round bottom flask, previously dried with three vacuum-nitrogen cycles, and dispersed in 10 ml of dry DMF. H_2THPP (10 mg, 0.0147 mmol) was added and the mixture stirred overnight at room temperature, under nitrogen. The resulting solid was centrifugated twice in

DMF (5 min x 5000 rpm), twice in water (5 min x 5000 rpm) and twice in acetone (5 min x 5000 rpm).
The solid was then dried and analyzed by TGA

Conjugation of the nanowires with H_2TCPP-H_2TAPP porphyrins

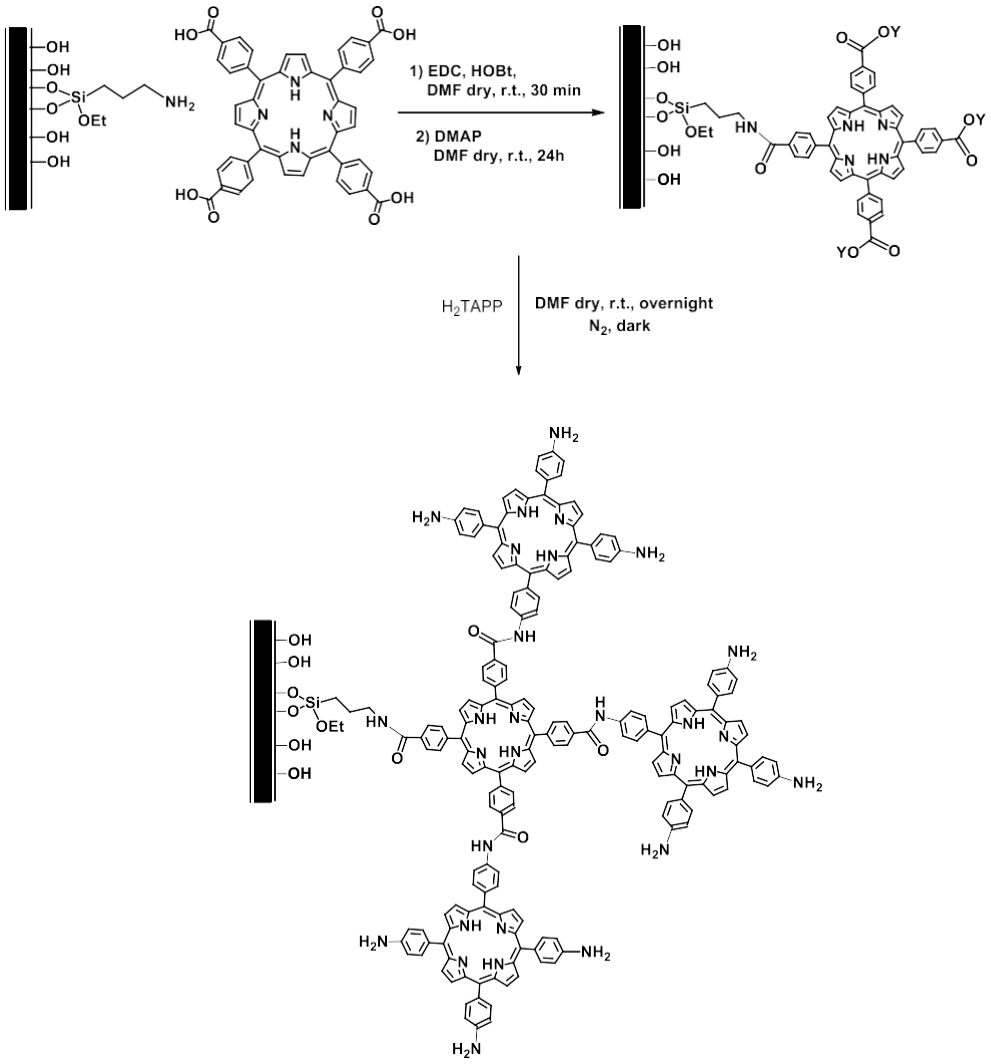

After activation with boiling conc. HCl, the NWs were reacted with APTES (4 μL of a 5mM solution in dry toluene) by refluxing the system in dry toluene (T ≥ 120°C) overnight.

Then H_2TCPP porphyrin (10.4 mg, 0.0132 mmol) was introduced in a 50 ml two-necked round bottom flask, previously dried with three vacuum/nitrogen cycles, and dissolved in 3 ml of dry DMF. EDC (15 mg, 0.0787 mmol) and HOBt (10 mg, 0.0740 mmol) were added and the mixture was stirred for 30 minutes under nitrogen. After that, the wafer covered by the nanowires was introduced and DMAP (14 mg, 0.1146 mmol) was added, together with further 4 ml of anhydrous DMF. The reaction mixture was stirred overnight at room temperature, under nitrogen atmosphere. After that time, the red solution was completely removed from the flask and the wafer was washed several times with dry DMF, until the solution was colorless. The wafer was then covered with 6 ml of anhydrous DMF and a solution of H_2TAPP in dry DMF was added. The flask containing the wafer was then covered with tinfoils to darken it and the reaction was left overnight at room temperature, under stirring and under nitrogen atmosphere.

The wafer was washed very well with DMF, until the solution was colorless, then transferred into a 50 ml round bottom flask and washed with water for about four hours. After that, it was washed with ethanol, dried and stored in the dark at 4°C.

The nanowires were finally detached from their support by sonication in ethanol with an ultrasound microtip (Misonix Sonicator). The suspension of nanowires in ethanol was then divided into many Eppendorf tubes and was centrifugated (14.000 rpm, 10-15 min). The precipitated nanowires were recovered and collected, then dried in the air, covered with a glass funnel and kept in the dark.

Chapter 3

Determination of porphyrin loading on SiC/SiOx nanowires

Introduction

The evaluation of the porphyrin amount bound to SiC/SiOx nanowires is an important issue in the frame of X-Ray-excited Photodynamic Therapy. Porphyrins, in fact, act as photosensitizers in our nanosystem, and are responsible for the amount of singlet oxygen which can be produced in the process: this cytotoxic agent determines the success of the nanosystem in killing cancer cells.

The amount of oxygen produced in X-PDT is directly related to the amount of photosensitizer in the whole nanosystem: thus, it is very important to know how much porphyrin is bound to the nanowires.

A quantitative analysis of charged porphyrin, however, is not simple and can't be carried out with traditional methods, like elemental analysis, for instance. A possible strategy would be that of considering the number of nitrogen atoms before and after the reaction of the nanowires with H_2TCPP porphyrin: such a strategy, however is neither simple nor precise, due to the huge number of nitrogen atoms in the whole nanosystem. For these reasons we considered other possible paths to determine the amount of loaded porphyrin on nanowires. We thought that an interesting strategy could be a kind of "indirect" quantification of a metal porphyrin exploiting an atomic absorption measure of the metal. We planned to synthesize a metal porphyrin, starting from *tetrakis*(4-carboxyphenyl) porphyrin, the compound that we usually conjugate to nanowires. The choice of a suitable metal, however, is crucial: it must fit the porphyrin cavity and it must be robust enough so that the final complex might not easily release the metal. For this reason we ruled out zinc, since it can be easily removed in mild conditions (e.g. slightly acidic environment) or simply over time.

After searching in the literature, we thought that copper could be a proper choice: copper porphyrins, in fact, are easy to be synthesized, while can't be easily demetallated under mild conditions. The only way to completely remove copper from a porphyrin cavity is the acidic treatment with concentrated sulfuric acid: no other acid works well for this purpose.

Results and discussion

The idea at the base of this study is to prepare a nanosystem containing a Cu(II) porphyrin (Figure 1): we planned to carry out all the reactions leaving the nanowires attached on their metallic support, but employing CuTCPP instead of H_2TCPP porphyrin.
The functionalized nanowires, after detaching from their support, were dispersed in concentrated H_2SO_4, in order to remove Cu(II) from the conjugated porphyrin, then centrifugated and washed with water more times. The resulting supernatant, an acidic solution of Cu(II), was collected into flasks and analyzed by atomic absorption spectroscopy.

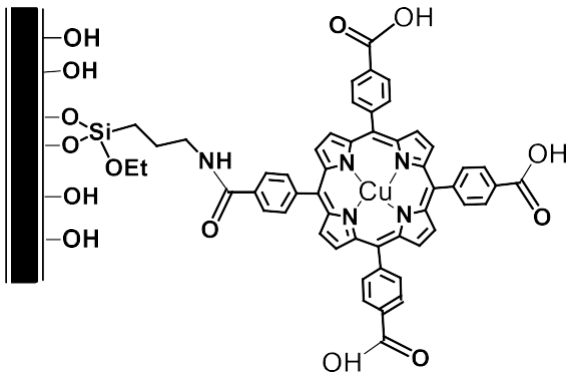

Figure 1: *Cu(II)TCPP porphyrin bound to SiC/SiOx nanowires*

The Cu(II) *tetrakis*(4-carboxyphenyl) porphyrin was synthetized as reported in Scheme 1.

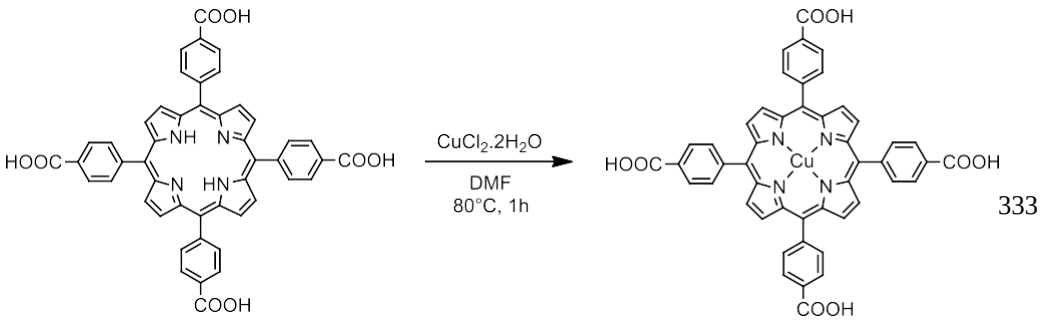

333

Scheme 1: *Synthesis of Cu(II)TCPP porphyrin*

The metal compound can be easily prepared starting from commercial *tetrakis*(4-carboxyphenyl)porphyrin and $CuCl_2$. $2H_2O$. The reaction was carried out in DMF at 80°C for an hour and a red solution was observed in the flask. The solvent was removed by distillation and the solid was obtained by simple precipitation from acetone, without any chromatographic purification, in 76% yield.

Since the porphyrin contains paramagnetic Cu(II), it is not possible a characterization by ^{1}H NMR spectroscopy. The compound was analyzed with UV-VIS and fluorescence spectroscopy in solution (Figures 2 and 3).

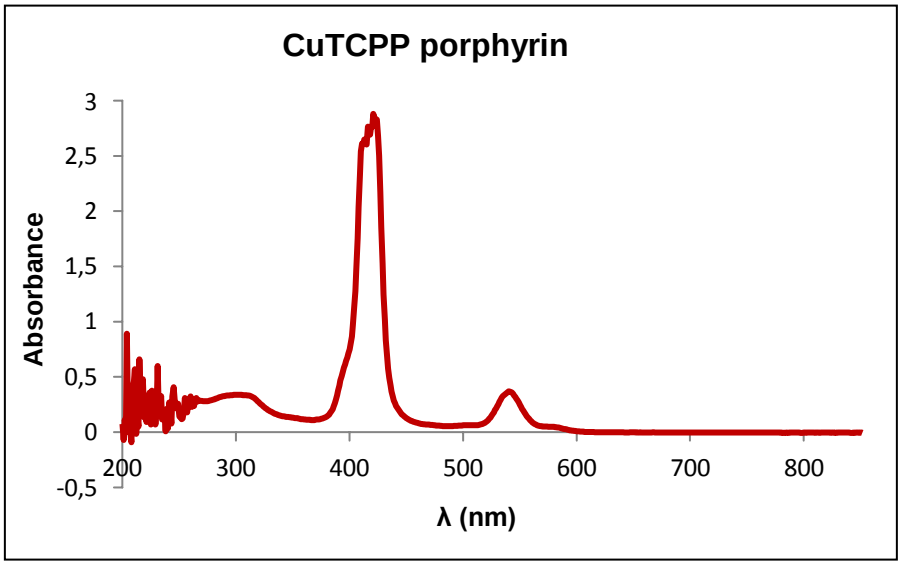

***Figure 2**: UV-VIS spectrum of CuTCPP*

UV-VIS shows the presence of only one Q band at 546 nm, with a poor visible shoulder, instead of four Q bands of non-metal porphyrin, proving that the reaction was carried out successfully.

Another confirm of the copper salification was given by fluorescence spectrum, which shows a complete quenching of fluorescence: this phenomenon is well-known for copper metal compounds and porphyrins are not an exception in this frame.

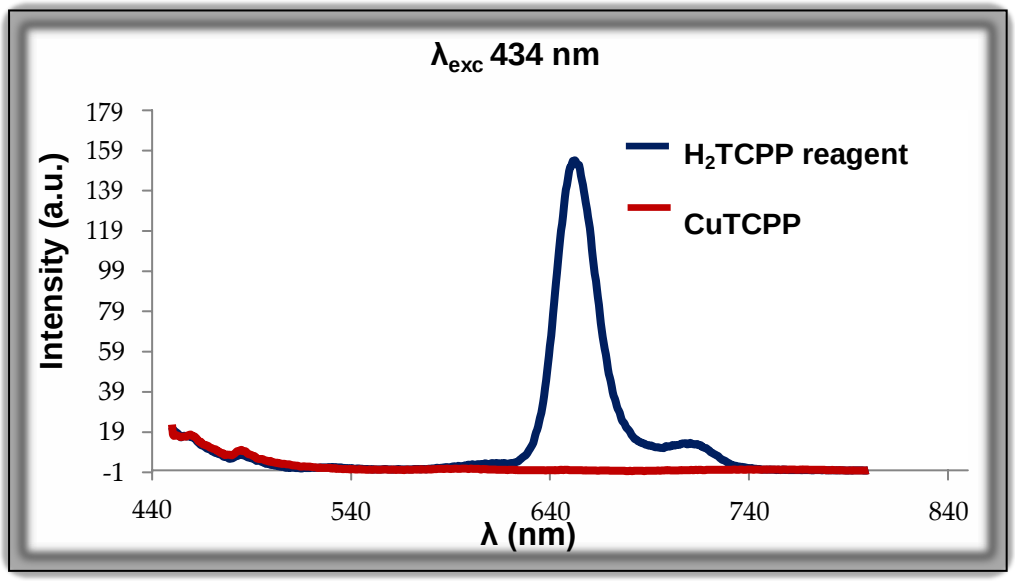

***Figure 3**: Fluorescence spectra of H_2TCPP and CuTCPP*

Copper-porphyrin was then incorporated into the nanosystem. Also in this case, all the reactions involving the nanowires were carried out leaving them attached to their Si solid support. The nanowires were activated by refluxing the wafers in concentrated HCl for 2 hours. The plate was then washed with water to neutral pH, then with ethanol, and finally dried in the air.

The amino groups were introduced on the nanowires surface by reacting the free hydroxy groups with (3-aminopropyl)triethoxysilane (APTES): the reaction was carried out at reflux in dry toluene, under inert atmosphere of nitrogen. The reaction was repeated twice, washing the wafer with dry toluene and acetone between the first reaction and the second one. In the third step the carboxy groups of CuTCPP, previously activated with condensing agents (EDC, HOBt and DMAP), were coupled to the amino functions on the nanowires, leading to amide bond formation.

In the last step, the residual active esters of CuTCPP were hydrolyzed with distilled water to restore carboxylic functions on porphyrin (Scheme 2).

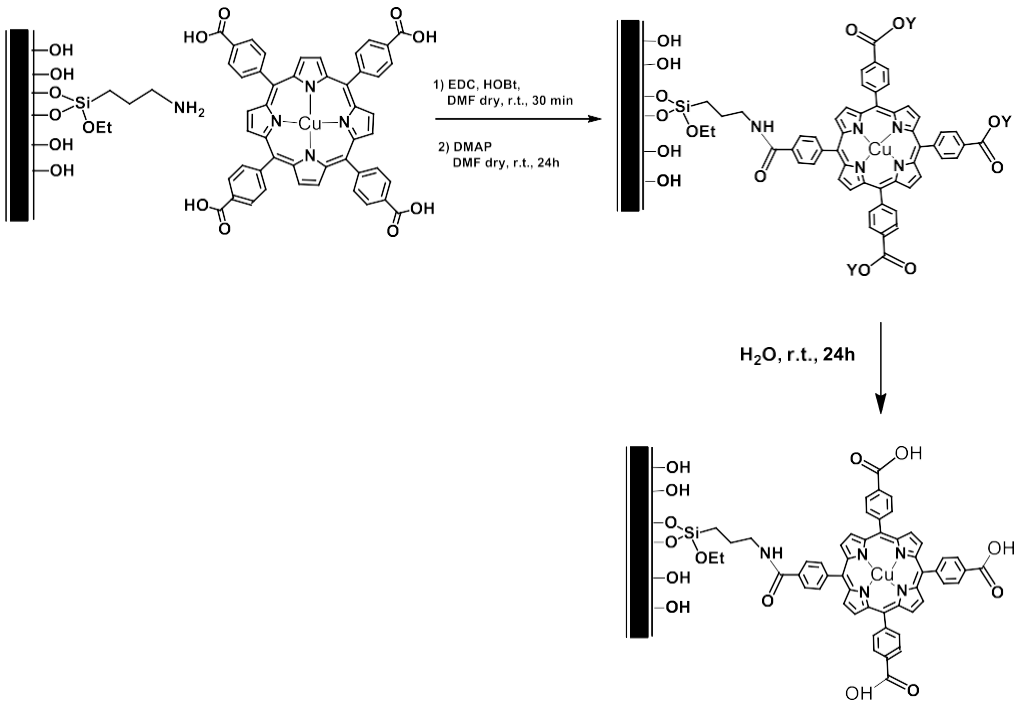

Scheme 2: *Preparation of the nanosystem containing Cu(II)TCPP porphyrin*

For this nanosystem it was not possible to check the success of conjugation carrying out an analysis with fluorescence spectroscopy at the solid state, since this is quenched by copper. Indeed, we verified that the fluorescence was quenched by copper.

To overcome this difficulty, we decided to analyze the functionalized nanosystem by removing copper from porphyrin.

A preliminary attempt to check the presence of CuTCPP on the nanowires was performed employing concentrated nitric acid, but only a partial removal of copper was observed.

Considering that the most convenient way to remove copper from porphyrin is to use concentrated sulfuric acid, we dipped the wafer with CuTCPP functionalized nanowires in concentrated H_2SO_4 (97%): in a few minutes, the solution became green, thus indicating that copper was removed from porphyrin.
Curious of knowing what happened to the nanowires on the plate, we tried to record another fluorescence spectrum, which showed that nanowires were fluorescent after copper removal. This was an important result, which allowed us to know that it was possible to de-metallate porphyrin once bound to the nanowires, without spoiling them with an acidic treatment.

Prompted by this good result, we managed to apply the same treatment on detached nanowires.
Functionalized nanowires, as usual, were detached from their metallic support by sonicating them in ethanol with an ultrasound microtip (Misonix Sonicator).
The obtained suspension was centrifugated many times, then the resulting nanowires were collected in an eppendorf, dried and weighed. The nanowires were dispersed in concentrated H_2SO_4 (97%) that instantly turned green (Figure 4). Then water was added and the resulting suspension was centrifugated many times, till to reach a 5% v/v acid solution. his solution, which contains free Cu(II) ions, was transferred in calibrated vessels and then analyzed by atomic absorption spectroscopy.

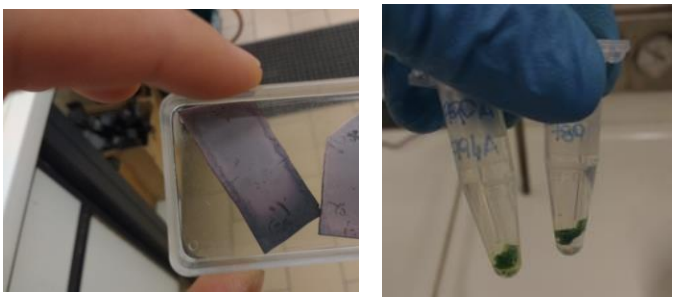

Figure 4*: Nanowires on their metallic supports (before acidic treatment, left) and detached (after acidic treatment, right)*

Experimental section:

Synthesis of Cu(II) 5,10,15,20-Tetrakis(4-carboxyphenyl)porphyrin

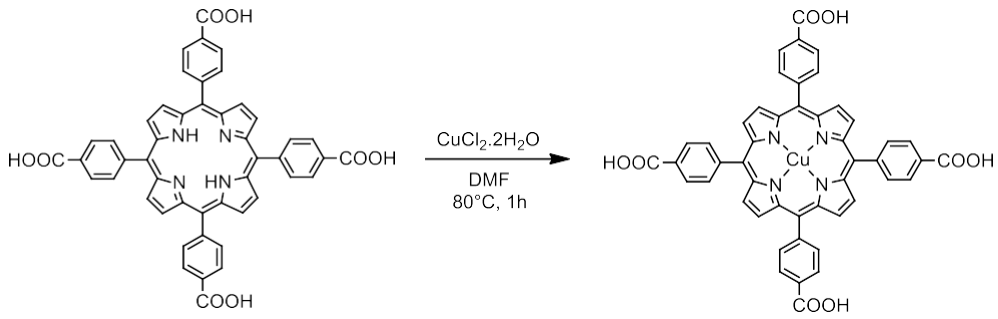

$CuCl_2.2H_2O$ (118 mg, 0.6955 mmol) was introduced in a 100 ml round bottom flask and dissolved in 5 ml of DMF. The resulting yellow solution was stirred for a few minutes, then H_2TCPP porphyrin (100 mg, 0.1265 mmol), dissolved in 25 ml of DMF, was added. The mixture was stirred for an hour at 80°C, then DMF was removed by distillation. The crude was dissolved in the least amount of DMF and recrystallized by addition of acetone. The flask was left overnight at -20°C, then the resulting solid was filtered on a Buchner funnel, washed several times with acetone and dried. Dark red solid, 82.3 mg, 76% yield.

UV-VIS (DMF)
λ max = 427 nm
λ = 546 nm (Q band)

MALDI-TOF MS
Matrix: alpha-cyano-4-hydroxycinnamic acid

m/z calculated: 852,34
m/z experimental: 852,07

Functionalization of the nanowires with Cu(II) 5,10,15,20-Tetrakis (4-carboxyphenyl)porphyrin

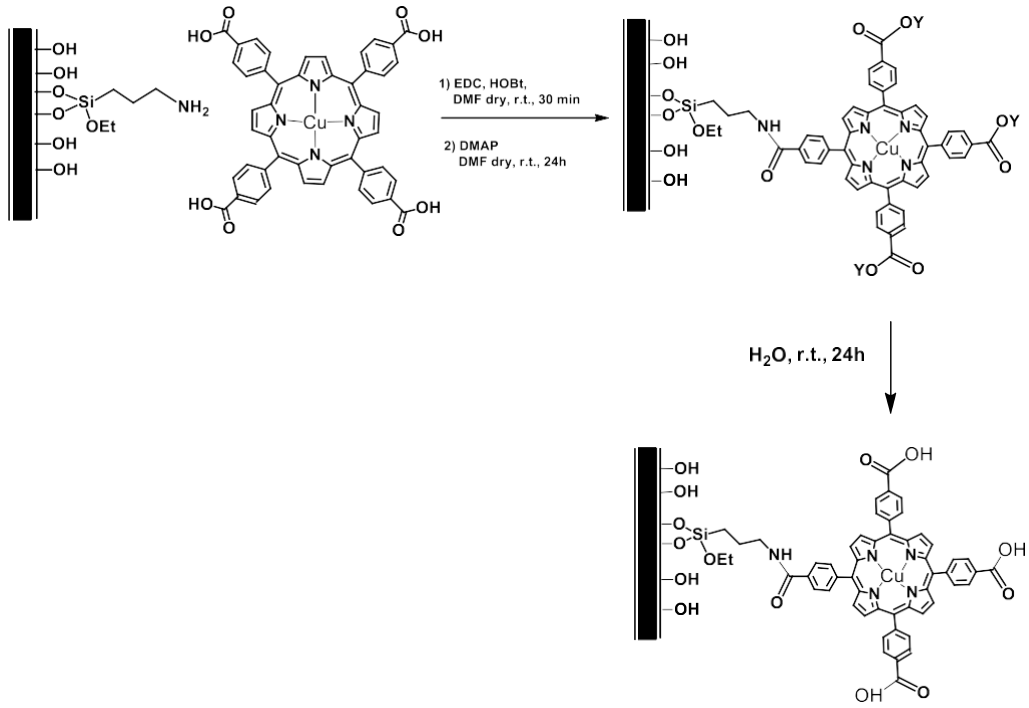

As previously described, activated nanowires were reacted with APTES in dry toluene to introduce amino functions.

Then, CuTCPP porphyrin (10.4 mg, 0.012 mmol) was introduced in a 50 ml two-necked round bottom flask, previously dried with three vacuum/nitrogen cycles, and dissolved in 3 ml of dry DMF. EDCI (15 mg, 0.0787 mmol) and HOBt (10 mg, 0.0740 mmol) were added and the mixture was stirred for 30 minutes under nitrogen. After that, the wafer covered by the nanowires was introduced and DMAP (14 mg, 0.1146 mmol) was added, together with further 4 ml of anhydrous DMF. The reaction mixture was stirred at room temperature for 24 hours under nitrogen flux. After that time, the wafer was removed from the flask and washed with

DMF and water, then was put into another flask and covered with distilled water, in order to hydrolyze active esters of porphyrin. The reaction was stirred at room temperature for 8 hours, then the nanowires were washed with further distilled water, ethanol and dried in the air.
The nanowires were detached from the support by sonicating the wafers in ethanol with an ultrasound microtip (Misonix Sonicator): the suspension of nanowires in ethanol was then divided into many Eppendorf tubes and was centrifugated (14.000 rpm, 10-15 min). The precipitated nanowires were finally recovered and collected in one Eppendorf, then dried in the air and weighted.

TEM analysis of nanowires functionalized with CuTCPP porphyrin

In order to check the presence of Cu in the previously illustrated nanosystem, a wafer containing nanowires functionalized with CuTCPP porphyrin was analyzed by TEM spectroscopy.
EDX spectra are here reported in Figures 5a and 5b.

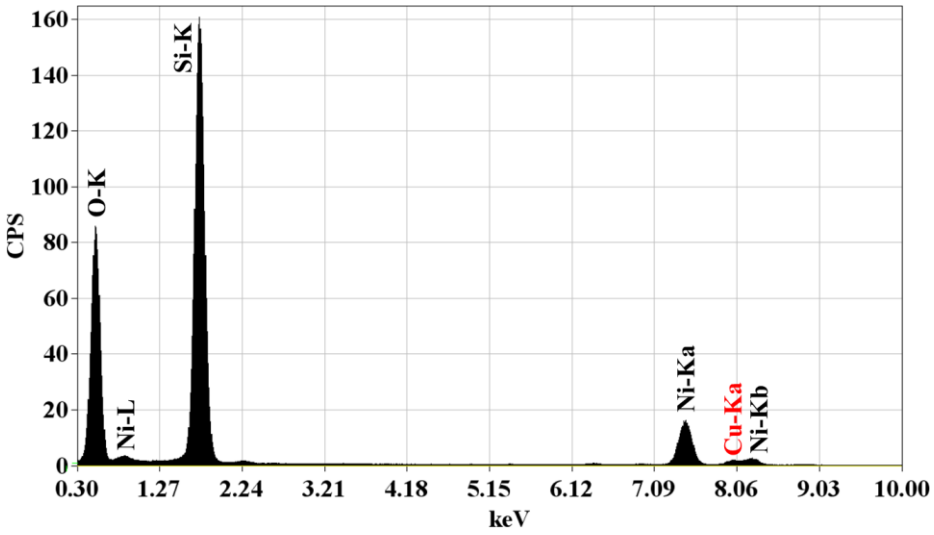

Figure 5a: *EDX spectrum of CuTCPP functionalized nanowires*

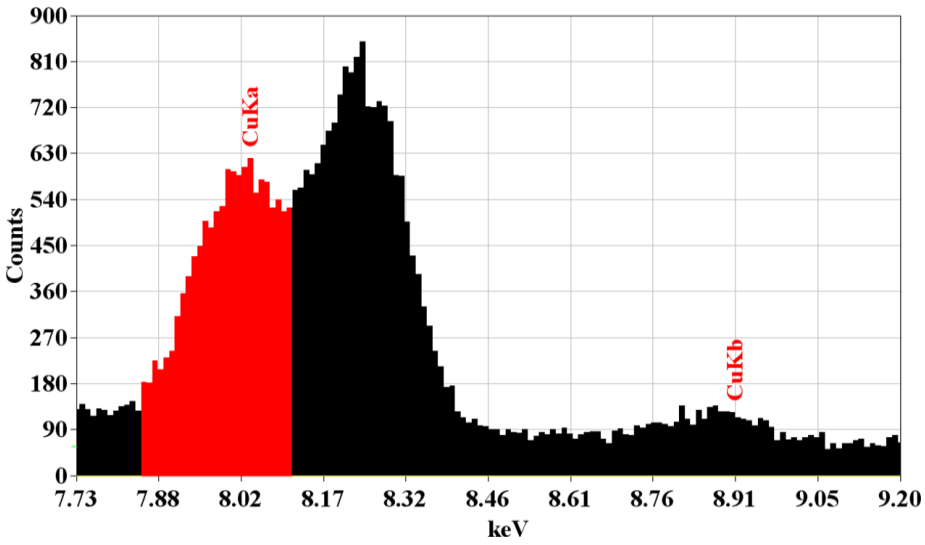

Figure 5b: *EDX spectrum of CuTCPP functionalized nanowires (zoom on Cu zone)*

EDX spectra show the presence of Cu in the nanosystem, with associated Si and O peaks from nanowires.
Ni peak is due to the fact that the sample was analyzed on a TEM grid made up of a Ni supported carbon film.

Quantitative analysis of Cu(II) in a 5% v/v solution of H_2SO_4 in water

Dried nanowires were treated with concentrated H_2SO_4 (97 %, 100 µL), then distilled water (900 µL) was added. The resulting green suspension of nanowires was sonicated in a sonicating bath, then centrifugated (14.000 rpm, 15 min). The supernatant was removed and transferred into a 2 ml flask, then the nanowires were washed again with distilled water (500 µL x 2) and centrifugated. The remaining supernatant was added to the previously collected in a 2 ml flask, thus leading to a 5 % v/v solution of H_2SO_4 in water, which underwent a quantitative analysis via atomic absorption.
The present analysis was carried out for two samples functionalized with two different methods.

Sample 1 (wafers 785 A and 789 A) was functionalized with CuTCPP porphyrin according to the already described procedure, leaving the nanowires on their metallic support.
Sample 2 (wafers 790 A and 794 A), on the other hand, underwent a different procedure of functionalization: the nanowires, after being reacted with APTES, were detached from their support, centrifugated and dried. After that, they were reacted with CuTCPP porphyrin. In this second procedure the final functionalization was carried out in solution.
This was thought to be functional in order to compare the efficiency of two different possibilities of functionalization and to establish which allows to obtain a better porphyrin loading.
Both the samples underwent atomic absorption measures.
Sample 1 lead to a 0.0217 mmol/g porphyrin loading, whereas Sample 2 yielded a 0.096 mmol/g loading.
This important result shows that performing the functionalization on detached nanowires leads to a remarkably increased porphyrin loading (four times more), with respect to reactions carried out using the nanowires on the supports where they were grown, which is the procedure that I usually employed.

Chapter 4

Open topic: determination of the number of functional groups of porphyrins anchored to SiC/SiOx nanowires

Introduction

An interesting issue in the frame of our project is to know the arrangement of the porphyrin with respect to the surface of the nanowires. Indeed, this could influence some properties of the final nanosystem, like its dispersion in aqueous medium and in culture broth, for instance, according to the exposed substituents on the macrocycle.
The arrangement of the porphyrin depends on the number of the functional groups involved in the conjugation to the nanowires. Indeed, we could suppose an orthogonal or tilted arrangement if the linking arm is only one or two vicinal arms, as depicted in Figure 1. Another possibility is a parallel arrangement, if two opposite functional groups are involved in the linkage

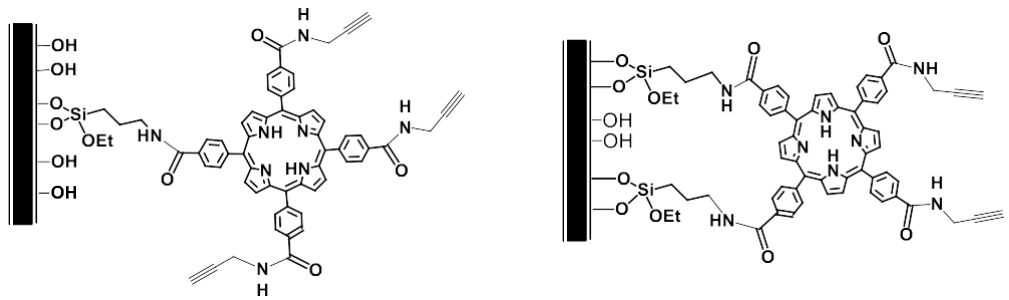

Figure 1*: Two different ways in which porphyrin can be bound to the nanowires: with one functional group (left) and with two vicinal functional groups (right)*

To estimate the number of linkages between porphyrin and a solid support is not a trivial issue: we thought that a possible analysis could be carried out with XPS spectroscopy, in order to distinguish different kinds of nitrogen atoms in the nanosystem. However, this was not possible since only a large N signal appeared, thus evidencing the inability to distinguish the different kinds of N atoms: this first attempt led us to partially abandon this approach. However we tried to bypass this problem attempting a similar method, with the same technique, but exploiting a different criterion and a different

compound: we thought to exploit 5,10,15,20-Tetrakis[4-(4-bromobenzanilide) phenyl] porphyrin in order to evaluate the ratio of the XPS signals of C=O and bromine, considering 5,10,15,20-Tetrakis(4-carboxyphenylphenyl) porphyrin as reference.

Results and discussion

To obtain information on the arrangement of the porphyrin with respect to the surface of the nanowires and aiming to understand the physical processes leading to the luminescence observed for the porphyrin conjugated nanowires, it was planned to perform XEOL experiments.
XEOL (X-ray excited optical luminescence) is a spectroscopy that excites mainly deep core electrons and has high site selectivity.

For this purpose, we prepared two different samples, consisting of *core-shell* SiC/SiOx nanowires functionalized with 5,10,15,20-Tetrakis(4-carboxyphenylphenyl) porphyrin and with different ending carboxylic groups, i.e. an amidic derivative or free carboxylic acids. *Core-shell* SiC/SiOx nanowires were activated as usual, refluxing the wafers in 37% HCl for two hours. After washing and drying well, amino groups were introduced on the nanowires surface by reaction with 3-(aminopropyl) triethoxysilane (APTES), refluxing in dry toluene overnight (reaction repeated twice). In the third step the carboxylic groups on H_2TCPP, previously activated with condensing agents (EDC and HOBt), were coupled to the amino functions on the nanowires in the presence of DMAP, leading to the formation of amide bonds
The first sample (580 A) was prepared converting the unreacted active ester groups in amide functions by adding butylamine in dry DMF.
The second one (536 B) was prepared by hydrolysis of the unreacted active esters to free carboxylic acids (Scheme 2).

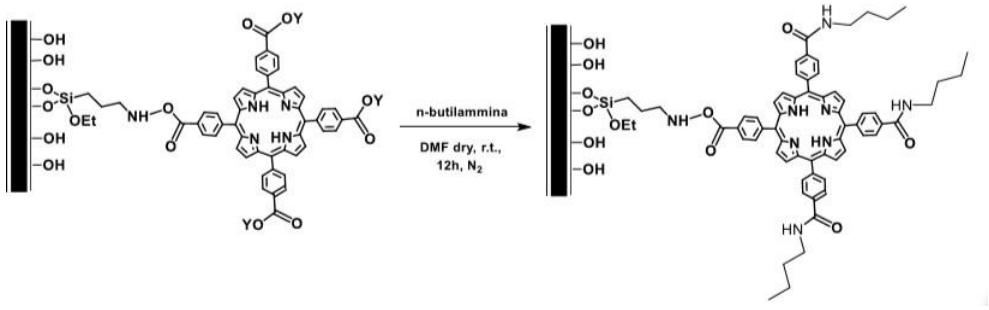

Scheme 1*: Synthesis of the nanosystem containing the n-butylamine amidic derivative of H_2TCPP*

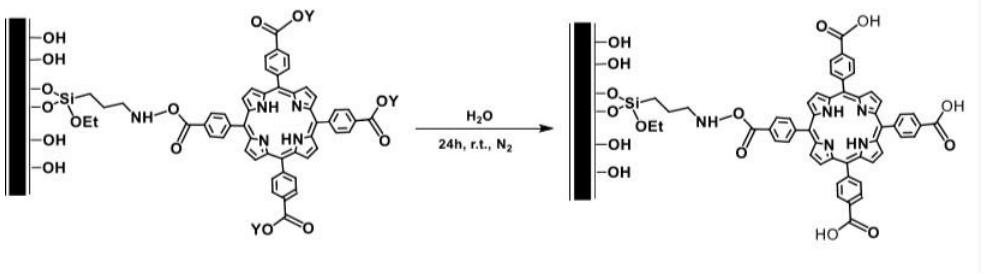

***Scheme 2**: Synthesis of the nanosystem containing H_2TCPP with restored carboxylic groups*

These samples were analyzed by solid state fluorescence spectroscopy Fluorescence spectra, collected employing a laser at λ = 473 nm as excitation source, evidenced that the functionalization occurred successfully for both the samples, since SiC fluorescence is negligible with respect to that of porphyrins (Figures 2 and 3).

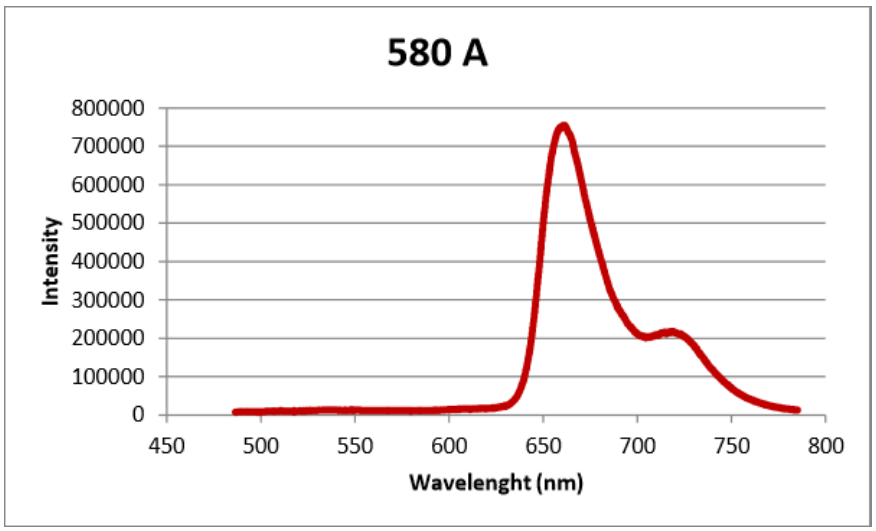

***Figure 2**: Fluorescence spectra of wafer 580 A, functionalized with butylamine*

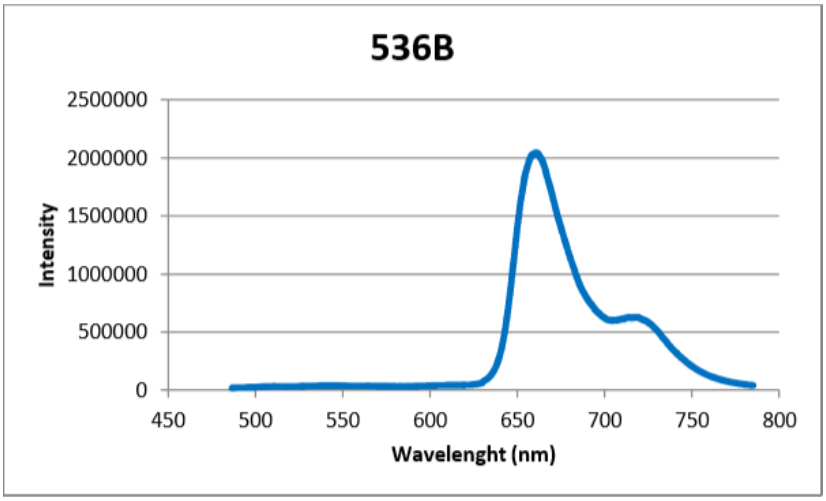

***Figure 3**: Fluorescence spectra of wafer 536 B, containing restored -COOH groups on H_2TCPP porphyrins*

Both the wafers were sent to the M. Nardi's group at IMEM-CNR institute in Trento to carry out XEOL experiments at ELETTRA (Trieste).
XEOL measurements were performed via synchrotron radiation using photon energies lower than those typical for radiotherapy. The spectra were collected using X-ray with photon Energy = 130 eV. Unfortunately, the spectra resembled that of bare nanowires, evidencing that with that XEOL setup it is not possible to see a porphyrin monolayer.

Since no usefull information was obtained, a XPS study was undertaken to determine the number of porphyrin functional groups involved in the conjugation to the nanowires. XPS (X-ray photoelectron spectroscopy) is a spectroscopic technique used to analyse the surface chemistry of a material. Indeed it is used to measure the elemental composition at the parts per thousand range.

The XPS spectra recorded on the two samples (580A and 536B) showed not resolved N1s signals associated to different kinds of porphyrin nitrogen (N, NH and NC=O) due to the large amount of N atoms present on the nanowire surface.

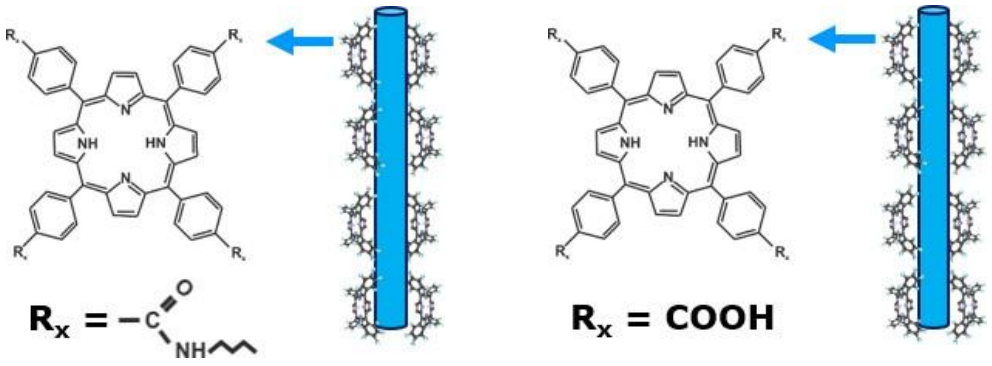

Figure 4: *Different number and kind of N atoms in samples 580 A and 536 B*

Also the C 1s XPS spectrum showed a large signals, with a shoulder at higher energy (Figure 5).

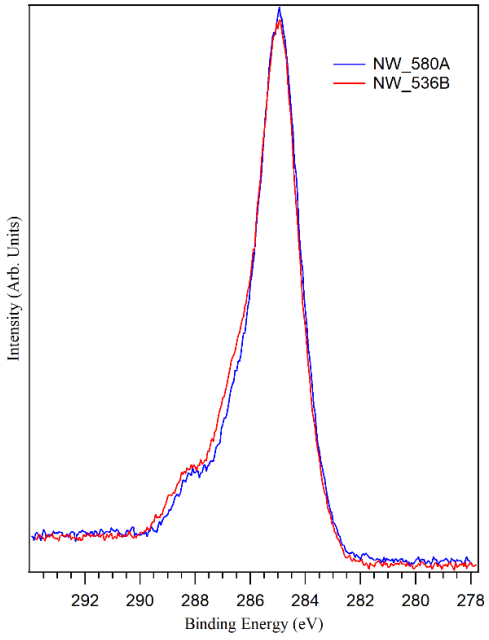

Figure 5: *C 1s signals for samples 536 B and 580 A*

The spectrum reported in Fig. 5, shows the large C 1s signal scaled accordingly to the position of the C-C and C=C components in standard porphyrin compounds (i.e. 285 eV). The binding energy shift of the spectra (about 2 eV) is due to charging effects of the analyzed samples, this is related to the intrinsic insulator character of the coreshell SiC/SiOx nanowires.

Also in this case the contribution of the alkyl chain Si-(CH2)3-NH2 on the nanowires surface lies under the same main components at 285 eV as well as the C-C and C=C of the porphyrin.

Before abandoning this kind of study, we decided to check if the presence of a different atom could help us in determining the number of linkages. To verify if it is possible to evaluate the ratio between the signals of C=O and a heteroatom such as Br, and consequently the number of linkages between porphyrins and solid supports, we planned to prepare as model reference a H_2TCPP derivative functionalized with
4-bromoanyline (5,10,15,20-Tetrakis[4-(4- bromobenzanilide) phenyl] porphyrin).

This derivative and H_2TCPP porphyrin as reference compounds (Figure 6) were deposited on Pt plates by drop-casting for XPS analyses.

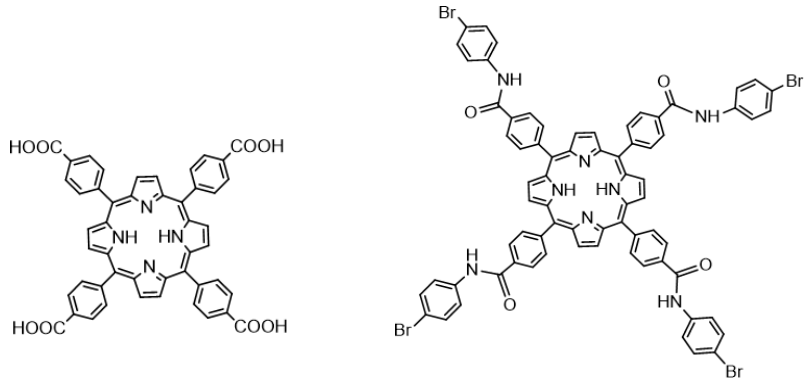

Figure 6: *Left: 5,10,15,20-Tetrakis(4-carboxyphenyl) porphyrin*
Right: 5,10,15,20-Tetrakis[4-(4-bromobenzanilide) phenyl]

Before proceeding with the deposition, a pre-treatment was carried out for the solid substrates in order to remove any impurities: Pt covered wafers were sonicated in isopropanol using a sonicating bath (15 min, freq. 59 KHz, power 100%), then were dried in the air for a few minutes. Porphyrins were dissolved in DMF till to reach a 5 μM solution and drop casted on pre-treated wafers, heating at 70°C, until a homogeneous layer was observed (Figure 7).

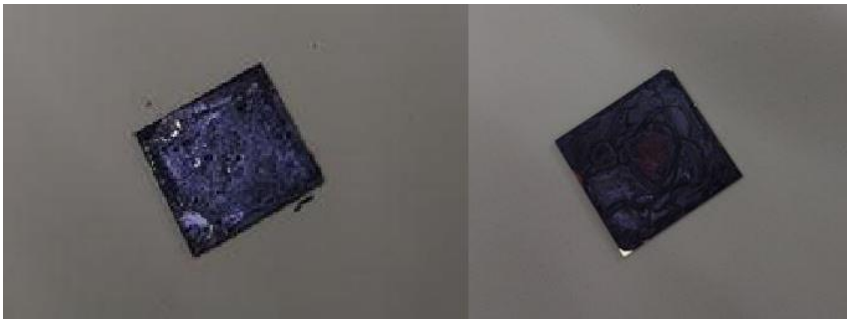

.

Figure 7: *Left: 5,10,15,20-Tetrakis(4-carboxyphenyl) porphyrin*
Right: 5,10,15,20-Tetrakis[4-(4-bromobenzanilide) phenyl]porphyrin)

Chapter 5

Zeta potential analysis of nanowires

Zeta potential is a term to define electrokinetic potential[1] in colloidal dispersions.
The zeta potential is largely employed to quantify the extent of the charge in a suspension and is an indicator of the stability of colloidal dispersions. The extent of the zeta potential indicates the degree of electrostatic repulsion between adjacent, similarly charged particles in a dispersion. For molecules and particles that are small enough, a high zeta potential will confer stability, i.e., the solution or dispersion will not tend to aggregate. When the potential is small, attractive forces may overtake this repulsion and the dispersion may break and flocculate. So, colloids with high zeta potential (in modulus, negative or positive) are electrically stabilized while colloids with low zeta potentials tend to coagulate or flocculate as explained in the following table (Table 1).[2][3]

Zeta potential [mV]	Stability behavior of the colloid
from 0 to ±5,	Rapid coagulation or flocculation
from ±10 to ±30	Incipient instability
from ±30 to ±40	Moderate stability
from ±40 to ±60	Good stability
more than ±61	Excellent stability

Table 1: *Table indicating the relation between zeta potential magnitude (in modulus) and stability of a colloidal suspension*

Zeta potential measures were carried out for different types of prepared nanosystems, in order to analyze the stability of their suspensions both in physiological solution and in biological medium.
In a previous work bare nanowires had already undergone zeta potential analysis: The Z potential values were –(37 ± 3) mV in water,

(12 ± 2) mV in RPMI 1640 medium, and +(2 ± 3) mV in a RPMISV medium. These values indicated that the material in water has a negative surface charge, related to O terminating the NW shell surface, and a good stability.

The modification of the Z potential in cell culture media, where it becomes smaller and eventually changes sign, suggested that the medium components (e.g. proteins) interact with the NWs and cover their surface causing a different charge compensation. [4]

As a further characterization of functionalized nanowires, we decided to carry out zeta potential analysis for three samples functionalized in three different ways. This was thought as useful to understand the influence that a specific kind of functionalization has on nanowires behavior in solution.

The samples we prepared are here reported.

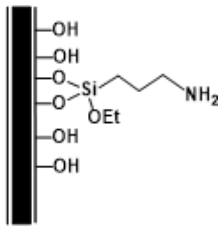

NWs 769 A

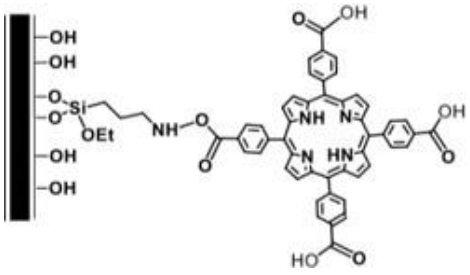

NWs 771 B

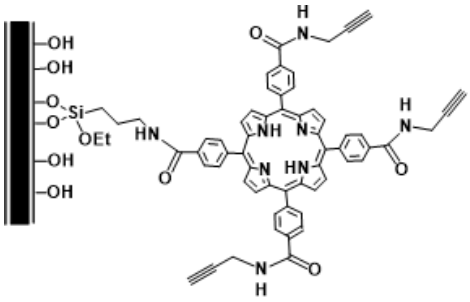

NWs 771 A

The first one consists of simple core-shell SiC/SiOx nanowires functionalized with 3-(aminopropyl)trieyhoxysilane, whereas the others contain native H_2TCPP porphyrin (NWs 771 B) or H_2TPAPP (NWs 771 A).

All the measurements were carried out employing a 1mM solution of NaCl in distilled water as physiological solution, whereas the other measures were carried out in RPMI 1640 medium. The results are reported in the table below (Table 2).

Sample	Physiological solution	RPMI 1640 medium
769 A	+16.49 mV	-5.26 mV
771 B	-49.38 mV	-6.79 mV
771 A	-29.24 mV	+6.90 mV

Table 2: *Summary on zeta potential measures carried out on our nanowires*

It can be noticed that, for all the samples, relatively high values of zeta potential (in modulus) were obtained from the measures in physiological solution. All the analyzed samples have a good stability in aqueous medium. For sample 769 A a positive zeta potential value was observed, which can be due to exposed NH_2 groups on nanowire functionalized with APTES. Negative zeta potential values, on the other hand, were found for samples 771 A and 771 B, both containing porphyrins.
As observed in previous works, zeta potential became smaller (in modulus) in biological medium and also changed sign for samples 769 A and 771 A, since many components in culture broth can interact with nanowires.

References

[1] Definition of electrokinetic potential in "IUPAC. Compendium of Chemical Terminology", 2nd ed. (the "Gold Book"). Compiled by A. D. McNaught and A. Wilkinson. Blackwell Scientific Publications, Oxford (1997). XML on-line corrected version: http://goldbook.iupac.org (2006-) created by M. Nic, J. Jirat, B. Kosata; updates compiled by A. Jenkins. ISBN 0-9678550-9-8. doi:10.1351/goldbook.

[2] R. Greenwood, K. Kendall, "Electroacoustic studies of moderately concentrated colloidal suspensions", *Journal of the European Ceramic Society, 19* (4), pp. 479–488, **1999**

[3] D.A.H. Hanaor, M. Michelazzi, C. Leonelli, C.C. Sorrell, "The effects of carboxylic acids on the aqueous dispersion and electrophoretic deposition of ZrO_2", *Journal of the European Ceramic Society, 32* (1) pp. 235-244, **2012**

[4] A. Cacchioli, F. Ravanetti, R. Alinovi, S. Pinelli, F. Rossi, M. Negri, E. Bedogni, M. Campanini, M. Galetti, M. Goldoni, P. Lagonegro, R. Alfieri, F. Bigi, and G. Salviati "Cytocompatibility and Cellular Internalization Mechanisms of SiC/ SiO_2 Nanowires", *NanoLetters., 14* (8), pp. 4368−4375, **2014**

Chapter 6

Synthesis of Zn (II) porphyrins functionalized with phosphonic acid groups

Introduction

In order to explore different type of linkers, we planned to functionalize a tetraphenylporphyrin with alkyl chains ending with phosphonic acid groups. The ability of phosphonic acid groups to bind the metal oxide surface was reported to be higher than other groups, like carboxy groups, for instance. In addition it was reported a study showing that a phtalocyanine functionalized with two long alkyl chains was arranged parallel to the ZnO surface with a very short distance.

To study the possible effect of very short distance between the photosensitizer and the inorganic surface on the energy transfer process, we planned to synthesize a porphyrin bearing four alkyl chains ending with free phosphonic acid groups.

Similar linkers were reported in the literature for porphyrins and phtalocyanines mainly used in the field of electron transfer processes, in particular anchored on metal oxides. Thus the synthesis of this kind of porphyrins opens the way to an application field different from energy transfer.

They are interesting for many applications: in addition to use as catalysts, they are employed as photosensitizers for photodynamic therapy in cancer treatment.

In order to improve different characteristics, it was possible to tune their properties by different substituents and/or by different metals

Indeed, porphyrins have specific electronic properties, which make them interesting also for functionalizing electrodes on metal oxides surfaces: electronic devices based on organic-inorganic hybrid systems are now being intensely studied, especially in the field of organic photovoltaic, to turn solar energy into electric, and in the field of photoelectrochemical cells (DSSC, Dye Sensitized Solar Cells) for water splitting, to turn solar energy into fuel [2].

Functionalizing an electrode with a porphyrin allows tuning of the electrode properties. In particular, porphyrins functionalized with phosphonic acids can be employed as sensitizers on TiO_2, ZnO, SnO_2 and on hybrid oxides metal surfaces (Figure 1).

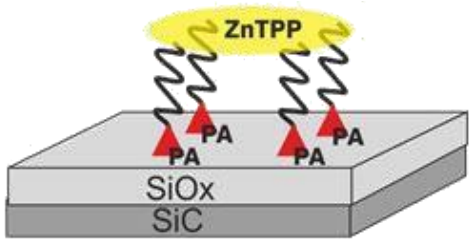

***Figure 1**: Schematic representation of a supported porphyrin*

Orientation and distance between the organic components and the oxide surface play a central role
in improving the efficiency of energy transfer processes from the chromophore excited state to the conduction band in the oxide: the efficiency of this process depends on how fast is holehopping between adjacent chromophores and on how fast is holes recombination. Moreover, the presence of a metal showed an improvement in the electron transmission from the porphyrin to the electron withdrawing acceptor [3].

Recently, a *self-assembled* monolayer of phosphonated phtalocyanine was used to functionalize a ZnO surface, so that it was possible to analyze how the phosphonic groups were bound to the metal surface [4] (as monodentate, bidentate or tridentate ligands).

Then, it was evidenced that photosensitizers bearing phosphonic acid groups are the most efficient in the field of photoelectrochemical cells: this was demonstrated in a work in which photosensistizers functionalized with various groups were linked to a TiO_2 surface. Their efficiency was then tested and those bearing phosphonic acid groups gave the best results[5].

In the literature there are many synthetic routes to prepare phosphonated porphyrins bearing phosphonic groups in different positions on the macrocycle: some of these are functionalized on pyrrolic rings, whereas others on phenyl rings, when present, or in meso positions [6] [7] [8] (Figure 2).

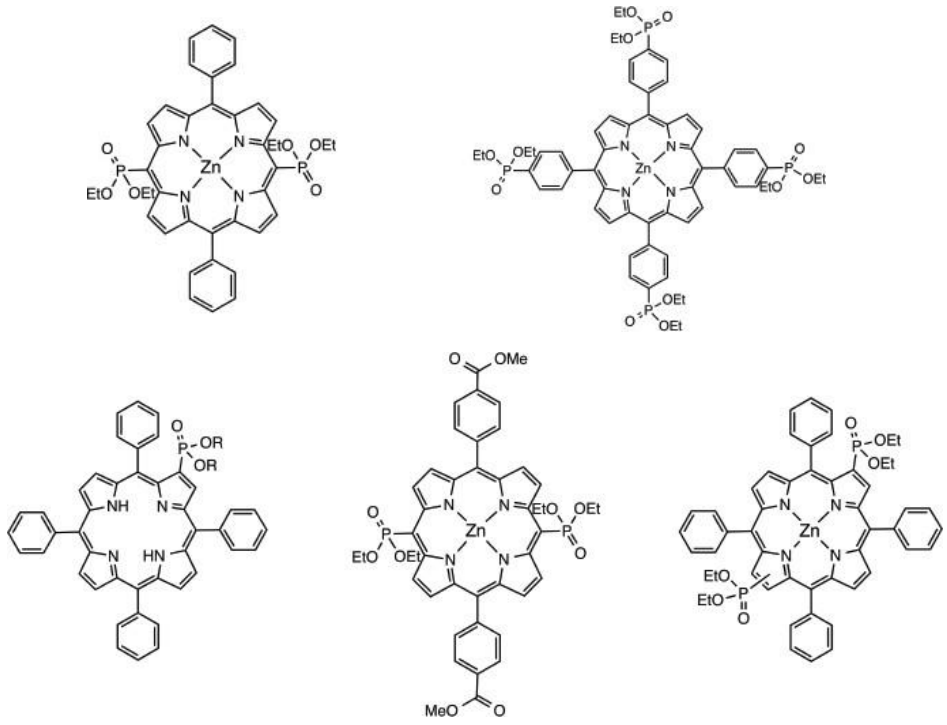

***Figure 2**: Examples of phosphonated porphyrins bearing substituents in different positions*

Results and discussion

In this work, the synthesis of a Zn porphyrin functionalized with four phosphonic acid groups was carried out, starting from *tetrakis*(4-hydroxyphenyl)porphyrin (H_2THPP). The obtained porphyrin, depicted below (Figure 3) is a new compound not reported in the literature.

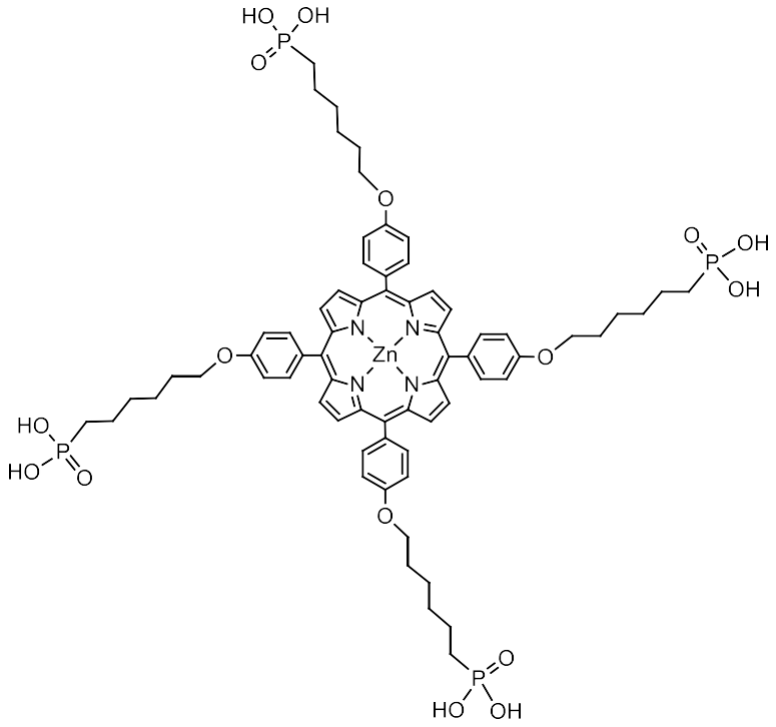

***Figure 3**: Zn porphyrin functionalized with four phosphonic acid groups, obtained starting from tetrakis(4-hydroxyphenyl)porphyrin (H_2THPP)*

We decided to functionalize H_2THPP porphyrin with six membered chains ending with phosphonic acids, so that this compound could be anchored to a nanostructure or a metal oxide surface in order to study the macrocycle orientation. This is done to understand in which way the organic compound is linked to the substrate: how many phosphonic groups are bound and how the macrocycle is oriented with respect to the surface is linked to.

A recent work reported in the literature demonstrated that the use of at least three linkers is functional for a better control of the immobilization process of the dye on the substrate: this leads to the formation of a monolayer with minimal aggregation and a narrower molecular orientation distribution that is parallel to the surface plane.

According to this study, the best choice would be to have a porphyrin containing alkyl chains ending with phosphonic groups in all four position on

the phenyl rings: this would force the dye to be parallel to the support. It was noticed that a parallel orientation of the dye with respect to the electrode surface is directly connected with a greater rate of charge transfer: this seems functional to make the most of these compounds in charge transfer processes. For this study we decided to synthetize a porphyrin tetrafunctionalized with phosphonic acids. We also planned to introduce a zinc atom in the porphyrin core, since it is known that the presence of a metal atom can optimize electron transfer processes.

The synthetic route we employed is reported in Scheme 1.

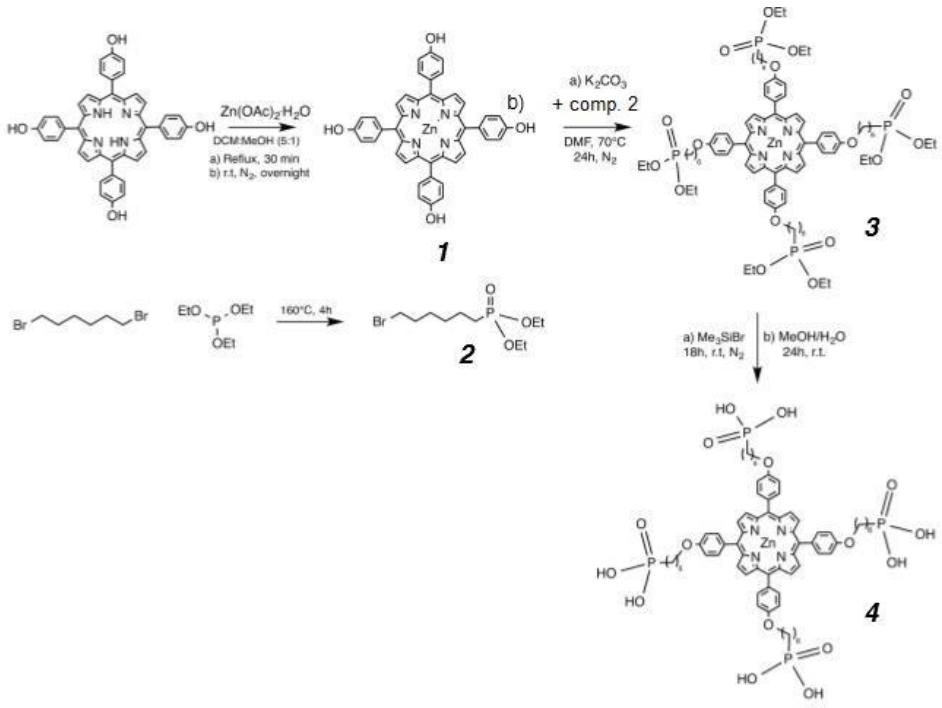

Scheme 1*: Synthetic route employed to synthesize zinc (II) 5,10,15,20-Tetrakis[4-(6-phosphonohexaoxy)phenyl] porphyrin (Compound 4)*

It starts from the salification of the pyrrolic core with zinc acetate; then, four six members alkyl chains ending with diethyl phosphonates were introduced on the phenyl rings in ZnTHPP. To this purpose, the chain diethyl-6-bromohexylphosphonate was synthetized apart. After the hydrolysis of diethylphosphonate groups, porphyrin bearing four free phosphonic acid groups was obtained.

The first step is the metallation of *tetra*(hydroxyphenyl)porphyrin (H_2THPP) with zinc (II). The reagent employed is zinc acetate dihydrate, used in large excess (8:1 ratio), to give a quantitative yield. The reaction was carried out in a mixture of DCM:MeOH 5:1, in which the starting macrocycle is completely soluble. At the end of the reaction, we found out a work-up simpler than that reported in literature[5] for a generic porphyrin, that involved washing with water and then sodium bicarbonate solution. Observing that in our case the addition of water caused a solid precipitation, we added a large amount of water to cause the complete precipitation of the Zn-porphyrin.
After metallation, the porphyrin changed its color from dark red to dark violet. Accordingly the UV-VIS spectrum reported below, it shows a slight shift of the Soret band to the blue zone (from 420 nm to 427 nm) (Figure 4). The most striking feature to confirm that the metallation was carried out successfully, however, is the reduction of the Q bands number. These are four in non metal porphyrin, whereas only two in the metal one. This is due to the increased symmetry of the molecule: non metal porphyrin has a D_{2h} symmetry, whereas zinc porphyrin belongs to D_{4h} punctual group.

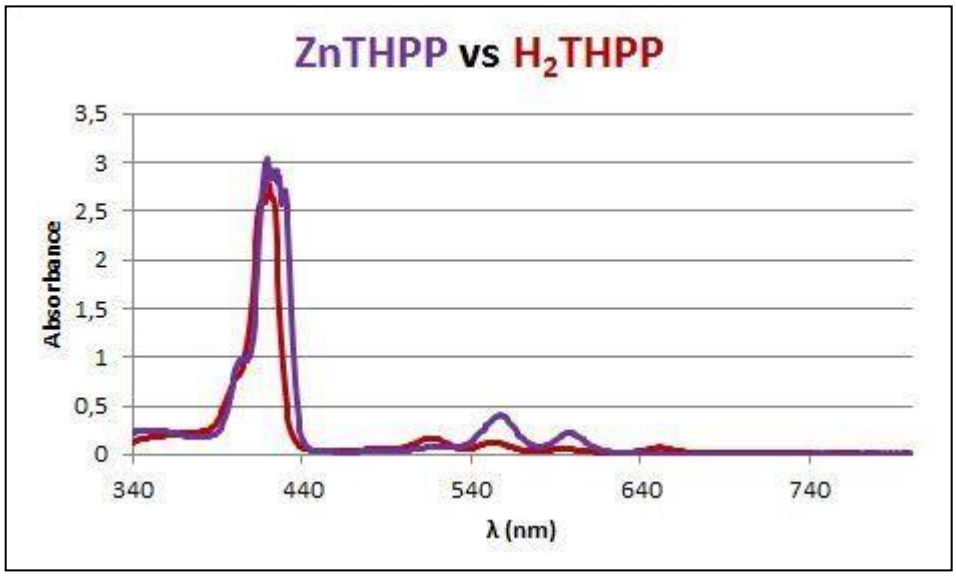

***Figure 4**: UV-VIS spectrum of H_2TPP and ZnTPP porphyrins*

Also ^{1}H NMR analysis allows an immediate detection of the metallation process (Figure5). Indeed, we observe the disappearance of the signals due to NH pyrrolic protons, which is at negative δ (-2.87 ppm) in the non metal compound. The product, recovered by Buchner filtration, was obtained pure in a quantitative yield (98%).

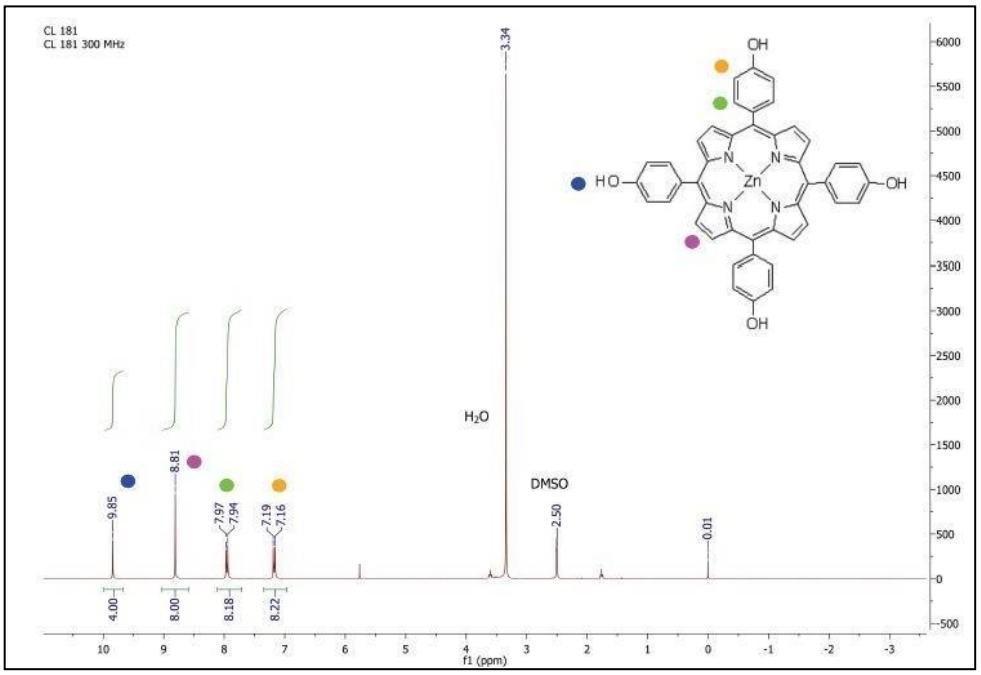

***Figure 5**: [1]H NMR spectrum of ZnTPP*

The synthesis of six member chain was carried out through the Michaelis-Arbuzov reaction, one the most employed reactions to form carbon-phosphorous bonds. In its most simple form, Arbuzov rearrangement is a reaction between an alkyl halide and a trialkyl phosphite $(RO)_3P$ to give a dialkyl alkylphosphonate. (Scheme 2). During the reaction trivalent phosphorous (P_{III}) is converted into pentavalent phosphorous (P_V).

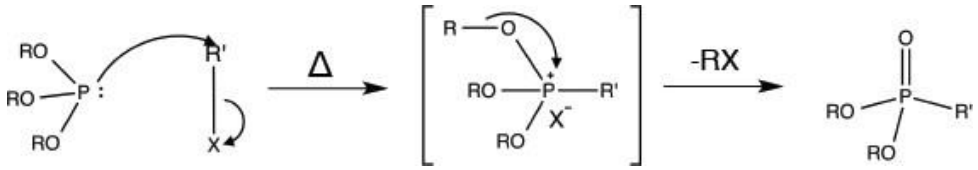

***Scheme 2**: Mechanism of Michaelis-Arbuzov rearrangement*

The electron lone pair on phosphite attacks the alkyl halide, according to a S_N2 mechanism, to form an addition intermediate in which the alkyl group in the halide is linked to the phosphorous. Then, an alkyl group of the phosphite dissociates from this, leading to the formation of a P=O double bond. This alkyl group binds the halide, producing a novel alkyl halide. The overall result is the conversion of phosphorous from trivalent to pentavalent. The driving force for the rearrangement is the conversion of >P-O-C bond into >P(=O) double bond that leads to an increase of its stability.

In the second step of the reaction, X^- group attacks the alkyl R according to a S_N2 mechanism: X^- attacks on the opposite side with respect to the leaving group. A further proof of this mechanism was the inversion of configuration observed in presence of asymmetric carbons.

Also S_N1 mechanism, which involves the formation of a carbocation as intermediate, can be observed in some cases, but just seldom.

Usually, Michaelis-Arbuzov rearrangement proceeds with no need of catalysts, but in some cases nichel or copper catalysts were employed. Primary alkyl halides are particularly reactive in this reaction, as expected in a typical S_N2 mechanism. Moreover, the nature of halide has an influence on the rate of the rearrangement, according to the order RI>RBr>RCl.

Since the reaction consists of the donation of a lone pair on phosphorous to the alkyl halide, the reaction is hindered if R groups on the phosphonic ester are electron withdrawing, whereas is favored if R groups are electron donor. The elimination step of the R group by X^-, according again to a S_N2 mechanism, is influenced by the nature of R group, in the order Me > Et > i-Pr.

The solvent is generally not employed and only in some cases allowed a better control of the reaction. [9][10]

In our specific case, according to a literature procedure [11], a mixture of 1,6-dibromohexane and triethylphosphite was refluxed at 160°C for four hours without solvent.

The use of a dibromide, instead of the corresponding monofunctional compound, may cause the attack of the phosphite on both sides of the chain: to avoid this, it is important to employ a large excess of halide with respect to the phosphite (6:1 ratio in our case).

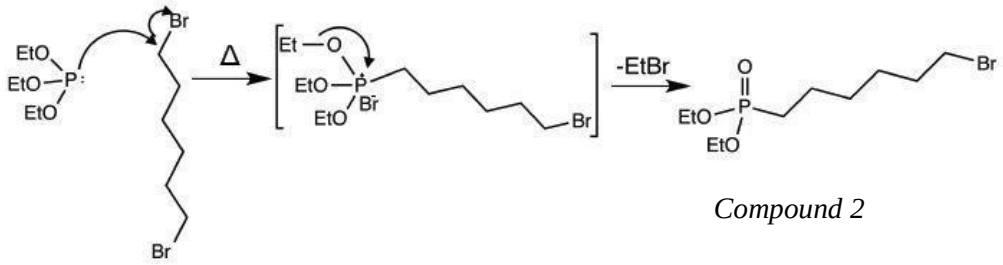

Compound 2

***Scheme 3**: Mechanism of formation of Compound 2, through Michaelis-Arbuzov reaction between triethylphosphite and 1,6-dibromohexane*

The crude was purified with flash chromatography and analyzed with ^{1}H NMR and ESI-MS. The product was obtained pure in 38% yield, a lower value than that reported in literature [11].

This may be due to a partial loss of product during chromatographic purification; furthermore, ESI-MS analysis and ^{1}H NMR of the crude allowed the identification of many by-products, which are typical of Michaelis-Arbuzov reaction (Figure 6).

These by-products are partially due to the different length of the R group on the phosphite and the R' group on the bromide: during the reaction a novel primary alkyl halide is formed (in our case ethyl bromide) and this can react with triethylphosphite instead of 1,6-dibromohexane.

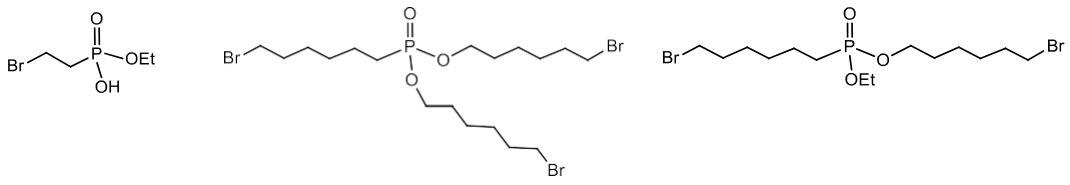

***Figure 6**: By-products observed with ESI-MS analysis*

For these reasons, the purification of the raw was quite laborious, due to this complex reaction mixture.
In the next step the alkyl chain is bound to the four phenolic groups on the previously metal porphyrin.

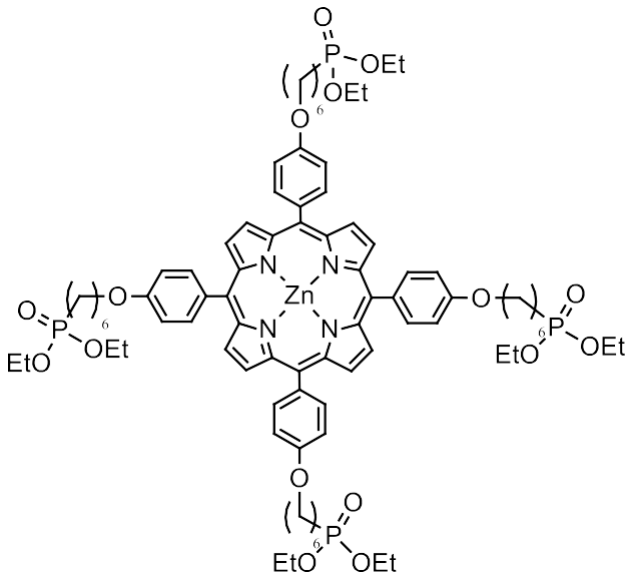

Figure 7: *Compound 3*

According to a S_N2 mechanism, the reaction occurs between a phenate and a primary halide. First, K_2CO_3 was added to a solution of the metal porphyrin in dry DMF to deprotonate the four phenolic OH. After stirring for 30 minutes, the primary halide Compound 2 was added and the reaction was stirred overnight at 70°C. In the preliminary reaction I carried out, only a slight excess of alkyl halide was employed (4.67:1), as suggested in a literature procedure [3].
A mixture of various compounds was obtained, difficult to separate. The desired tetrasubstituted product was formed in a small amount, being the main products a mixture of two disubstituted isomers in 5,10 or 5,15 on the macrocycle (Figure 8). These isomers were well identified by ^1H NMR and ESI-MS (Figures 9, 10 and 11).

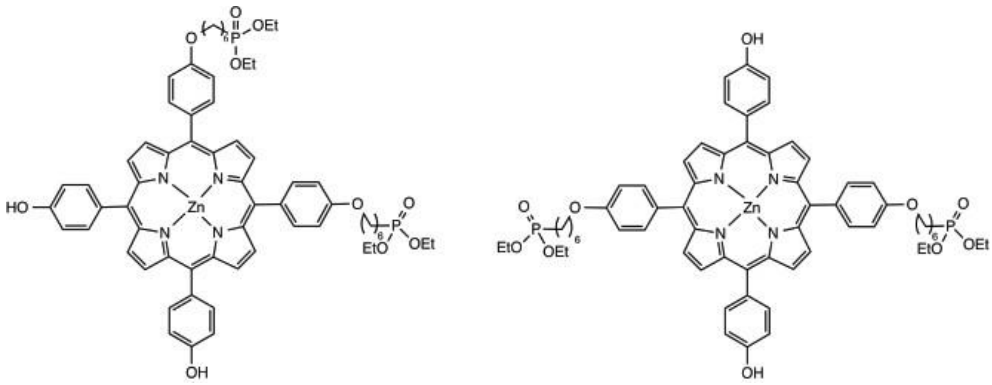

Figure 8: *Disubstituted isomers obtained from a preliminary reaction between ZnTHPP and Compound 2*

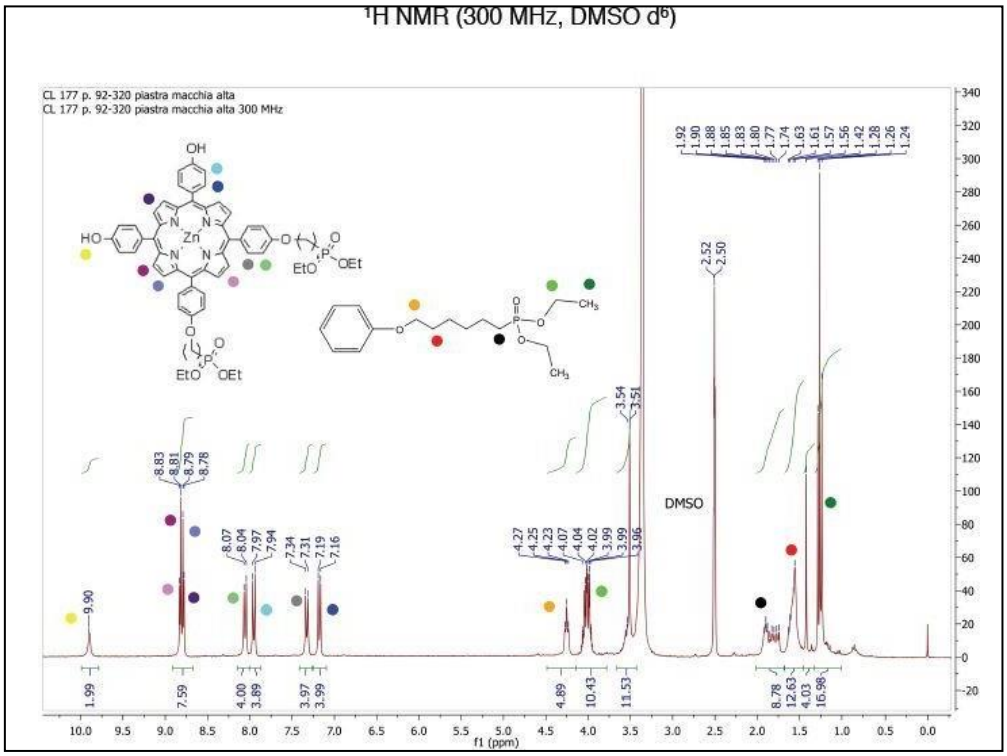

Figure 9: *[1]H NMR spectrum of disubstituted isomer in positions 5,10 on ZnTHPP porphyrin*

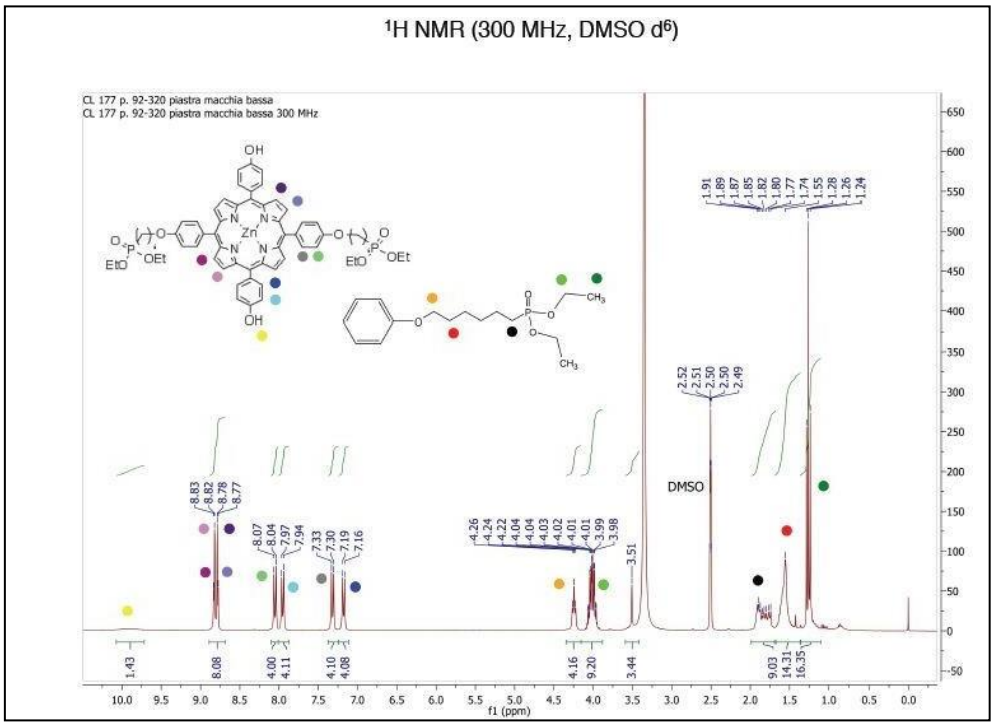

Figure 10: *^{1}H NMR spectrum of disubstituted isomer in positions 5,15 on ZnTHPP porphyrin*

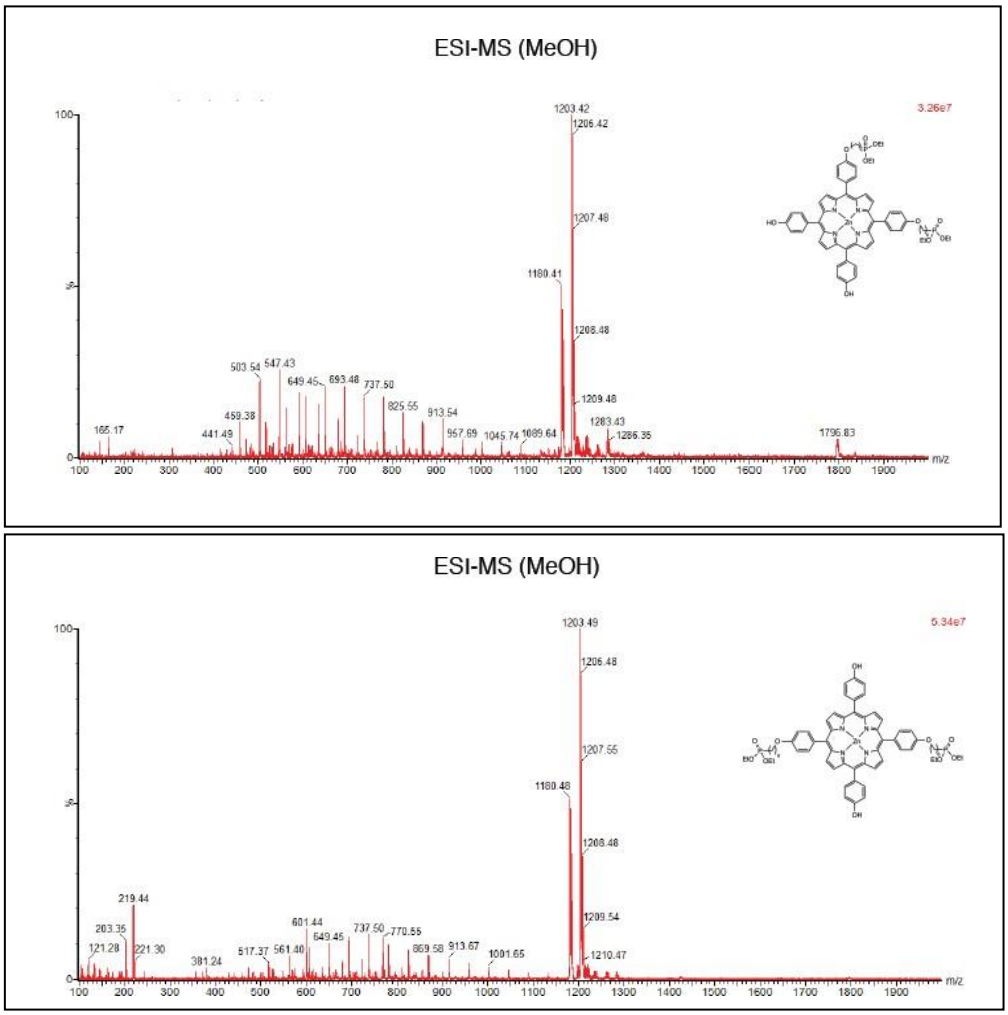

Figure 11: *ESI-MS spectra of disubstituted isomers on ZnTHPP porphyrin*

Therefore, we decided to employ a two-fold excess of Compound 2 with respect to the porphyrin, in order to obtain the tetrasubstituted product. We expected to obtain in a larger part the desired tetrasubstituted product, together with the trisubstituted one.

The crude was purified with preparative TLC, which allowed to obtain pure tetrasubstituted porphyrin in 40% yield. Also trisubstituted porphyrin was obtained pure and isolated in 30% yield. Disubstituted products were still

present, but only in a small amount. Pure products were analyzed with ^{1}H NMR and ESI-MS. ^{1}H NMR spectrum (Figure 12) showed a few signals, as expected for the high symmetry of the tetrasubstituted macrocycle, which are easily assigned. The ^{1}H NMR spectrum of trisubstituted product (Figure 13) is far more complex, since the molecule is not symmetrical. Pyrrolic and phenyl protons are not chemically equivalent, as in the case of tetrasubstituted compound, giving rise to different signals in the ^{1}H NMR spectrum.

The most intense peak in the ESI spectrum (Figure 14), corresponding to the value m/z = 1645.74, is due to the Na^{+} adduct of the tetrafunctionalized compound, leading to an immediate identification of the desired product.

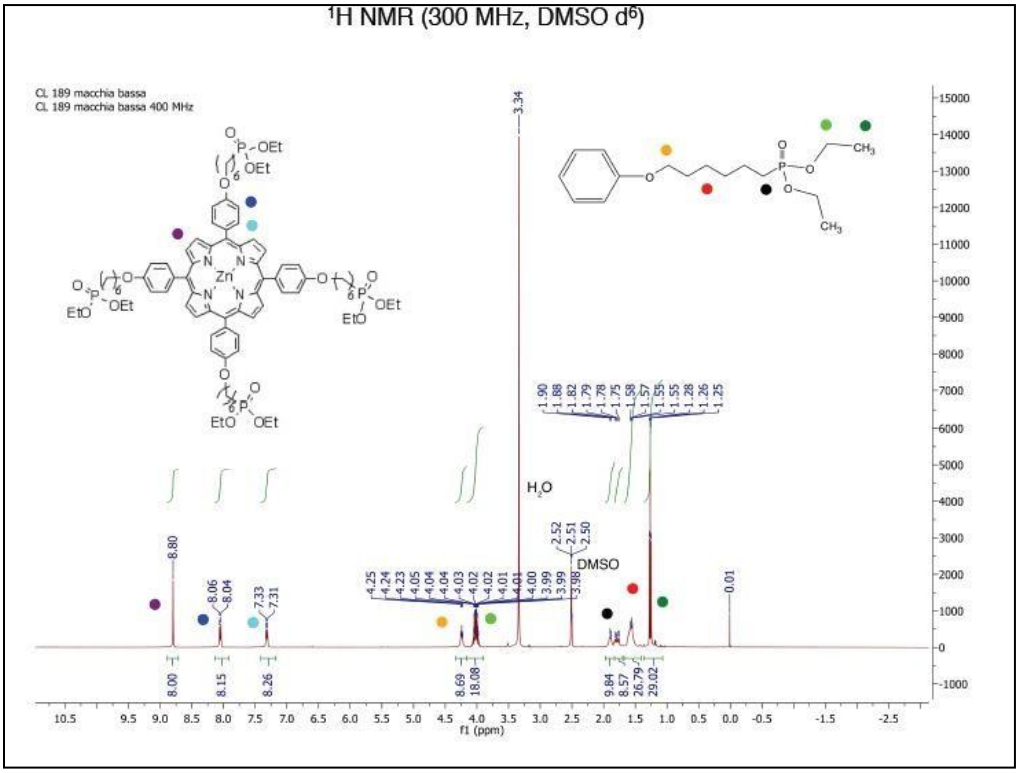

Figure 12: *^{1}H NMR spectrum (300 MHz, DMSO d6) of tetrasubstituted Compound 3*

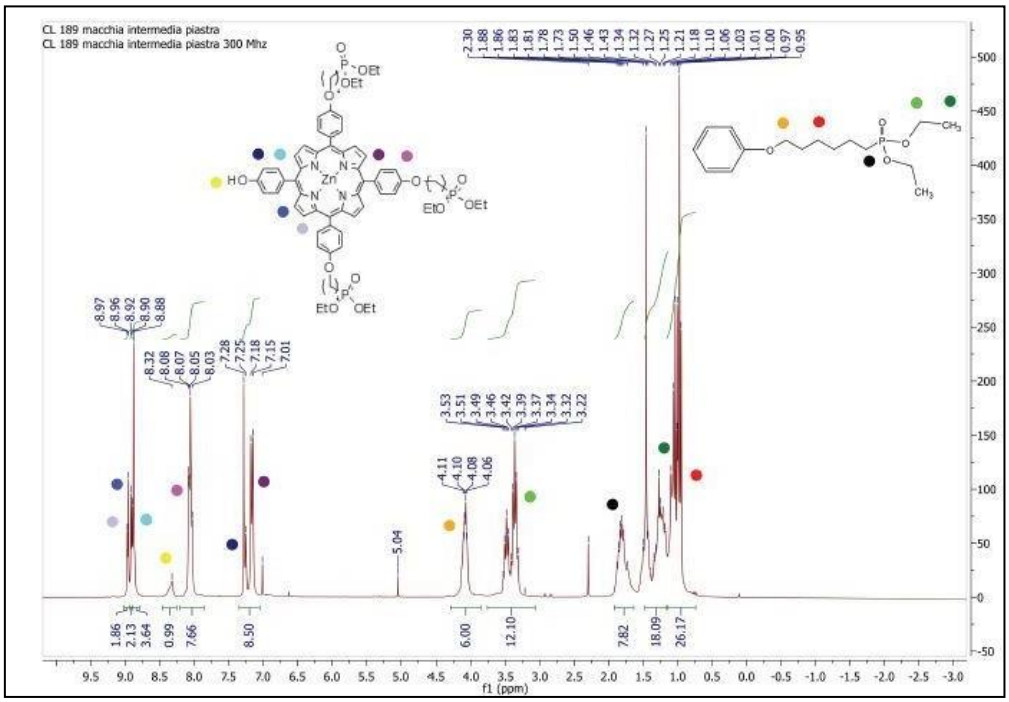

Figure 13: *^{1}H NMR spectrum (300 MHz, DMSO d6) of trisubstituted compound*

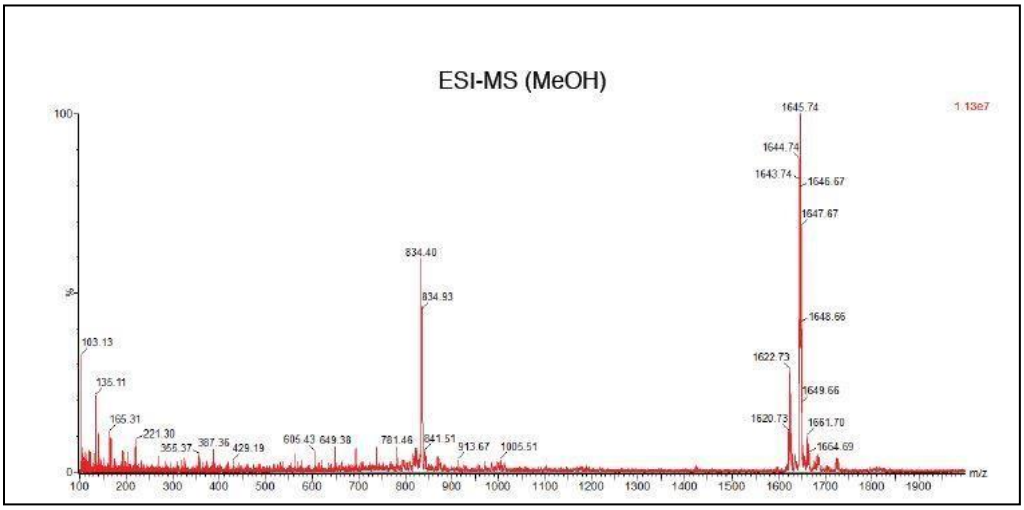

Figure 14: *ESI-MS spectrum (MeOH) of tetrasubstituted Compound 3*

The last synthetic step is the hydrolysis of the phosphonates, to yield free phosphonic acid groups. Phosphonic acids $RP(O)(OH)_2$ can be obtained with a dealkylation reaction of the corresponding diethyl phosphonate esters, using trimethylbromosilane as reagent [6]. An acid catalyzed hydrolysis is not convenient, since it requires too hard conditions, which may spoil the R groups on the phosphonate; furthermore, acid conditions would also remove the metal from the porphyrin core. The hydrolysis reaction of phosphonate occurs in two steps: in the first one the oxygen atom of the ethylphosphonate ester attacks the bromosilane, producing an active intermediate [12]. The latter, containing P-O-Si bond, is hydrolyzed in the second step.

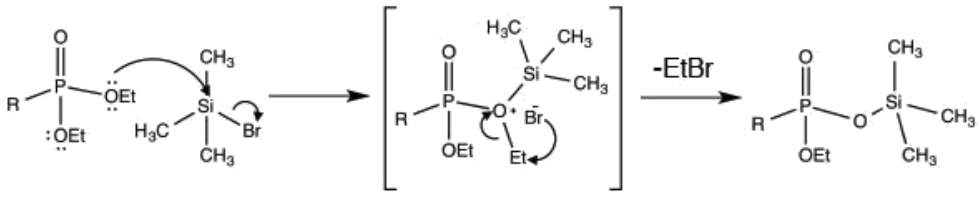

Scheme 4: *Formation of the active intermediated in the reaction between ethylphosphonate ester and bromotrimethylsilane*

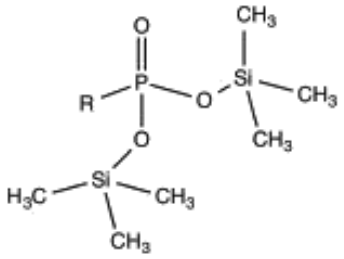

Figure 15: *Silyl ester intermediate*

The reaction was carried out in dry dichloromethane to avoid the hydrolysis of the forming silane.

Then, the intermediate is hydrolyzed to phosphonic acid by adding a mixture of water and methanol (1:4 ratio) and stirring at room temperature for 24 hours. Water is acid enough to destroy the silyl ester intermediate, whereas methanol is necessary to dissolve the macrocyclic compound.

During the hydrolysis the mixture changes color from brilliant violet to green.

After adding H_2O/MeOH the precipitation of a green solid was observed. When the reaction went at completion, the solid was recovered by filtration with a buchner funnel. The green powder was washed very well with MeOH and THF, then analyzed with ^{1}H NMR, UV-VIS and ^{31}P NMR spectroscopies. The product was isolated pure in a 50% weighted yield. ^{1}H NMR spectrum (Figure 16) shows the disappearance of the ethyl phosphonic ester signals and the presence of a very broad signal due to phosphonic acids at 4.21 ppm. In the spectrum other low signals are present, that we attributed to a partial demetallation of the porphyrin, as suggested by the presence of NH signals at δ -2.90 ppm.

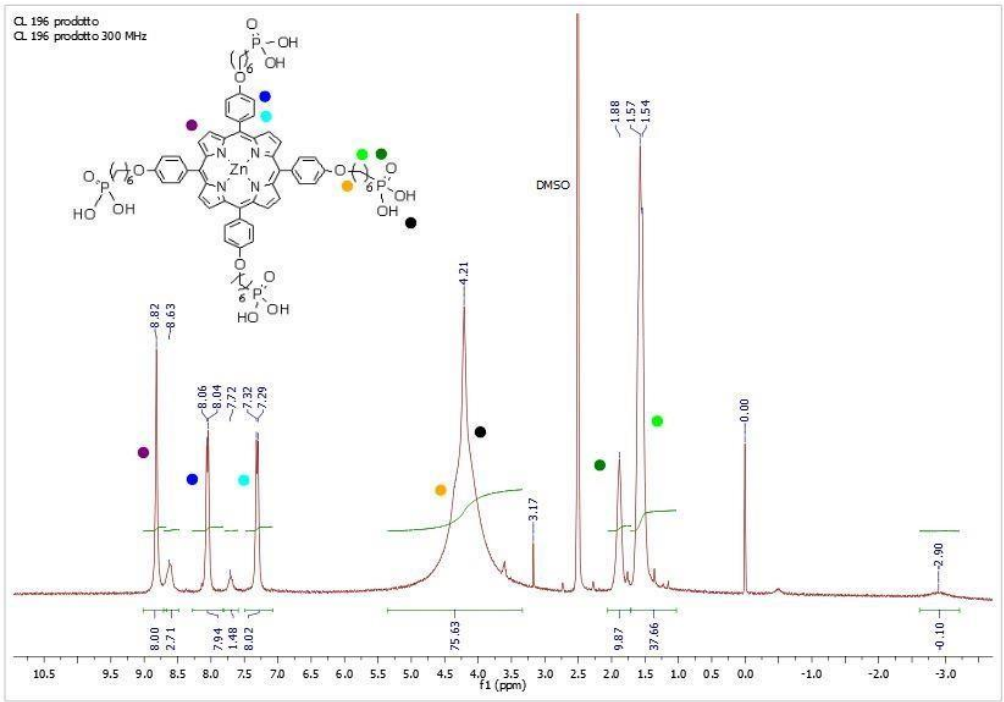

Figure 16: *^{1}H NMR spectrum (300 MHz, DMSO d^{6}) of Compound 4*

The final product, bearing four chains ending with phosphonic acids, was supposed to be anchored to the inorganic support, in order to carry out studies on energy transfer process, related to the orientation of the chromophore with respect to the support surface.
This work will be performed in collaboration with researchers of IMEM-CNR institute in Trento.
For a tetrafunctionalized TPP porphyrin the most convenient way to arrange is expected to be parallel with respect to the solid surface, according to a so called "flat-lying" conformation. On the contrary, a monofunctionalized TPP porphyrin will probably be in an "upright-standing" conformation, with respect to the solid surface. The energy transfer process should be more or less efficient according to how the porphyrin is arranged on the solid.
The technique that will be employed to determine the arrangement of porphyrins on solid supports is X-ray excited optical luminescence (XEOL). This is an X-ray photon in/optical photon out technique (Figure 17).
This is based on the conversion of the X-ray energy absorbed by the system in optical photons often involving multi-step cascade processes. XEOL is often used together with XANEFS/NEXAFS to provide site specificity which in turn can help to reveal the electronic structure and optical properties of interest.

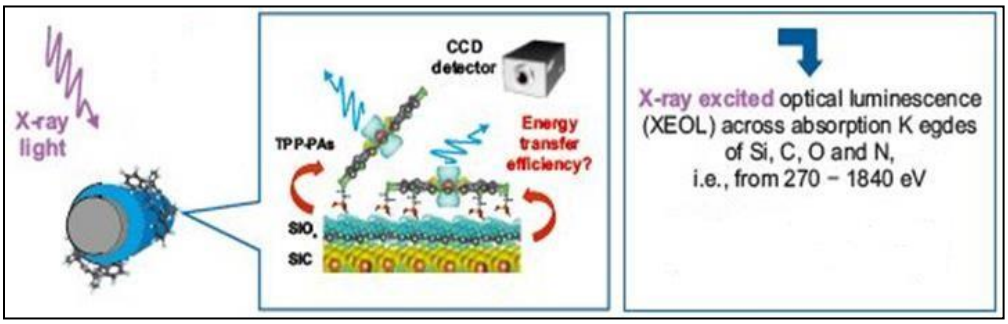

Figure 17: *XEOL technique to determine the conformation of porphyrins on metallic supports*

It is well known that XEOL signal is increased when a metal is present in the environment: for this reason we decided to employ a Zn porphyrin.

Unfortunately, zinc porphyrins are quite labile, thus they can undergo demetallation in a slightly acidic environment or simply in time.
Our zinc TPAA$(PA)_4$ porphyrin was characterized with UV-VIS and photoluminescence (PL) spectroscopies (Figure 18)

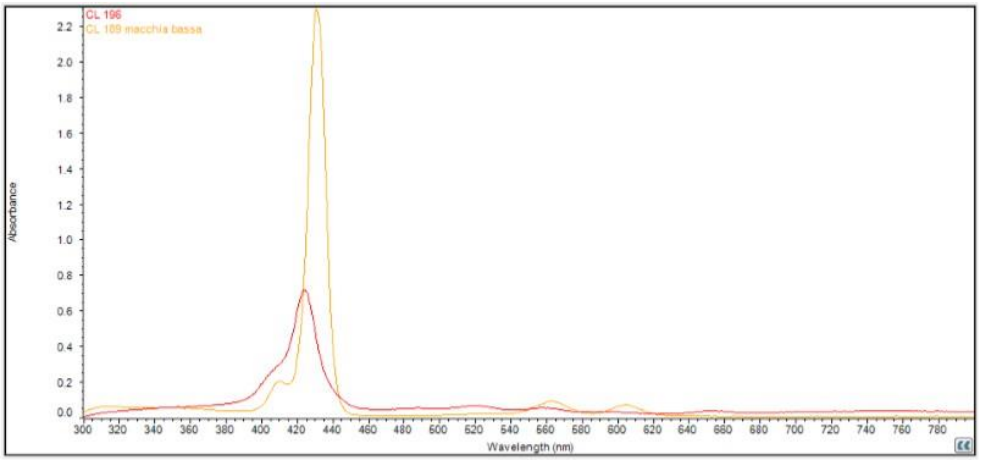

Figure 18: *UV-VIS spectrum showing a superimposition of Compound 3 (orange line) and Compound 4 (red line)*

Experimental section

Synthesis of Zn(II) 5,10,15,20-Tetrakis(4-hydroxyphenyl)porphyrin (Compound 1)

The reaction was carried out under nitrogen atmosphere, using a 25 ml Schlenck, previously dried with 3 vacuum/nitrogen cycles.
Tetrakis(4-hydroxyphenyl)porphyrin (0.500 gr; 0.737 mmol) was dissolved in 40 ml of a mixture of CH_2Cl_2/MeOH (5:1). Then, zinc acetate dihydrate (1.2936 g, 5.893 mmol) was added under stirring. For the first 30 minutes the mixture was refluxed at 70°C, then was left at room temperature overnight under nitrogen.
The reaction was quenched by adding distilled water until a violet precipitate was observed. The solid was filtered on a Buchner funnel, washed with distilled water and dried at the vacuum pump. Pure metal porphyrin was obtained and analyzed with ^{1}H NMR, ESI-MS and UV-VIS (brilliant violet solid, 0.5354 g, 98% yield).

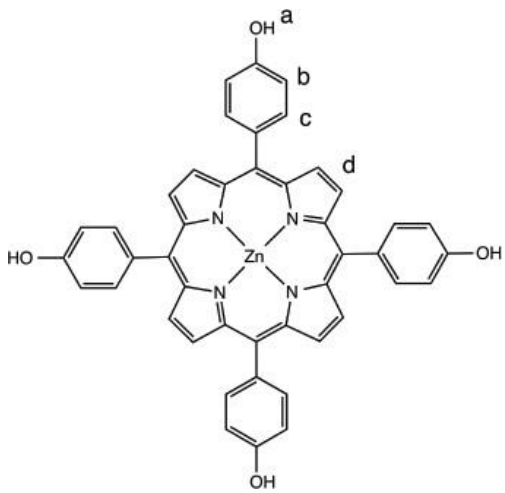

^{1}H NMR (300 MHz, DMSO d6)

δ(ppm) = 9.85 (4H, s, Ha); 8.81 (8H, s, -CHd); 7.955 (H, d, Hc); 7.175 (8H, d, Hb).

UV-VIS (DMF)

λ max = 427 nm

ESI-MS (MeOH)

m/z = 217.19 Zinc acetate

m/z = 371.23 [Compound 1]$^{+2}$

m/z = 740.28 [Compound 1]$^{+1}$

Synthesis of diethyl-6-bromohexylphosphonate (Compound 2)

The reaction was carried out in a 50 ml two-necked round bottom flask, equipped with a condenser and a bubble counter, under nitrogen. 1,6-dibromohexane (15.494 ml, 100.6 mmol) and triethylphosphite (2.85 ml, 16.6 mmol) were introduced in the flask, previously dried with 3 vacuum/nitrogen cycles, and the mixture was refluxed 4 hours at 160°C. After cooling to room temperature, the mixture was distilled under reduced pressure (0.018 mbar) heating at 150°C, in order to remove unreacted 1,6-dibromohexane and ethyl bromide generated in the reaction.
The crude containing the product was purified with flash chromatography using a mixture of hexane and ethyl acetate 1:15 as eluent. The product was collected, dried at the rotary evaporator and at the vacuum pump, then analyzed with ^{1}H NMR and ESI-MS. Pure product was obtained as a light yellow liquid (1.895 g, 38% yield).

Note: It is possible to purify the crude also with an automatic column, using a gradient of hexane and ethyl acetate.

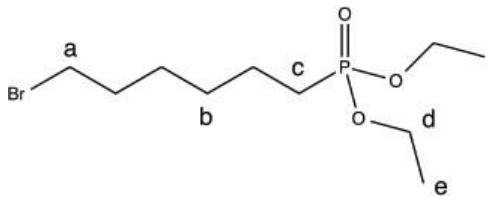

^{1}H NMR (300 MHz, CDCl3)

δ(ppm) = 4.095 (4H, m, Hd); 3.40 (2H, t, Ha); 1.74 (8H, m, Hb); 1.46 (2H, m, Hc); 1.32 (6H, t, He).

ESI-MS (MeOH)

m/z = 301.145 $[Compound\ 2]^{+1}$

m/z = 323.147 $[Compound\ 2 + Na]^{+1}$

m/z = 603.205 Dimer of $[Compound\ 2]^{+1}$

m/z = 623.178 Dimer of $[Compound\ 2 + Na]^{+1}$

Synthesis of zinc (II) 5,10,15,20-Tetrakis[4-(6-diethylphosphonohexaoxy)phenyl] porphyrin (Compound 3)

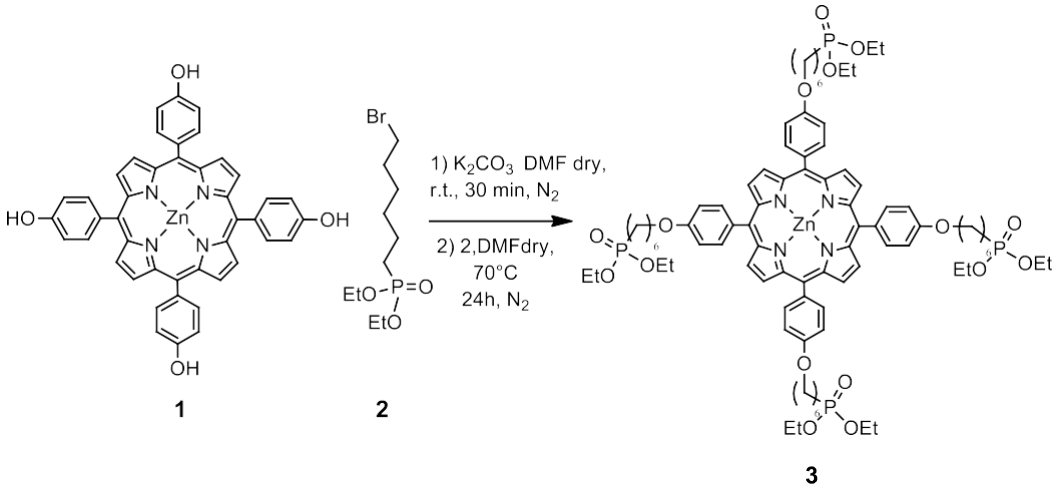

1 **2** **3**

The reaction was carried out under dry conditions, employing Schlenck glassware properly dried with 3 vacuum/nitrogen cycles.

Compound 1 (0.3315 g, 0.447 mmol) was introduced in the flask and dissolved in 8 ml of dry DMF.

K_2CO_3 was then added and the mixture was stirred at room temperature for 30 minutes.

Compound 2 (1.0834 g, 3.574 mmol), dissolved in 6 ml of dry DMF, was added and the mixture was stirred at 70°C for 24 hours, under nitrogen.

The reaction was quenched by addition of 100 ml of distilled water, which caused the precipitation of a violet solid: the latter was filtered over a Buchner funnel, washed with distilled water, dried at the rotary evaporator and at the vacuum pump.

The crude was purified with preparative TLC, using THF as eluent.

The desired tetrasubstituted product (together to the trisubstituted compound) was removed from the silica and extracted with THF and methanol. After getting rid off silica, the solution containing the compound was dried at the

rotary evaporator and at the vacuum pump to yield the desired product as a brilliant violet solid (0.2151 g, 40% yield). The product was characterized with ^{1}H NMR, ^{31}P NMR, UV-VIS and ESI-MS.

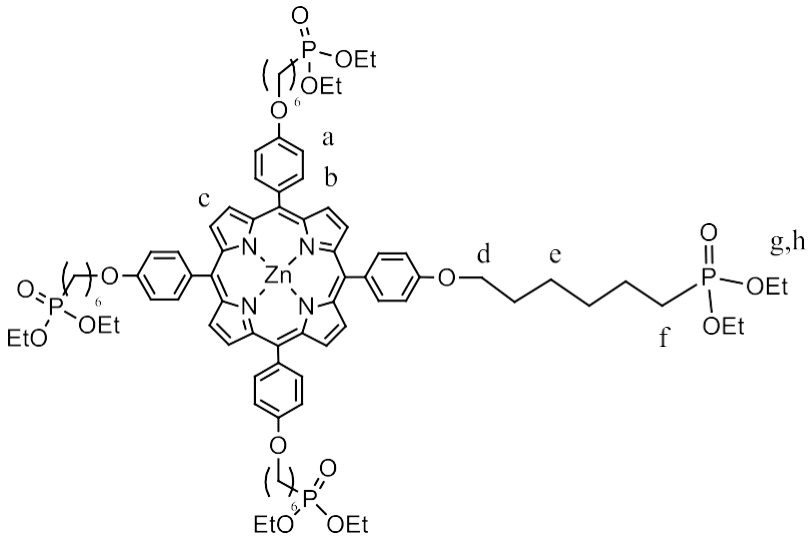

3

^{1}H NMR (400 MHz, DMSO d6)

δ(ppm) = 8.80 (8H, s, Hc); 8.05 (8H, d, Ha); 7.32 (8H, d, Hb); 4.24 (8H, t, Hd); 4.015 (16H, m, CH_2 in –OEt, Hg); 1.90 (8H, t, Hf); 1.47 (32H, m, He); 1.26 (24H, t, CH_3 in -OEt, Hh).

^{31}P{H} NMR (400 MHz, CDCl3)

δ(ppm) = 31.99

ESI-MS (MeOH)

m/z = 834.40 [Compound 3 + Na]$^{+2}$

m/z = 1622.73 [Compound 3]$^{+1}$

m/z = 1645.74 [Compound 3 + Na]$^{+1}$

UV-VIS (DMSO)

λ max = 430 nm (Soret band)

λ = 554 nm Q(0,0) band

λ = 607 nm Q(1,0) band

Disubstituted isomers:

Isomer O:

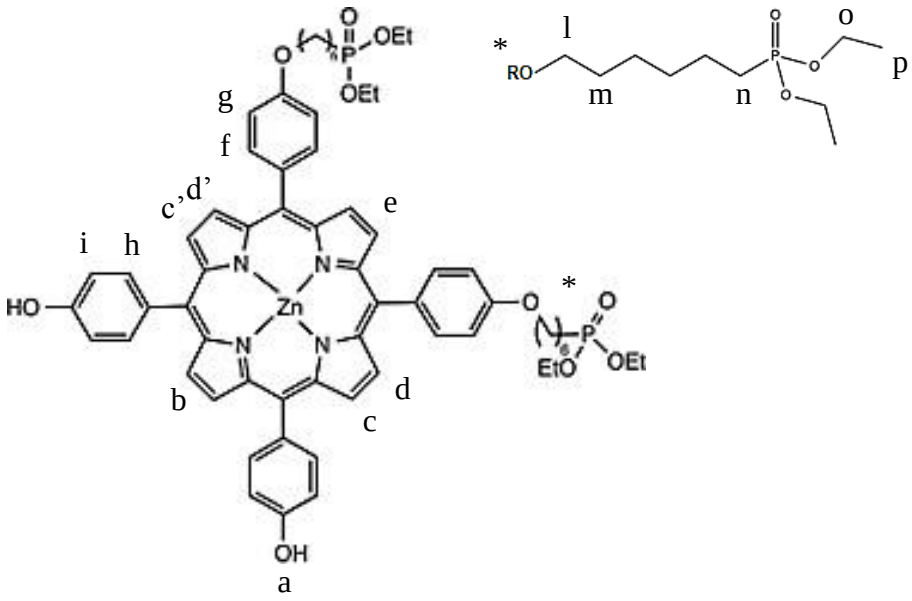

^{1}H NMR (300 MHz, DMSO d6)

δ(ppm) = 9.90 (2H, s, Ha); 8.80 (8H, m, Hb, Hc,c', Hd,d' He); 8.06 (4H, d, Hg); 7.96 (4H, d, Hi); 7.33 (4H, d, Hf); 7.18 (4H, d, Hh); 4.25 (4H, t, Hl);

4.015 (8H, m, CH_2 in –OEt, Ho); 1.90 (4H, t, Hn); 1.51 (4 H, m, Hm); 1.26 (12H, t, CH_3 in -OEt, Hp).

ESI-MS (MeOH)

m/z = 1180.41 $[Isomer\ O]^{+1}$

m/z = 1203.42 $[Isomer\ O + Na]^{+1}$

Isomer P:

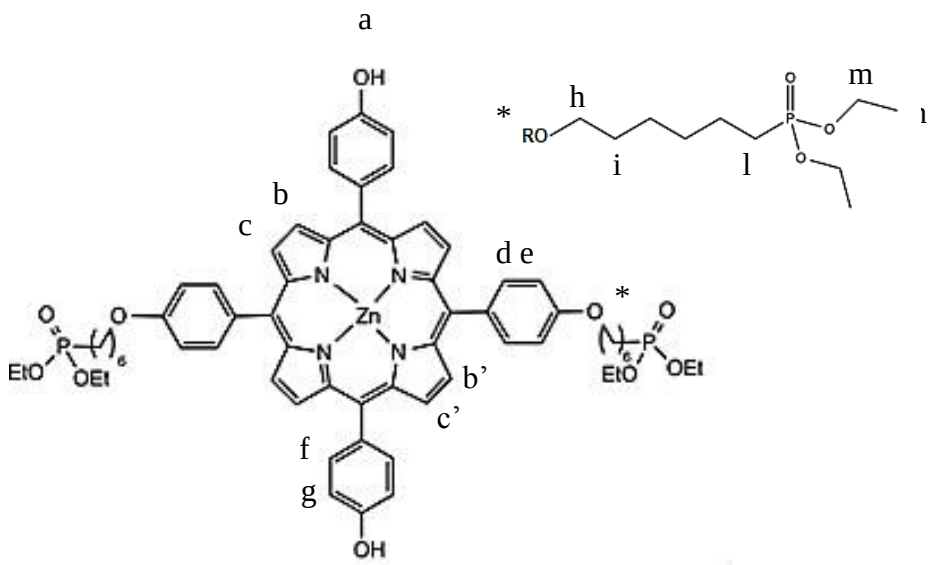

^{1}H NMR (300 MHz, DMSO d6)

δ(ppm) = 9.90 (2H, s, Ha); 8.80 (8H, m, Hb, Hc); 8.06 (4H, d, He); 7.96 (4H, d, Hg); 7.32 (4H, d, Hd); 7.18 (4H, d, Hf); 4.24 (4H, t, Hh); 4.02 (8H, m, CH_2 in –OEt, Hm); 1.89 (4H, t, Hl); 1.55 (4 H, m, Hm); 1.26 (12H, t, CH_3 in -OEt, Hn).

ESI-MS (MeOH)

m/z = 1180.48 [Isomer P]$^{+1}$

m/z = 1203.49 [Isomer P + Na]$^{+1}$

Trisubstituted compound:

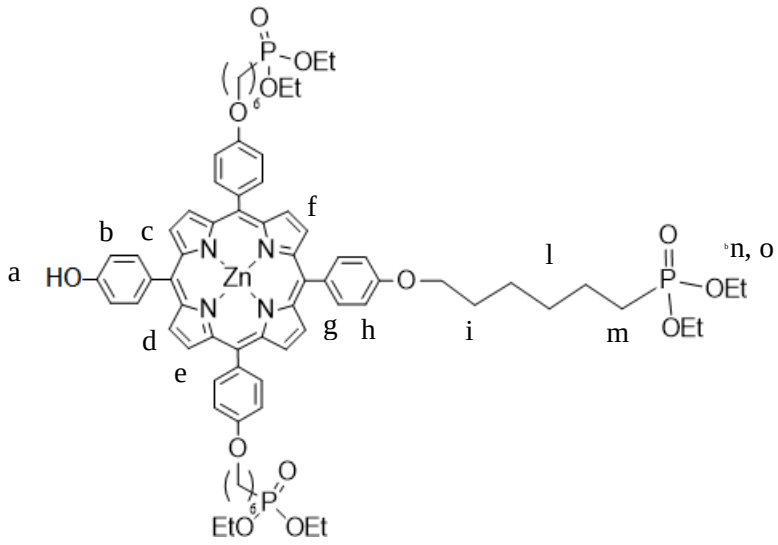

^{1}H NMR (300 MHz, $CDCl_3$)

δ(ppm) = 8.97 (2H, d, Hd); 8.96 (2H, d, He); 8.90 (4H, s, Hf); 8.32 (1H, s, Ha); 8.075 (2H, d, Hb); 8.04 (6H, d, Hh); 7.22 (2H, d, Hc); 7.10 (6H, d, Hg); 4.09 (6H, m, Hi); 3.42 (12H, m, CH_2 in –OEt, Hn); 1.80 (6H, t, Hm); 1.26 (18H, m, Ho); 1.02 (24H, m, CH_3 in -OEt, Hl).

Synthesis of zinc (II) 5,10,15,20-Tetrakis[4-(6-phosphonohexaoxy)phenyl] porphyrin

(Compound 4)

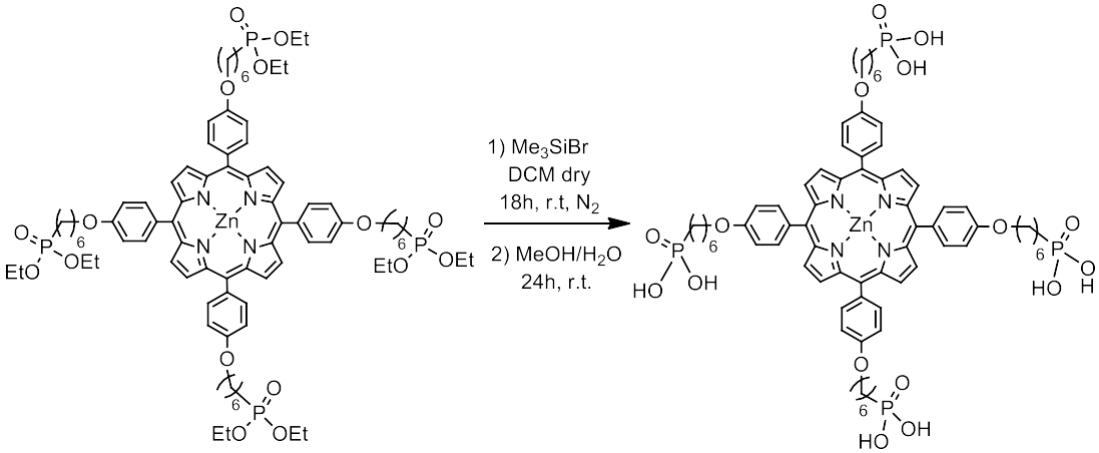

4

The reaction was carried out under dry conditions, employing a 25 ml round bottom flask, previously dried with 3 vacuum/nitrogen cycles.

Compound 3 (0.2005 g, 0.104 mmol) was introduced in the flask and dissolved in 6.33 ml of dry CH_2Cl_2. Bromotrimethylsilane (0.3730 g, 2,627 mmol) was then added under nitrogen flux.

The reaction was stirred at room temperature for 18 hours under nitrogen, then CH_2Cl_2 was removed at the rotary evaporator.

The remaining green solid was redissolved in a mixture of distilled water (1.52 ml) and MeOH (6.073 ml) and the reaction was stirred at room temperature for further 24 hours.

The precipitated green solid was filtered on a Buchner funnel, washed with MeOH and THF, then dried. The solid was redispersed in 25 ml of THF and refluxed an hour, then filtered again and collected as a brilliant green powder (0.0727 g, 50% yield), which was analyzed with ^{1}H NMR, ^{31}P NMR and UV-VIS.

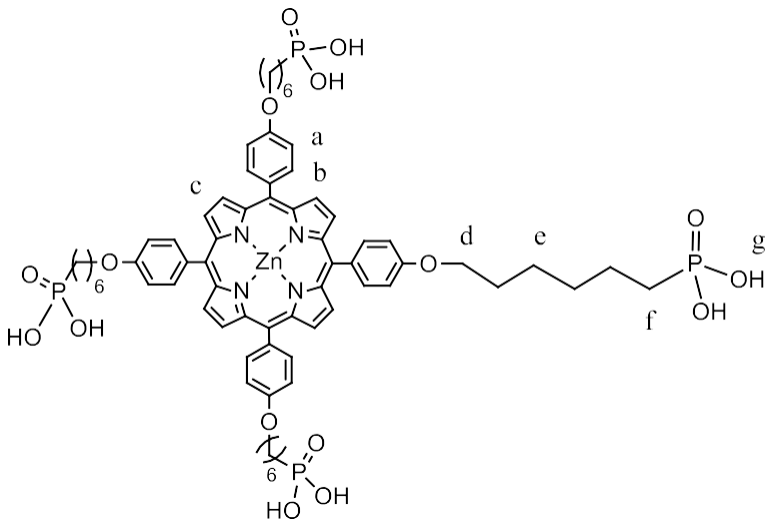

4

[1]H NMR (300 MHz, DMSO d6)

δ(ppm)= 8.82 (8H, s, Hc); 8.05 (8H, d, Ha); 7.305 (8H, d, Hb); 4.21 (8H, broad, Hg); 3.17 (8H, broad, Hd); 1.88 (8H, broad, Hf); 1.56 (32H, broad, He).

[31]P{H} NMR (400 MHz, DMSO d6)

δ(ppm) = 26.76

UV-VIS (DMSO)

λmax = 423 nm (Soret band)

λ = 520 nm Q(0,0) band

λ = 548 nm Q(1,0) band

References

[1] F. Rossi, E. Bedogni, F. Bigi, T. Rimoldi, L. Cristofolini, S. Pinelli, R. Alinovi, M. Negri, S.C. Dhanabalan, G. Attolini, F. Fabbri, M. Goldoni, A. Mutti, G. Benecchi, C. Ghetti, S. Iannotta and G. Salviati, "Porphyrin conjugated SiC/SiOx nanowires for X-ray-excited photodynamic therapy", *Scientific Reports, 5*, p. 7606, **2015**

[2] L.A. Martini, G.F. Moore, R.L. Milot, L.Z. Cai, S.W. Sheehan, C.A. Schmuttenmaer, G.W. Brudvig and R.H. Crabtree, "Modular Assembly of High-Potential Zinc Porphyrin Photosensitizers Attached to TiO_2 with a Series of Anchoring Groups", *J. Phys.Chem. C, 117* (28), pp. 14526-14533, **2013**

[3] H. Lin, G.A. MacDonald, Y. Shi, N.W. Polaske, D.V. McGrath, S.R. Marder, N.R. Armstrong, E.L. Ratcliff and S. Scott Saavedra, "Influence of Molecular Orientation on Charge-Transfer Processes at Phthalocyanine/Metal Oxide Interfaces and Relationship to Organic Photovoltaic Performance", *The Journal of Physical Chemistry, 119* (19), pp. 10304-10313, **2015**

[4] M. Timpel, M.V. Nardi, S. Krause, G. Ligorio, C. Christodoulou, L. Pasquali, A. Giglia, J. Frisch, B. Wegner, P. Moras and N. Koch, "Surface Modification of ZnO(0001)-Zn with Phosphonate-Based Self-Assembled Monolayers: Binding Modes, Orientation, and Work Function", *Chemistry of Materials, 26,* (17), pp. 5042-5050, **2014**

[5] B.J. Brennan, M.J. Llansola Portolés, P.A. Liddell, T.A. Moore, A.L. Moore and D. Gust, "Comparison of silatrane, phosphonic acid, and carboxylic acid functional groups for attachment of porphyrin sensitizers to TiO_2 in photoelectrochemical cells", *Physical Chemistry Chemical Physics, 15* (39), pp. 16605-16614, **2013**

[6] E.V. Vinogradova, Y.Y. Enakieva, S.E. Nefedov, K.P. Birin, A.Y. Tsivadze, Y.G. Gorbunova, A.G. Bessmertnykh-Lemeune, C. Stern and R.

Guilard, "Synthesis and Self-Organization of Zinc β-(Dialkoxyphosphoryl)porphyrins in the Solid State and in Solution", *Chemistry – A European Journal, 18* (47), pp. 15092-15104, **2012**

[7] Y. Fang, Y.G. Gorbunova, P. Chen, X. Jiang, M. Manowong, A.A. Sinelshchikova, Y.Y. Enakieva, A.G. Martynov, A.Y. Tsivadze, A. Bessmertnykh-Lemeune, C. Stern, R. Guilard and K.M. Kadish, "Electrochemical and Spectroelectrochemical Studies of Diphosphorylated Metalloporphyrins. Generation of a Phlorin Anion Product", *Inorganic Chemistry, 54* (7), pp. 3501-3512, **2015**

[8] A.G. Bessmertnykh-Lemeune, C. Stern, Y.G. Gorbunova, A.Y. Tsivadze and R. Guilard, *Macroheterocycles, 7* (2), 122-132, **2014**

[9] A.K. Bhattacharya, G. Thyagarajan, "Michaelis-Arbuzov Rearrangement", *Chemical Reviews, 81* (4), pp. 415- 430, **1981**

[10] A.Y. Garner, E.C. Chaplin and P.M. Scanlon, "Mechanism of the Michaelis-Arbuzov reaction: olefin formation", *The Journal of Organic Chemistry, 24* (4), pp. 532-536, **1959**

[11] M.A. Derbanne, V. Besse, S. Le Goff, M. Sadoun, T. Pham, and Stability, "Hydrolitycally stable acidic monomers used in two steps self-etch adhesives", *Polymer Degradation, 98* (9), pp. 1688-1698, **2013**

[12] C.E. McKenna, M.T. Higa, N.H. Cheung and M. McKenna, "The facile dealkylation of phosphonic acid dialkyl esters by bromotrimethylsilane" *Tetrahedron Letters, 18* (2), pp. 155-158, **1977**

Conclusions

My thesis work was focused on the preparation of novel hybrid nanosystems for possible applications in nanomedicine, in particular for X-ray excited photodynamic therapy, with the aim of treating deep solid tumours.
During my PhD period, I developed different kinds of hybrid inorganic/organic nanosystems, all based on *core-shell* SiC/SiOx nanowires, functionalized with various porphyrins and substituents. Whereas in previous PhD works developed in our laboratory the *tetra*(4-carboxyphenyl)porphyrin (H_2TCPP) was covalently linked to the SiC/SiO_x NWs by a 'click' reaction, during my thesis work I conjugated the selected porphyrin to the nanowires by the formation of the covalent amide bond and introduced different ending chains in the porphyrin moiety.
Amide bond formation required the preliminary introduction of amino groups on the nanowire surface: silica hydroxyl groups were reacted with APTES (aminopropyltriethoxysilane). To bind the porphyrin to the nanowire surface, the carboxylic groups of H_2TCPP porphyrin were previously activated with typical condensation agents (EDC, HOBt, and DMAP) and then reacted with the amino groups to give the amide bond formation.
This novel conjugation strategy lead to a higher degree of porphyrin loading, as evidenced by fluorescence spectra, and occurred under very mild conditions, with respect to those employed in click reactions.
The aim of my PhD was to develop nanosystems with a better dispersion in biological medium, with respect to those previously prepared. All the nanosystems I synthetized were characterized with solid state fluorescence spectroscopy, in order to check that functionalization with porphyrins was carried out successfully, and underwent in vitro tests employing A549 cells (human adenocarcinoma epithelial cellular line). The antiproliferative activity was tested and compared for each nanosystem.
My PhD activity, on the whole, consisted in:

1) *Synthesis of hybrid nanosystems functionalized with PEGylated porphyrins*

   a) Synthesis of a hybrid nanosystem containing H_2TCPP porphyrin conjugated with PEG_6-CH_2COOH

$NH_2CH_2CH_2(OCH_2CH_2)_5OCH_2CO_3$ chain was synthetized with a multistep reaction starting from hexaethylene glycol, then was bound to activated carboxylic groups of H_2TCPP porphyrin on the nanowires.
Finally, deprotection with trifluoroacetic yielded free acid carboxylic groups at the end of the PEG-chains. After detaching nanowires from their metallic support, clonogenic tests performed on the adenocarcinoma human alveolar basal epithelial (A549) cell line evidenced the ability of the nanosystem to significantly reduce the survival fraction with respect to simple radiotherapy.

b) Synthesis of a hybrid nanosystem containing H_2TCPP porphyrin conjugated with PEG_8-OH

The second short PEG chain I prepared, NH_2-PEG_8-OH, was synthetized from tetraethylene glycol by a multistep synthesis. The residual activated carboxylic groups of the H_2TCPP porphyrin conjugated to the nanowires were reacted with this chain giving a less polar nanosystem, without a ionizable carboxylic group. The activity of the nanowires, after detaching from their support, was checked by *in vitro* tests on A549 tumoural cell line. A lower activity was observed with respect to the previous nanosystem based on PEG_6-CH_2COOH. This could be ascribed to lower internalization due to the formation of boundles in the biological medium.

2) Synthesis of a hybrid nanosystem containing H_2TCPP and H_2TAPP conjugated porphyrins

We thought to link a second different porphyrin on the conjugated H_2TCPP porphyrin in order to thicken the photosensitizer layer on nanowires. This was supposed to improve energy transfer processes and, thus, the production of singlet oxygen. In particular, tetra(4-aminophenyl)porphyrin (H_2TAPP) was successfully reacted with H_2TCPP. The present nanosystem was characterized with fluorescence spectroscopy and its antiproliferative activity against A549 cell line was tested.

3) Evaluation of porphyrin loading on nanowires via quantitative analysis of Cu(II) in solution

Cu-TCPP porphyrin was synthetized so that it could be conjugated to the nanowires. A copper metal porphyrin was chosen since it is stable enough not to undergo demetallation in mild conditions. Cu-TCPP porphyrin was successfully conjugated to nanowires. The complete removal of copper from the porphyrin was achieved by an acidic treatment of detached nanowires with concentrated sulfuric acid. The determination of Cu amount by atomic absorption was performed.

4) Synthesis of Zn (II) porphyrins functionalized with phosphonic acids

We choose tetra(4-hydroxyphenyl)porphyrin (H_2THPP) as starting compound in order to obtain a metal tetra-phosphonated porphyrin: such a compound can be conjugated to a solid support and phosphonic groups could be an alternative linker to anchor porphyrins on solid supports. In this frame it was possible to obtain the Zn-THPP functionalized with four phosphonic acid chain ($-CH_2)_6PO_3H$), a compound that is not reported in the literature. This type of porphyrins is of great interest for both energy transfer process and electron transfer process.
The conjugation of this porphyrin on a flat silicon support will be useful to study the porphyrin position on the surface, parallel or not, by X-ray excited optical luminescence (XEOL): porphyrin orientation on a solid support, in fact, is an important parameter in determining the efficiency of energy and electron transfer processes.

Future perspectives

The results obtained in my PhD work confirm the $^1O_2$ production by the conjugated NW-porphyrin system, occurring through the self-lighted photodynamic process, and demonstrated that our novel approach is very efficient to enhance radiation therapy effects for cancer treatments.

It was noticed that to irradiate nanowires with a 4Gy radiation is not useful to increment the production of singlet oxygen. All future experiments will be carried out employing a 2Gy radiation. Furthermore, it seems convenient to reduce the energy of employed X-ray during the treatment.

The results observed from quantitative determination of Cu on nanowires evidenced that a remarkably increased loading of porphyrin can be achieved by conjugating detached nanowires, after the introduction of amino groups on their surface. For this reason, it is convenient to carry this approach through and to repeat also the conjugation via "click" chemistry in this conditions.

Another important challenge is to find different strategies to bind phosphonic acids on silica surface, a difficult reaction to achieve. We thought about possible ways, consisting of formation of covalent amide bonds or ionic bonds, for instance. The aim is to achieve a stable conjugation between phosphonic groups and silica, instead of simple chemisorption.
A stable conjugation is the basis to make the most of this compounds for a variety of applications.

In addition, porphyrins functionalized with phosphonic acids are of great interest for both energy and electron transfer processes, when conjugated in a stable way to flat solid supports. Their possible application in photodynamic therapy, on the other hand, has not been already explored: it could be interesting to create novel nanosystems containing this kind of compounds (with or without metal), in order to study their cytotoxic activity and efficiency in producing singlet oxygen.

Energy transfer studies on porphyrins functionalized with phosphonic acids will be carried out with XEOL technique, employing less energetic X-ray.

Acknowledgments

First of all I would like to thank my tutor, prof. Franca Bigi, for all that she taught me during these years. Thanks to her I learned to work accurately and I became more and more fond of organic chemistry. She gave me the opportunity to work in BioNiMed project, within which I learned a lot of new things and I became more self-confident, both chemically and not chemically.
Thanks to all the members of BioNiMed project and to all the people who helped me in these years. Thanks to the members of IMEM-CNR institute of Parma, in particular to Dr. Bosi's Material Growth group and prof. Salviati's Material Characterization group. Special thanks to two members of this group, Paola and Francesca, very nice people, whom I appreciate a lot. Thanks to the members of IMEM-CNR institute of Trento for XPS and XEOL studies of my samples. Thanks to the members of Toxicology Department of Parma Hospital: to Matteo Goldoni for atomic absorption analysis of my samples, to Rossella Alinovi and Silvana Pinelli for clonogenic tests and for teaching me something more in biomedical and biological field. Thanks to the members of Cristofolini's group (Physics Department) and especially to Davide Orsi for fluorescence analysis of my samples and for the reliability and kindness showed in these years.
Special thanks, of course, go to my parents, who always supported me during these years at university and gave me the opportunity to do what I like most. Thanks to my mum, the most important person in my life, with which I share everything and who supports me in everything I do.
Thanks to my dad, who always believes in me and is always enthusiastic about what I do in the lab.
Thanks to Gianmaria, who supports me, believes in me and with which I shared more than three years.
Thanks to my lab-mates, with which I shared these years too: Emanuele, who always helped me whenever I needed, Matteo and Alessandra, who turned out to be good friends in and outside the lab, the amazing Spez, Anna, Chiara and other people I met in these years.
Special thanks go to Martina, a very nice person and a good friend, with which I shared many adventures and misadventures in the lab and tiring workouts in the gym!
Thanks to my amazing bachelor students, Luca, Giulia, Francesca, Dario and

Kevin: I was very lucky and glad to work with all of you in the lab! I couldn't ask for better students to collaborate with!
Special thanks to Dario, a true good friend, as well as an excellent bachelor student. Special thanks also to Kevin, the most funny bachelor student ever!

Thanks to the research fellows who helped me during this years: Antonio (Pacio), a hard-working and helpful colleague, and Davide, who helped me and made me laugh a lot during our days in the lab.
Thanks to all the '94 students. This experience allowed me to know you and many of you became good friends of mine.
Special thanks to Marine, maybe one of my best friends, that knows everything about me. Thanks to Damiano, a good friend and a very funny person, and, of course, to Gigi ("my favourite student"), who always fools me and makes me laugh. During these years I had the opportunity to meet such nice friends!
Thanks to these people that I met at university and became good friends of mine also in everyday life: Martina, Jessica, Veronica, Luca, Kevin, Riccardo and Filippo.
Thanks to all these people for sharing with me these beautiful years.

Cecilia Loffi

21/03/1990: Born in Cremona (Italy)

07/2009: Liceo Classico Daniele Manin High School, Cremona, Italy 100/100

26/10/2012: Bachelor Degree in Chemistry, University of Parma, Parma, Italy 110/110 with praise

24/10/2014: Master Degree in Chemistry, University of Parma, Parma, Italy 110/110 with praise

11/2014-10/2017: PhD Student with Prof. F. Bigi, University of Parma (Italy)